1997

Eddy current automatic flaw detection system for heat exchanger tubes in steam generators

Sheng-Fa Chuang
Iowa State University

INFORMATION TO USERS

This manuscript has been reproduced from the microfilm master. UMI films the text directly from the original or copy submitted. Thus, some thesis and dissertation copies are in typewriter face, while others may be from any type of computer printer.

The quality of this reproduction is dependent upon the quality of the copy submitted. Broken or indistinct print, colored or poor quality illustrations and photographs, print bleedthrough, substandard margins, and improper alignment can adversely affect reproduction.

In the unlikely event that the author did not send UMI a complete manuscript and there are missing pages, these will be noted. Also, if unauthorized copyright material had to be removed, a note will indicate the deletion.

Oversize materials (e.g., maps, drawings, charts) are reproduced by sectioning the original, beginning at the upper left-hand corner and continuing from left to right in equal sections with small overlaps. Each original is also photographed in one exposure and is included in reduced form at the back of the book.

Photographs included in the original manuscript have been reproduced xerographically in this copy. Higher quality 6" x 9" black and white photographic prints are available for any photographs or illustrations appearing in this copy for an additional charge. Contact UMI directly to order.

UMI

A Bell & Howell Information Company
300 North Zeeb Road, Ann Arbor MI 48106-1346 USA
313/761-4700 800/521-0600

Eddy current automatic flaw detection system for heat exchanger tubes in steam generators

by

Sheng-Fa Chuang

A dissertation submitted to the graduate faculty

in partial fulfillment of the requirements for the degree of

DOCTOR OF PHILOSOPHY

Major: Electrical Engineering (Communication and Signal Processing)

Major Professor: John P. Basart

Iowa State University

Ames, Iowa

1997

Graduate College

Iowa State university

This is to certify that the doctoral dissertation of

Sheng-Fa Chuang

has met the dissertation requirements of Iowa State University

Signature was redacted for privacy.

Major Professor

Signature was redacted for privacy.

For the Major Program

Signature was redacted for privacy.

For the Graduate College

TABLE OF CONTENTS

ACKNOWLEDGEMENTS

The completion of the dissertation would not have been possible without the help and support of many individuals. My deepest thanks go first to my advisor professor John P. Basart for his guidance, encouragement, and genuine concern throughout my stay at Iowa State University. His commitment to excellence has been a great inspiration in course of my graduate research. His willingness to share his knowledge of signal processing is sincerely appreciated.

Special thanks go to John C. Moulder for numerous and enlightening conversations whenever needed. His great sense of humor made my serious research topic more enjoyable. I acknowledge his input in the field of nondestructive evaluation (NDE) using eddy current technique.

I also thank members of my graduate committee, Dr. Satish S. Udpa, Dr. Lalita Udpa, Dr. David K. Hsu, and Dr. William Q. Meeker for their time and advice. Suggestions and criticisms made by this group helped my study more productive.

Special acknowledgment to my colleagues and friends who provided continuos encouragement and assistance, in particular, I would like to thank Bing Wang, Zhong Zhang, lunxiong He, Han-Yi Hsieh, and Amneh Akour.

Last but not the least, I wish to thank my wife Yu-Ju Chen for her endless patience and understanding. Without her support, I could not have accomplished what I had set out to do. The arrival of our son, Alan, during this experience provides proper perspective to all of my pursuits.

Finally, my deepest thanks go to my parents, Mr. Chien-Tsung Chuang and Mrs. Mei-Yin C. Chuang, who always gave me the utmost freedom, love, and confidence to become what I am today.

CHAPTER 1. INTRODUCTION

1.1 Statement of Problem

Proper inspection of steam generators is critical to the safe and economical operation of nuclear power plants. In the past, eddy current inspection has proven to be both fast and effective in detecting and sizing most of the degradation mechanisms that occurred in the early generators. However, as the nation's generators have aged, newer and much more subtle forms of degradation have appeared that require more intelligent application of eddy current tests. Especially, the generators have accumulated a variety of damage that makes it difficult to detect the defects. Recent eddy current inspections at a few plants have demonstrated the need for improved eddy current inspections. Both the accuracy and the speed of the present inspections need to be improved, so that we can do a better job of preventing tube failures before they occur rather than determining why a tube failed after the fact.

Conventional eddy current data analysis is carried out by human analysts. Normally, during the inspection signals from multiple channels of different frequency and probe type (absolute or differential) are recorded. Analysts combine their experience and information from the shape of the signal, the shape of the lissajous pattern of the signal and the phase of the signal in each channel to make a decision. Through the use of multiple-frequency ET systems, modern equipment is capable of acquiring the necessary data to correctly diagnose the indications. Applying consistent and reliable analysis techniques, however, is required to achieve improved test results. Human nature itself will cause some variance in analysis.

Also, the combination of many different properties in the eddy current signal makes it very difficult to analyze. Inspection results are often not consistent with prior inspections or are inconsistent among different analysts. To overcome these obstacles, an eddy current automatic analysis system is needed to improve the test results.

1.2 Significance of the Work

An automatic flaw detection system for eddy current inspection of steam generator tubes has been developed. It is based on techniques developed previously and the knowledge of experts, combined in an automatic flaw detection system to predict and prevent tube failures.

The inspection of steam generator tubing is a difficult and complex problem. Traditional signal processing techniques are not very suitable to solve this particular problem. It requires integration of many novel techniques to optimize the solution of the problem. We developed a new detection technique which is a combination of statistical analysis and the wavelet transform to find the possible flaw indications. We also investigated a template matching technique and a fuzzy decision making system to help analyze the tube inspection data. The development of new detection techniques and the integration of these novel techniques in a comprehensive software analysis package are the fundamental contributions of this research.

1.3 Dissertation Objectives

The objectives of this study can be summarized as follows:

1. Study the characteristics of eddy current tubing inspection data obtained from a bobbin coil. This study should provide sufficient understanding of the flaw-probe interaction, properties of noise sources, and the formation of the inspection data under complex test conditions. This study is the basis for investigating signal processing and flaw detection techniques.
2. Investigate eddy current signal processing and flaw detection techniques to perform automatic data analysis, to reduce the workload of human analysts, and to improve the quality of data analysis. Based on the techniques studied, an automatic flaw detection system should be developed and tested using real-world inspection data.
3. Study techniques that can be used to compare two data sets obtained from the same tube at different times. Such techniques are very important to industrial practice because they allow one to study the changes in a tube over time. Several key techniques must be studied: (1) data alignment techniques to compensate for the variation in pulling speed in different inspections; (2) Flaw characterization techniques to obtain estimates on flaw sizes; and (3) Techniques to resolve inconsistencies in results obtained from the two data sets.

1.4 Organization of the Dissertation

In Chapter 2, the technological background of eddy current non-destructive evaluation (NDE) technique and its application to steam generator tubing inspection are introduced. The

fundamental concepts of eddy current testing (ET) is described so that one can understand what ET is and how the signal is formed. Traditional human analysis methods are described to illustrate how the data is processed and evaluated. In Chapter 3, a comprehensive literature survey on the development of eddy current data analysis will be presented. The survey includes signal processing techniques, feature extraction, flaw classification, and expert systems. From Chapter 4 to Chapter 6, we present our automatic flaw detection system. There are three major components in the automatic flaw detection system: signal preprocessing, wavelet flaw identification, and fuzzy decision-making, in a consecutive order. In Chapter 4, we discuss the first stage of the eddy current automatic flaw detection system--signal preprocessing. Three efficient procedures--initial set-up, automatic data alignment, and background removal are discussed. In Chapter 5, we introduce the wavelet flaw identification method, which is stage two of the flaw detection system. The concepts and fundamental theory of wavelets are presented first. Then the wavelet flaw detection algorithm, based on the wavelet theory, is given. This algorithm consists of four procedures: fast wavelet transform, extrema algorithm, denoising procedure, and transient detection algorithm. In Chapter 6, the fuzzy evaluation system, stage three of the flaw detection system, is discussed. The fuzzy evaluation system is based on a template matching technique and a fuzzy inference system. In Chapter 7, we give the results of a rigorous test of the flaw detection system. From the test results, we evaluate the performance of the system and also point out the strengths and limitations. Finally, in Chapter 8 we present a summary of the research effort towards the development of an automatic flaw detection system and discuss the future direction of this work.

1.5 Summary of Major New Contributions

1. The data alignment approach provides a new technique for data comparison (section 4.3). It offers an efficient way to compare data from sequential inspections. The problem of identifying the same location on the tube has been solved. Especially, the growth of a flaw can be easily determined after the data are aligned.
2. The wavelet flaw detection method offers a new means for analyzing the eddy current differential probe signals, which are localized in both time and frequency. Especially, the noise and the flaw signal can be separated in the wavelet domain by using multiresolution analysis. It also provides new features for classifying flaw signals. In addition, in the wavelet domain the position of a flaw can be preserved. All these properties make wavelet analysis an ideal tool for eddy current data analysis.
3. The fuzzy inference system developed in this study provides an effective and flexible frame work for an automatic flaw detection system. The fuzzy inference system combines the information obtained from wavelet analysis and template matching to improve the reliability and accuracy of analysis results. Another attractive property of the fuzzy inference system is that it allows easy integration of new features with existing features. Therefore, it can be further improved when data processing techniques become more mature and more expert knowledge is applied.

CHAPTER 2. BACKGROUND

2.1 Introduction

Eddy current testing is a widely used nondestructive testing (NDT) method. It is a technique based on electromagnetic field theory for detecting defects in materials or evaluating material properties. Eddy current testing uses relatively small size probes and has high sensitivity and high inspection speed. This makes it an ideal choice for inspecting metallic tubing structures such as heat exchanger tubes. The basic principle of eddy current testing (ET) is that a change in material properties or the presence of a flaw in the test piece perturbs the electromagnetic field of an interrogating probe. This perturbation produces a change in the electrical input impedance of the probe, which can be used to deduce the nature of the flaw.

Due to the relatively low cost and the one-side accessibility requirement of the test object, ET has been widely used in the inspection of the heat-exchanger tubes in steam generators of nuclear power plants. These tubes are used to separate the primary water and the secondary water of the nuclear reactor. While the primary water is radioactive, the secondary water is not radioactive. Since it is life-critical to make sure that there is no radioactive material in the secondary water, the safety of these tubes is very important. The inspection of these tubes is a critical component of the maintenance of the nuclear power plants [1].

In this chapter, we provide some background information on the eddy current NDE technique and its application to steam generator tubing inspection. First we review the

fundamental concept of the ET technique [2-4]. Understanding the fundamentals of ET technology is the basis for the correct interpretation of a defect signal. After explaining these we will then discuss the multi-frequency eddy current testing technique which are widely used in industrial practice to enhance flaw characterization capability. Conventional data analysis for steam generator tubing inspection data relies on well-trained human analysts. We give a description on the methods used by human analysts for interpreting the data and making decisions on flaw type and size. This background information is very helpful for the development of an automatic flaw detection system which simulates the process of the human expert based data analysis.

2.2 Fundamentals of ET Technique

A brief review of the ET technique is included here. The discussion is divided into two major parts: (1) an introduction to the basic eddy current behavior; and (2) methods to optimize the detection of defect signals. We introduce the basic concept of eddy current, some considerations on eddy current probe design, and the limitations of the ET defect detection. The skin depth and phase lag of ET is also addressed for giving a deeper understanding of the ET technique and explaining the reasons for the limitations of the ET technique. To understand how a defect can be characterized from its signal, we first describe how the probe impedance is changed by the presence of a defect. Then we explain how to select the test frequency for optimizing the defect detection capability. We also briefly review the basic principles for eddy current defect signal analysis.

2.2.1 Eddy current generation and flow

A sine current in a cylindrical coil produces an alternating magnetic field oriented perpendicular to the current or parallel to the coil's axis. When this field intersects an conductive metal testpiece, eddy currents are induced in it according to Faraday's and Ohm's laws. The eddy currents are normal to the magnetic field. The eddy currents in metal testpiece set up a magnetic field in opposition to the incident field causing partial cancellation according to Lenz's Law. This decrease in magnetic flux through a coil causes a change in coil impedance. By measuring the impedance of the coil and observing its change as the coil is moved around the test piece, it is possible to locate and characterize defects in the testpiece. As an eddy current probe is brought close to a conductor, both the resistive and inductive reactance components of the probe coil impedance are altered. When a probe passes over a defect the eddy current flow distorts, resulting in a change in probe coil impedance. Fig. 2.1 illustrates the eddy currents induced in a metal testpiece by an air-core coil.

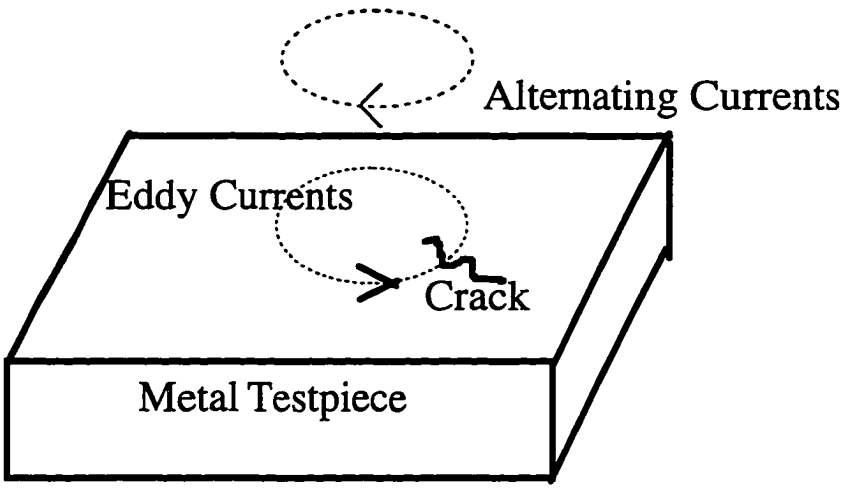

Figure 2.1 Eddy current generation and flow in a metal testpiece.

2.2.2 Probe design and defect detection

An eddy current instrument is generally built by combining a variable frequency excitation current source with an ac bridge to measure the small impedance changes due to defects. Probe coils are located on adjacent arms of the bridge as shown in Fig. 2.2 [3,5]. Bridge instruments normally use probes with two coils. If the probe has one test coil and one reference coil, it is called an absolute probe. If both coils sense the material under test equally it is called a differential probe. To be differential the coils must be connected in opposition. Absolute probes respond to all variables which affect eddy current flow, such as resistivity, magnetic permeability, geometry of test material and defects. By contrast, differential probes compare adjacent material sections. A differential probe will only yield an out-of-balance (defect) signal when a difference in eddy current distribution exists under the adjacent coils. The absolute probe is usually used for general inspection and especially for detecting the long and gradual defects. The differential probe is normally used for the inspection for localized defects.

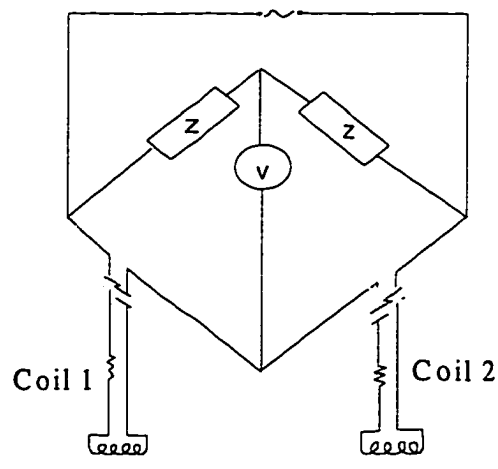

Figure 2.2 Probe coils in an ac bridge circuit.

In Figure 2.3 we illustrate typical one-dimensional defect signals from an absolute probe and a differential coil. As the absolute probe passes over a point defect, the signal produced has a shape similar to that of a Gaussian signal, centered on the defect, as shown in the figure. The differential bobbin probe produces a signal that is similar to the derivative of a gaussian, with the defect signal approaching a maximum as the first coil is under the defect, going to the zero as the defect is centered between the two differential coils, and becoming a minimum as the defect is under the second coil.

It is fundamental to ET that only those defects which in some way disturb or alter normal eddy current flow patterns are detectable. Since flaw detection in eddy current testing relies on impedance change in the coil, certain types of defects cannot be detected by an eddy

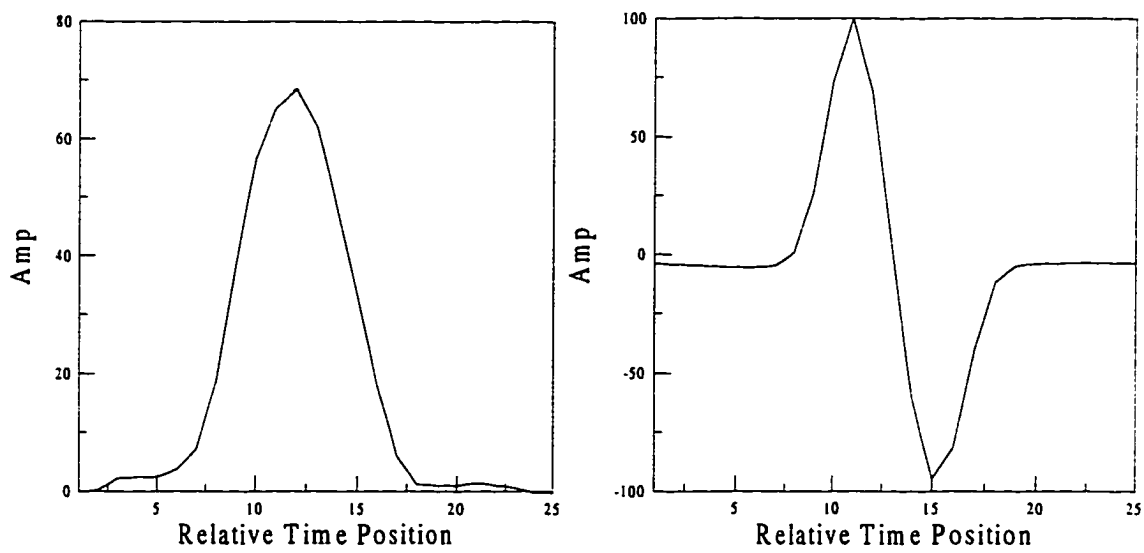

Figure 2.3 One-dimensional defect signals from an absolute probe (left) and a differential coil (right).

current probe because they do not impede eddy current flow. The major limitations of the ET technique are listed as follows:

(1) Eddy currents flow in closed paths and only are induced in conducting material. Therefore, ET can not be used for non-conducting material or material with very low conductivity.

(2) Eddy currents are governed by a diffusive field and are only capable of penetrating to a certain depth in the metal testpiece. The penetration depth is dependent on the test frequency. Therefore, eddy current testing is not sensitive to deep flaws unless a very low test frequency is used.

(3) If the coil axis is perpendicular to the testpiece surface, no eddy currents are induced along the center line of the coil so that defects located right below the coil center are not detectable.

(4) Eddy currents are parallel to coil windings so that a probe coil has poor sensitivity to laminar defects in plates or tubes and circumferential cracks in tubes or bars.

2.2.3 Skin depth and phase lag

Eddy currents are induced by a changing diffusive magnetic field which is concentrated near the surface of the metal testpiece. Eddy current density decreases with increasing depth and the variation with depth depends on the test frequency, electrical resistivity and magnetic permeability of the sample. Skin effect arises as follows: eddy currents flowing in the sample at any depth produce magnetic fields which oppose the primary field, thus reducing magnetic flux and causing a decrease in current flow at greater

depth. This result is an exponential decrease in eddy current density J with increasing depth. For infinitely thick material, a standard depth of penetration δ is defined as the depth at which eddy current density J_x has dropped to $1/e$ or 36.8% of the surface density J_0. The J_x is the eddy current density at depth x below the surface. The skin depth is given by the following equation [2]

$$\delta = \sqrt{\frac{2}{\omega\mu\sigma}}, \tag{2.1}$$

where ω is the radian test frequency, σ is the conductivity of the metal testpiece, and μ is the magnetic permeability. Sensitivity to subsurface defects depends on eddy current density at that depth. Current density at 3δ below the surface is only 5% of the surface density; 3δ therefore represents the practical limit of defect detection. In practice the useful depth is actually less than 3δ because of the large resultant phase lag.

Phase lag β in ET refers to the fact that subsurface eddy currents are not in phase but lag those at the surface. Phase lag increases linearly with depth for infinitely material. It is given by [2, 3]

$$\beta = x/\delta \text{ radians}, \tag{2.2}$$

where x is the depth below the surface and δ is the skin depth. Phase lag provides a simple way to classify detect type and to estimate the depth of the flaw. For the steam generator tubing inspection, the signal from a defect on the internal surface of the tube is different in phase from the signal from a defect on the external surface. Therefore, by examining the phase of the signal, we can determine whether the flaw is an inside diameter (ID) flaw or an outside diameter (OD) flaw. Also, we can differentiate the signal for a significant defect (for

instance, a crack) from signals for insignificant surface conditions (such as changes in tube diameter or dents).

2.2.4 Probe impedance, test frequencies, and defect signal analysis

Eddy current testing consists of monitoring the resistive and inductive reactance components of coil impedance. To aid analysis, impedance changes are normally plotted on an x-y graph called a *Lissajous pattern* with inductive reactance along the y axis and resistance along the x axis. Human inspectors utilize Lissajous patterns of the acquired data signals to further differentiate flaw indications from unwanted signals and noises. This is known as the impedance plane analysis method of eddy current testing.

To optimize the detection capability of eddy current testing for a certain testpiece, the test frequency must be carefully selected. Frequency is the only controllable test variable of the probe coil. The choice of test frequency for defect detection depends on the thickness of material to be inspected. As a general rule one should use a test frequency which makes the maximum thickness of material to be inspected about one standard depth of penetration. Lower frequencies might giver deeper penetration but would yield reduced sensitivity and poor discrimination between surface and subsurface defects. Higher frequencies would make subsurface defects undetectable. In industrial ET inspections, multiple-frequency ET systems are frequently used to combine the high sensitivity at high frequency and the good penetration at low frequency. For heat exchanger tubes, a low test frequency is used to detect tube support structures and a high frequency is used to detect surface defects. Through the use of multiple-frequency ET systems, tubing inspection data can provide necessary information for

human analysts to distinguish flaw signals from permanent structures and insignificant changes of the tubes.

Defect analysis of eddy current testing relies on the depth dependence of the phase of a defect signal. Phase lag is very important in ET since it permits defect characterization as well as reliable estimation of depth. Many signal sources are possible during ET since anything which affects sample resistivity or permeability will be detected as a change in probe coil impedance. Only some of these changes may be defects. Phase analysis allows one to decide which signals represent defects and which are irrelevant indications. Fig. 2.4 illustrates the impedance plane representation of a tube support plate signal, the signal from through wall flaw and 40% OD flaw. As can be seen in the figure, the three signals have distinctive phase characteristics. By examining the phase of an eddy current signal, we can determine the indication type and estimate the depth of the flaw. To correct for possible phase offset due to different probe response and instrumentation setup, a calibration process is used in industrial practice. During the calibration process, the eddy current signals from a set of artificial flaws on a calibration tube are measured and analyzed. The phase angles of those signals are recorded and a calibration standard is established. The calibration standard relates the phase angle of the eddy current signal with the depth of the defect. After the eddy current signal of a unknown defect is measured using the same probe, we can estimate the depth of the defect by using the calibration standard.

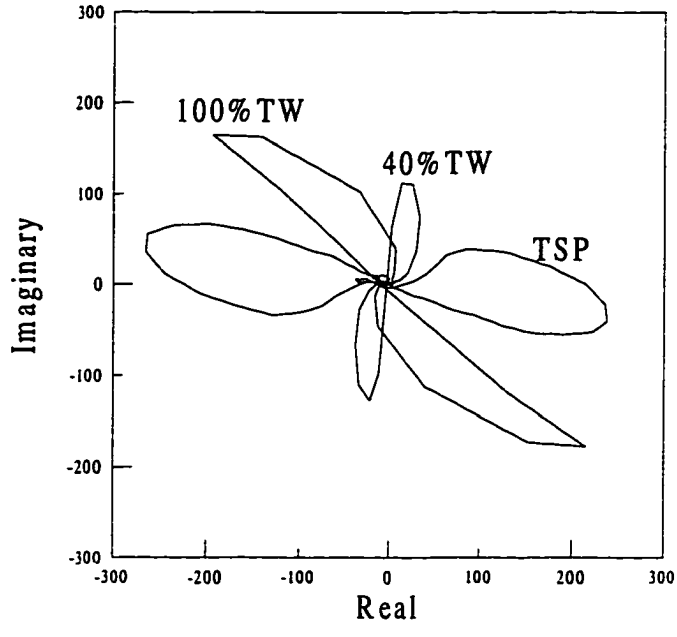

Figure 2.4 Eddy current impedance plane signals of TSP, 100%TW OD flaw, and 40%TW OD flaw on 400 kHz differential channel.

2.3 Multifrequency/Multiparameter Eddy-Current Technology

2.3.1 Overview

In the history of eddy-current testing, the development of multifrequency/multiparameter (MFEC/MPEC) eddy-current technology has significantly improved the quality of the inspection of steam-generator tubing. ET by its nature is sensitive to any change in the electrical or magnetic properties of the test part. For heat exchanger tubing, this includes not only defects, but also support structures, electrically conductive deposits, permeability variations, dents and bulges, roll expansions, and other phenomena. Indications from all these unwanted effects frequently combine with indications from defects so that both flaw detection and sizing are difficult. The invention of

MFEC/MPEC technology offers benefits in characterizing and interpreting defect signals. Especially with MFEC/MPEC technology we are able to separate the contribution of the various parameters that determine the coil impedance and to suppress the contribution caused by unwanted or disturbing parameters.

One important processing procedure in multifrequency testing is the mixing of the signals from different frequency channels. It can be used to separate a flaw signal from a support plate signal for flaws near support plate structures. Mixing can be implemented in hardware by using multipliers and adders. It can also be implemented in software by using a least squares (LS) algorithm or similar algorithms. Mixing provides an advantage which is not possible in single frequency eddy current testing: the mixed channel can be tuned to be sensitive to certain types of defects and to eliminate signals from structures which are of no interest to the inspector.

2.3.2 Multifrequency/Multiparameter methodology

The MFEC method is a data analysis method which analyzes the signal in the impedance plane at different frequencies. The data from each frequency may be treated as a separate single-frequency test which permits comparison of test responses as a function of frequency. In eddy current testing, different frequencies produce different responses for the same test object. In general, lower frequencies give deeper penetration but would yield reduced sensitivity and poor discrimination between surface and subsurface defects. Higher frequencies would make subsurface defects undetectable. According to the frequency dependence of the impedance change response, we can have different sensitivities of a defect

signal at different frequencies. With the MFEC method, we can analyze these signals simultaneously and use characteristics of the defects and other unwanted parameters on different frequencies to identify the flaw indications.

For the MPEC method, data from individual frequencies are combined by a vector addition process. This combination of data is referred to as mixing and is mathematically equivalent to simultaneous solution of multiple equations. This mixing process permits elimination of unwanted test parameters while those of interest are retained. In steam-generator inspection the desired information on tubing flaws can be masked by dents, support plates, probe wobble, and inside-diameter variations such as mandrel chatter or pilgering. With the MPEC method, we can suppress those unwanted test variables. This is especially important for flaws near tube support plate regions: an accurate estimation of the flaw depth is only possible after the support plate signal is removed.

2.4 Data Collection and Traditional Human Analysis Method

2.4.1 Introduction

The objective of developing an automatic flaw detection system is to reduce the work load of human analysts and to improve the speed, accuracy and reliability of eddy current data analysis. The basic principles of the automatic flaw detection system should be based on the decision process of human analysts. This means we need to establish a system which utilizes machine intelligence principles to simulate the human decision making process. Therefore, good understanding of traditional human analysis procedures is fundamental for the development of the automatic flaw detection system.

The traditional human analysis method is based on the basic eddy current probe-flaw interaction phenomenon and the experience of the human inspectors. Although it is relatively easy to understand the basic relationship between flaw characteristics and the shape and orientation of the corresponding Lissajous pattern, real-world inspection data is difficult to analyze because noise and many unwanted signals cause significant distortion of the flaw signal in the inspection data. For such distorted and noisy inspection data, the experience of human inspectors is very critical for correct flaw detection and accurate flaw characterization. Generally, each set of inspection data is analyzed by two human analysts individually. The two analysts are named the primary and the secondary analysts. Both of the two analysts have the responsibility for reporting all indications of degradation or imperfection, and for reporting all information that describes the indications. If there is any disagreement between the primary and the secondary analysts, the conflict will be resolved by a third analyst. To ensure the consistency of data analysis result, the analysts follow a set of eddy current analysis guidelines that describe the analysis set-up procedure, data screening rules, and the reporting criteria. The analysis set-up procedures are used to establish a reference standard by using a calibration standard for compensation of variations in probe characteristics and instrument settings. The data screening rules provide instructions for defining the "calls" of defects and setting up the main analysis frequency. The reporting criteria outline the report responsibility of two analysts and also describe what should be emphasized in the report. Here we concentrate on the analysis set-up procedure and the data screening rules. The data screening rules represent a significant part of the knowledge of a human inspection expert.

To provide a better understanding on the data analysis method, we give a brief introduction of the data collection procedure.

2.4.2 Data collection

Eddy current inspection data is collected by professional data operators from the heat exchanger tubes of the steam generator in a nuclear power plant. An operator controls a robot to put an eddy current probe into one end of a heat exchanger tube and push it till it reaches the other end. Then the probe is pulled out with a constant speed and the impedance change is measured and recorded as a function of time. Before the tubing data inspection data is acquired, a calibration tube is first inspected to calibrate the probe and the inspection instruments. Due to variations in probe characteristics and instrument setting, the inspection data must be calibrated to get rid of those variations and to adjust the acquired data to a common magnitude and phase reference. The calibration tube has the same dimensions and material properties as the tube to be inspected. Artificial defects are machined into the calibration tube to establish a reference for later data analysis.

In conventional steam generator inspection, a bobbin coil is used which gives one-dimensional impedance change data. Four test frequencies are used in a typical industrial type inspection. In a modern eddy current data acquisition instrument, the probes are designed to allow multifrequency testing under both the absolute mode and the differential mode. This type of probe combines both the advantages of an absolute probe and that of an differential probe which allows the inspectors to detect both localized defects and gradual changing defects. Through the use of multi-frequency testing, the inspector can differentiate

various types of defects. For example, four test frequencies are used in the inspection process in most industrial inspections. A typical set of frequencies is 600 kHz, 400 kHz, 200 kHz, and 35 kHz. The 400 kHz test frequency is the main test frequency which is close to the optimal test frequency. The 600 kHz and 200 kHz are the reference test frequencies which have better sensitivities to the ID defects and the OD defects, respectively. The lowest test frequency 35 kHz has the largest penetration depth and the lowest resolution. It is used to provide a signal which does not contain much flaw information but has good sensitivity to permanent structures such as tube support plates. For each frequency, both the absolute signal and the differential signal are recorded. There are eight data channels for the four test frequencies and the test modes. The eight channel signals provide enough information for a human inspector to differentiate different types of flaws. However, circumferential cracks cannot easily be detected by a bobbin probe because these cracks are parallel to the eddy currents induced by the bobbin coil.

2.4.3 The traditional human analysis method

The human analysis procedure can be divided into two major processes. The first process is the initial set-up procedure and the other one is the data screening process. The analysis set-up procedure is very important because it establishes a consistent analysis standard and ensures that the results of the analysis are reliable. It is accomplished by using the calibration standard. Five major steps are required to be completed in the set-up process, which are (1) settings for rotation, (2) mixes, (3) normalization, (4) calibration curves, and (5) landmark tables. The operation procedure and the order of the processing sequence are

crucial for the correctness of the analysis, hence some important guidelines must be followed in the set-up procedure. Before the raw data are analyzed, the set-up steps from (1) to (4) must be finished and applied to the calibration standard for obtaining set-up parameters that will be applied to the raw data later. The principles and operation criteria for the above five steps are outlined and explained as the following:

(1) Setting for span and rotation

A 100% through-wall (TW) OD flaw signal is defined as a phase rotation reference. A human inspector adjusts the 100% TW flaw signal in the calibration standard to be 40 degrees on all eight original channels and the mix channels [6].

(2) Mixes

A 400/200 kHz differential mix is established as the TSP suppression mix. This mix signal is obtained by using the broached TSP in the calibration standard.

(3) Normalization

The voltages of all channels are normalized based on the magnitude of the 400kHz differential channel. The broached TSP in the calibration standard is set to a voltage level of four volts in the 400 kHz channel. After the normalization, we can measure the size of a flaw by using the voltage of the flaw signal.

(4) Calibration curves

A 3-point phase calibration curve is set for the 100%, 60%, and 20% TW holes in each channel. The purpose of the calibration curve is to estimate the flaw depth (%TW) from the phase of the flaw signal. If the phase angle of a possible flaw indication is known, we

can use the calibration curve to decide whether it is a true flaw or not and also to calculate the %TW.

(5) Landmark table

The landmark table is used to transform the relative time positions of indications to their physical locations in the heat exchanger tube. This is accomplished by using the fixed positions of TSPs as landmarks. If the pulling speed of the probe is constant and the locations of the TSPs are known, we can map the relative time position of an indication into a physical location. For example, suppose the relative time position of an indication is 15800, the 10th TSP's position is 15000 and 11th TSP's position is 16200. The distance between the 10th and 11th TSPs is 36.00". Therefore, the location of the indication is about 10th TSP +24.00".

The whole scenario of the analysis set-up procedure is addressed as following: The human inspector sets up the calibration standard. The 100% TW flaw signal is located and its phase angle is adjusted to be 40 degree in higher frequency channels (600, 400, and 200 kHz). The 400/200 kHz differential mix is established as the TSP suppression mix. Then the phase rotation process is repeated for the mix channel. The voltage of the broached TSP in the 400kHz channel is set to be four volts. For higher frequency channels and the mix channel, the calibration curves are established. At this point, the human inspector saves the parameters obtained from the above procedures into a set-up file. Then the raw data is loaded and is automatically calibrated by using the set-up file. The analysis set-up process is finished after the landmark table has been built.

The data screening process is followed after the set-up procedures. During this stage, a human analyst display the data after calibration using an x-y plot to display a small segment of the tubing inspection data. As the analyst scrolls through the data, he/she looks at the Lissajous pattern of the signal in the current sliding window and tries to find patterns that are indications of defect signals. Ideally, the Lissajous pattern of a localized defect obtained using a differential probe has a figure 8 shape (see Fig 2.4). The angle of this phase 8 pattern indicates the depth of the flaw. Of course, this figure 8 pattern is usually severely distorted in the presence of noise and corrupting signals. For these distorted signals, the quality of the data analysis is dependent on the experience of the human analyst. He/she must be able to distinguish true indications from false indications even if they have similar Lissajous patterns. He/she should also be able to estimate the flaw depth based on the distorted signal. An automatic flaw detection system should mimic the decision process of a human expert to improve data analysis quality.

CHAPTER 3. LITERATURE REVIEW

3.1 Introduction

Although eddy current testing has been applied to industrial practice for a relatively long time, theories and methodologies for processing and analyzing eddy current inspection data have not been well studied in the literature. This is mainly due to the complexity of modeling the underlying physical phenomenon of eddy current testing. Because eddy current testing is governed by a diffusion equation, analytical solutions of the forward problem are difficult to obtain, and numerical models must be used in most cases. The task of analyzing and characterizing eddy current signal can be considered as an inverse problem whose solution is critically dependent on the accurate and fast solutions of the eddy current forward problem. Because of the slow speed and inaccuracy of currently available eddy current forward models, in industrial practice eddy current data analysis is still mainly dependent on empirical methods. Also, real-world inspection data is usually distorted by noise and signals from insignificant structural changes of the tube which further complicates the analysis process. Therefore, signal processing techniques must also be used to enhance signals from flaws under interests and suppress noise and signals from unwanted effects.

Since conventional eddy current data analysis relies on well trained human analysts, it is time consuming and has high cost. An automatic flaw detection system is thus highly desirable to improve processing speed and to reduce the work load of human analysts. An automatic flaw detection system should be based on the following processing techniques:

1. Signal processing techniques to remove noise and unwanted signals and to enhance flaw signals. Typical noise and interference sources in eddy current tubing inspection include liftoff, electromagnetic noise, tube ID noise and denting, and quantization noise. To remove some of the above stated interference signals, we must combine the information in different frequency channels which is made available by multi-frequency testing techniques.
2. Feature Extraction techniques to represent the signal of a possible flaw indication into a number of features. These features capture most of the discriminatory information in the raw data while greatly reducing the amount of data needed to be processed in later steps.
3. Flaw classification techniques to differentiate types of defects and also to separate unwanted signals from defect-induced signals. The flaw classification step makes decision on flaw type based on the information represented by the features of a possible flaw indication.
4. Flaw characterization techniques to determine the sizes of flaws. In this step, the sizes (length, width, depth, etc.) of a flaw is estimated by using features or characteristics of the flaw signal. This is actually an eddy current inverse problem. Because of the complexity of analytically solving the inverse problem, in industry practice empirical methods based on calibration standards are usually used.

In current industrial practice, there are several signal processing techniques for eddy current data analysis. One of the most important techniques is the mixing process [7, 8] which utilizes the frequency dependence of eddy currents to enhance signals of interests and to suppress other signals. One of the typical applications of the mixing operation is to

suppress large signals from tube support plates which may otherwise severely distort signals from flaws near the tube support plates. Other signal processing techniques include bandpass filtering [9] and the so-called correlation filtering [9]. They are conventional general purpose signal processing techniques which have achieved limited success in the area of eddy current data analysis.

Feature extraction techniques in the literature can be classified into two major categories: nonparametric methods and parametric methods. Nonparametric feature extraction methods were proposed by Doctor et al. [10] and Mucciardi [11]. In this type of approach, a feature vector containing elements drawn from the time, frequency, and spatial domains. Examples of such elements include auto-correlation and cross-correlation terms, spectral components, and phase angles. The feature vector is then compressed by using only a subset containing the largest amount of discriminatory information. The Fourier descriptor method suggested by Udpa and Lord [1] involves the derivation of a parametric model of the eddy current defect signal. The Fourier descriptors give rotational, scaling and translational invariant representation of the shape of a Lissajous pattern. Therefore, they are insensitive to changes in test conditions and probe characteristics.

To determine whether a signal is from a flaw indication and to classify flaw types, signal classification techniques must be used. For eddy current data analysis, the flaw classification can be directly based on the impedance change data [12, 13], or it can be based on a set of carefully selected features [10, 11, 14, 15]. The method proposed by Mucciardi [12] involves the use of a matched filter. Match filters have impulse responses that are reflected, shifted, and possibly scaled versions of the signals to be matched. The frequency

domain equivalent of the matched filter - conjugate spectrum was also proposed by Stepinski [13]. Among the methods based on feature extraction, the techniques proposed by Doctors et al. [10] used the Fisher linear discriminant method for feature reduction. The method proposed by Mucciardi [11] is based on adaptive learning network. More recently, fuzzy logic [14] and neural networks [15] were also applied to the eddy current flaw classification problem.

Flaw characterization is closely related to flaw classification. In fact, some of the flaw classification techniques, such as fuzzy logic and neural networks, can be applied to flaw characterization as well [15]. However, because this inverse problem is highly ill-posed, in industrial practice empirical methods based on calibration standards are still widely used [9].

Up to this date, the only complete automatic flaw detection system that has been presented in the literature is the Dodger expert system [14]. This expert system, concentrated on the consistency of interpretation, is based on the following five functional components: operator interface, knowledge system, machine pattern recognition, reasoning with uncertainty, and automatic calibration. Although the Dodger expert system has achieved sufficient robustness as indicated by test results on data containing small variations, it results should still need to be overchecked by human operators in cases where the conclusions are in doubt.

In this chapter we briefly review the above discussed processing techniques for eddy current data analysis. The purpose of the discussion is to give a comprehensive background of the current state of the eddy current data analysis field. In Section 3.2, we discuss signal

processing techniques such as mixing, bandpass filtering and correlation filtering. In Section 3.3, we discuss both the parametric and nonparametric feature extraction methods. In Section 3.4, we review various flaw classification techniques. Finally in Section 3.5, we give a brief introduction to the Dodger expert system and discuss its major design concepts.

3.2 Signal Processing Techniques

3.2.1 Mixing

In [16], a theory on the mixing of multifrequency eddy current data in both the time domain and the frequency domain was presented. A fundamental assumption made in this theory is that eddy current signals at two frequencies are RST (rotation, scaling, translation) transformation of each other. For the tube support plate regions, the steps for suppressing the contribution due to the tube support plates are described as follows,

1. Let $\underline{S}_a$ and $\underline{S}_b$ be the support plate signals at frequencies f_a and f_b.
2. Let $\underline{S}_b = (T)\,\underline{S}_a$ where the transformation T is a function of

   S_x : scaling in x direction

   S_y : scaling in y direction

   t_x : translation in x direction

   t_y : translation in y direction

   ϕ : rotation about the origin

Estimate the transformation parameters using $\underline{S}_a$ and $\underline{S}_b$

3. Let $\underline{c}_a$ and $\underline{c}_b$ be the composite (support plate +defect) signals at frequencies f_a and f_b.

4. Then the defect signal is given by

$$\underline{d}_{f_b} = \underline{c}_{f_b} - T \cdot \underline{c}_{f_a} \tag{3.1}$$

The most important step of mixing is to find the transformation parameters using the measured signals of the tube support plate (or other signals to be suppressed) at the two frequencies. The transformation can be implemented in both time domain and the frequency domain.

3.2.1.1 Time domain implementation

In time domain, the basic transformation of rotation scaling and translation (RST) can be combined to yield a single transformation matrix.

$$T = \begin{bmatrix} S_x \cos\theta & S_y \sin\theta \\ -S_x \sin\theta & S_y \cos\theta \\ S_x\left(t_x \cos\theta - t_y \sin\theta\right) & S_y\left(t_x \sin\theta + t_y \cos\theta\right) \end{bmatrix} \tag{3.2}$$

Using the support plate signals $\underline{S}_a$ and $\underline{S}_b$, the transformation parameters are obtained by least squares estimation procedures, i.e. by minimizing the error function

$$E = \left\| \underline{S}_b - T \cdot \underline{S}_a \right\|^2 \tag{3.3}$$

with respect to the transformation parameters. This results in a set of five nonlinear equations to be solved simultaneously. The solution of this nonlinear system is very difficult. Usually numerical methods must be used to obtain an estimation of the solution.

3.2.1.2 Frequency domain implementation

A simpler way to obtain the transformation parameters is to use frequency domain representation. In the frequency domain, the transformation equations are decoupled in the parameters by using Fourier descriptors. Fourier descriptors are a class of translational, rotational and scaling invariant shape descriptors. Since the impedance plane trajectories obtained from eddy current probes are closed curves, a point (x, y) on the signal can be represented as a function of the arc length l (from an arbitrary starting point), in terms of the complex contour function

$$u(l) = x(l) + jy(l), \qquad j = \sqrt{-1} \tag{3.4}$$

then

$$u(l + nL) = u(l), \qquad n = \ldots -1,0,1,2\ldots \tag{3.5}$$

where L is the total length of the curve, the periodic function $u(l)$ can be expanded in a Fourier series

$$u(l) = \sum_{n=-\infty}^{\infty} c_n \exp\left[\frac{j2\pi nl}{L}\right] \tag{3.6}$$

where

$$c_n = \frac{1}{L}\int_0^L u(l)\exp\left(\frac{-j2\pi nl}{L}\right)dl\,. \tag{3.7}$$

The linearity property of the Fourier series expansion yield a simple relation between the Fourier series coefficients of two curves that are transformed versions of each other. Let γ be a simply closed curve with Fourier series coefficients $(\underline{c}_n)$. Let γ' be obtained by rotation (θ), scaling (s) and translation (p) of the curve γ. Let $\left(\underline{c}_n'\right)$ be the Fourier series

coefficients of γ'. Using properties of Fourier transform, the relation between $(\underline{c}_n)$ and $(\underline{c}_n')$ is given by

$$c_0' = c_0 + p \tag{3.8}$$

$$c_n' = se^{j\phi}c_n \quad n = 1,2,\ldots \tag{3.9}$$

The transformation parameters s, ϕ, and p for the multifrequency algorithm are obtained by considering just one of the Fourier series coefficients of the two support plate signals at frequencies f_a and f_b.

3.2.2 Bandpass filtering

Bandpass filtering is a traditional signal processing technique used to remove both the low frequency and high frequency components in a signal. In eddy current data analysis, bandpass filtering has been widely used because it is effective in removing several types of noise and unwanted signals. Low frequency noise in eddy current inspection data include signals resulted from changes in liftoff, changes in tube diameter and vibration of the probe. High frequency noise in eddy current inspection data include quantization noise, electromagnetic noise and thermal noise. Although eddy current flaw signals are localized in time domain, their major frequency components are not overlapped with the above stated low frequency and high frequency noises. Therefore, by using a bandpass filter with proper low cutoff frequency and high cutoff frequency, it is possible to significantly suppress both the low frequency noises and the high frequency noises while keeping the flaw signals almost intact. The low and high cutoff frequencies determine the performance of the bandpass

filtering. They are dependent on the sampling rate, the probe pulling speed, and the signal-to-noise ratio. In industry practice the selection of the cutoff frequencies is usually done by trial and error.

To reduce computation time, the bandpass filter is usually implemented in time domain by using finite impulse response (FIR) filters. Once the sampling rate, the low and high cutoff frequencies, the pass band ripple, and the stopband suppression ratio are specified, a FIR filter of certain order can be designed to meet the requirements. Details on the design of FIR filters can be found in [17].

3.2.3 Correlation filtering

Another conventional signal processing technique that has been widely used in eddy current data analysis is so-called correlation filter. Although named as correlation filter, this type of filters actually compute the first-order or the second-order difference of the original data. The correlation filters are very effective in removing liftoff signal since they only output local changes in the data. After correlation filtering, flaw signals may exhibit certain features which distinguish them from noise and unwanted signals. For instance, a crack signal obtained using a differential probe has four closely spaced peaks after correlation filtering. By examining certain features in the correlation filtering output, a human operator can detect flaw signals with higher probability.

3.3 Feature Extraction

3.3.1 Overview

To classify and characterize a defect signal, the first thing we need to do is to extract a set of meaningful features from the raw impedance change data. The purpose of feature extraction is twofold: (1) by extracting and using only the significant features in flaw classification, we can greatly reduce the amount of data used in the decision process and thus reduce the amount of computation; (2) when flaw signals are represented by features, the difference between different types of flaws becomes more distinguishable and decisions on flaw type can be easily made. For the purpose of flaw characterization, nonparametric classification methods based on feature extraction techniques were proposed by Doctor et al. The Fourier descriptor method suggested by Udpa and Lord introduced a parametric model of the eddy current defect signal.

3.3.2 Nonparametric approach

In [10], three groups of features were studied: shape parameters, autocorrelation (time series) parameters, and frequency-domain parameters. The purpose of the shape features is to describe the Lissajous pattern in detail. There are a total of 19 features belong to the shape feature group. These features include power in horizontal channel, power in vertical channel, eigenvalues of the power matrix, and the area of Lissajous pattern, among many others.

The second group of features is based on the autocorrelation function. The autocorrelation function of a zero mean stationary complex random process is defined as

$$C_k = \frac{\sum_{l=1}^{N} v_k v_{k+l}^*}{\sum_{l=1}^{N} |v_l|^2}, \quad k = 0, 1, ..., N\text{-}1 \tag{3.10}$$

where k is the time delay, v_l is the random process, and N is the data length. The values of the autocorrelation function at certain time delays were used as features in the second group.

Features from the frequency domain were obtained using the fast Fourier transform (FFT) algorithm. Five frequency-domain features were used: the maximum frequency response, the frequency of the maximum response, and ratios of the first three moments of the frequency distribution. The moments in the frequency domain are defined by the following formulas

$$M_0 = \int_0^\infty p(\omega) d\omega, \tag{3.11}$$

$$M_1 = \int_0^\infty \omega p(\omega) d\omega, \tag{3.12}$$

$$M_2 = \int_0^\infty \omega^2 p(\omega) d\omega, \tag{3.13}$$

where $p(w)$ is the power spectral density.

The complete set of features were then reduced to a smaller set of features containing the largest amount of discriminatory information. The Fisher linear discriminant method for feature reduction was used for this purpose. The feature reduction process also revealed that the set of optimal features for flaw type classification are significantly different from that for flaw sizing.

3.3.3 Parametric approach: Fourier descriptors

In [6], an interesting and very useful Fourier descriptor method is described in detail. This method provides not only the features for eddy current defect classification but also other applications on the archiving, resampling, and filtering. Most difficulties on the eddy current data analysis arises from the complex nature of the eddy current technique itself. Variations of pulling speed, lift-off and changes of geometry are among those factors which always increase the complexity in dealing with signal analysis. The Fourier descriptors can overcome those above problems due to the insensitivity of the descriptors to zero, gain drift and variation in probe speed. These properties bring the Fourier descriptors to be suitable features for representing the shape of impedance plane trajectories of indications.

The concept of the Fourier descriptors is addressed as following: A contour function representing a closed curve is a complex periodic function which can be expended in a Fourier series. If the curve is smooth and it is a discrete function, we can approximate the curve by a m sides polygon with vertices at v_0, v_1, ..., v_{m-1}, as shown in Fig. 3.1.

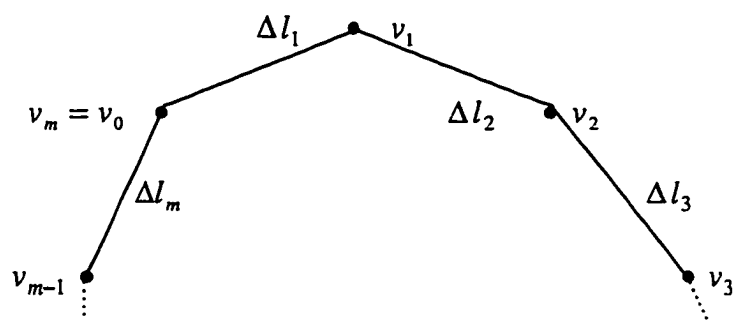

Figure 3.1 A polygon of m sides approximating the curve.

Then the expression of the Fourier coefficients is

$$c_n = \frac{L}{4\pi^2 n^2} \sum_{k=1}^{m} (b_{k-1} - b_k) \exp(\frac{j2\pi n l_k}{L}), \tag{3.14}$$

where

$$l_k = \sum_{i=1}^{k} |v_i - v_{i-1}|, \quad k > 0 \text{ and } l_0 = 0 \tag{3.15}$$

and

$$b_k = \frac{v_{k+1} - v_k}{|v_{k+1} - v_k|}. \tag{3.16}$$

However, the above complex coefficients c_n is dependent on the rotation, translation, and scaling transformation of curve. In addition, the expression is sensitive to the choice of the starting point.

In order to obtain descriptors that are without the variances caused by zero and gain drift in the eddy current instrument, an functions of descriptors are derived so that the coefficients are insensitive to the transformation of the curve and starting points of the curve. The functions of descriptors are

$$b_n = \frac{c_{1+n} c_{1-n}}{c_1^2}, \quad n \neq 1. \tag{3.17}$$

The functions of descriptors are then incorporated into a feature vector and pattern recognition algorithms are used for signal classification. An approach based on K-Means clustering algorithm is applied by Udpa and Lord. Another approach based on neural networks was proposed by L. Udpa and S. S. Udpa[15]. It involves the use of neural

networks for interpreting eddy current signals. The network was implemented by using a multilayer perceptron with backpropagation algorithm.

3.4 Flaw Classification

3.4.1 Matched filter

A straightforward way to do flaw classification is to use matched filters [12]. Matched filters have been widely used in radar systems for the detection of echo signals. The concept of matched filter is very simple: consider a complex signal $z(t)$, $t \in [0, T]$, the filter that gives the maximum output at time instant T is given by

$$h(t) = z^*(T-t),\ t \in [0, T]. \tag{3.18}$$

It is easy to show that the output of the matched filter at time instant T is equal to the output of a correlator

$$x * h(T) = \int_0^T x(t)h^*(T-t)dt. \tag{3.19}$$

By using a number of matched filters (each of them is based on a certain type of flaw signal), it is possible to decide the flaw type of the signal for a possible flaw indication. The outputs of the matched filters are compared and the flaw type is determined by the matched filter with the largest output. If all the matched filters give a output that is below a certain threshold value, the signal is considered not from a significant flaw indication.

3.4.2 Conjugate spectrum filter

The frequency domain equivalent of the discussed matched filter is the so-called conjugate spectrum filter [13]. Given the spectrum $Z(\omega)$ of the complex signal $z(t)$, the spectrum of the conjugate spectrum filter is given by

$$H(\omega) = Z^*(-\omega), \tag{3.20}$$

which is the frequency domain equivalent of equation (3.18). Depending on the application, the CSFs can be designed both for enhancement and suppression of the selected ET patterns. Two types of conjugate spectrum filters can be designed in such cases: the phase-matched and the orthogonal filters. The phase-matched filter suppresses all the ET patterns with the phase angle different from that of the prototype. The orthogonal filter suppresses the prototype and all the signals with the similar phase angles and the shapes.

3.4.3 Adaptive learning networks

Nonparametric methods of defect characterization rely on selecting a set of features that give the largest amount of discriminatory information. Examples of such methods include the well-known adaptive learning network and the fisher linear discriminant method.

First proposed by Mucciardi for characterizing defects [11], the adaptive learning network attempts to fit a nonlinear polynomial model between a defect characteristic y of interest and a set $(x_1, x_2, \cdots, x_n)$ of features, i.e.,

$$y = f(x_1, x_2, \cdots, x_n). \tag{3.21}$$

The adaptive learning network accomplishes this using a layered network built from quadratic elements. In the training phase, the available data are partitioned into two groups

called the training set and the testing set. The parameters of the network are determined by using the training set. After the training process, a nonlinear relationship between the input features to the network and the output flaw characteristic (defect parameter) is established.

3.4.4 Neural networks

Eddy current flaw classification using artificial neural networks was proposed by L. Udpa and S. S. Udpa [15]. In this work, the features for flaw classification are Fourier descriptors. A two-layered perceptron was used and the training algorithm was the back-propagation algorithm. Based on differentiable nonlinear node transfer function, a multilayer perceptron has the capability of approximating complex nonlinear decision surface. This learning property makes it ideal for the eddy current flaw classification problem. In the test, the training data set contained 40 flaw signals from 4 different flaw classes. The four classes were identified using only two output nodes, thereby minimizing the weights to be estimated. The inputs to the network were eight Fourier descriptors. Test results on this neural network classifier are significantly better than that of a partially trained K-means clustering algorithm. Neural nets also offer the advantage of being able to flag ambiguous data rather than misclassify them.

3.5 Expert System for Eddy Current Evaluation

3.5.1 Overview

Eddy current testing is a widely used nondestructive testing method, particularly for inspecting tubing material. ET's speed ,sensitivity, and ease of use make it an ideal choice. For all its benefits, however, ET can also be among the most frustrating of NDT methods. Although the technique itself is simple and reliable, inspection data and results frequently are contradictory and misleading due to the many material variables that influence the ET measurements.

Most difficulties with ET arise from data analysis. The conventional eddy current data analysis are done by human analysts. Human nature itself will cause some variance in analysis. More important, the expertise to analyze data most proficiently is very often distributed among several individuals. To overcome these obstacles, an eddy current expert system had been developed by Levy et al [14]. The expert system, called Dodger, was developed to satisfy the following functional requirements. They are consistency of interpretation, comprehensive knowledge base, flexibility for growth, decreased reliance on an operator, and quantification of uncertainty. The design of the expert system is based on the premise that the best evaluation results from cooperation of a team of analysts with diverse knowledge.

3.5.2 The Dodger expert system

The Dodger expert system is composed of the following major functional components: operator interface, knowledge system (rule base plus knowledge base), machine

pattern recognition, reasoning with uncertainty, and automatic calibration. Each of these components is briefly described next.

Operator Interface The operator interface presents a graphical display of ET data, including time-based strip charts that show horizontal and vertical components of an ET signal separately, and Lissajous plots.

Knowledge System The knowledge system is composed of a knowledge base and a rule base. The knowledge base consists of a collection of a facts and observations derived from the data being analyzed. The rule base consists of a set of rules that embody the interpretation guidelines and practical experience of several expert ET analysts.

Machine Pattern Recognition The machine pattern recognition component emulates the visual skills of an analyst. It analyzes ET signals in the form of impedance plots, and extracts significant geometric characteristics such as phase and amplitude.

Reasoning with Uncertainty The reasoning with uncertainty system gathers parameters representing phase and amplitude measurements from ET signals at several frequencies and combines them in order to develop a strategy for the expert system to follow in pursuing a diagnosis. Fuzzy set theory is used to associate the parameters with one or more possible material conditions.

Automatic Calibration The automatic calibration system processes ET data from ASME standard tubes to calibrate the operation of the rest of the system.

CHAPTER 4. SIGNAL PREPROCESSING (STAGE #1 OF SYSTEM)

The objective of this research is to determine the feasibility of automatically screening eddy current bobbin coil data from sequential inspections of steam generator tubes in order to determine whether or not there are significant differences in two data sequences. To achieve this objective, the two data sets must be aligned and calibrated so as to eliminate the differences due to changes in probe condition and instrument setting. The signal preprocessing step, which is the first stage of the eddy current automatic flaw detection system, was developed for this purpose. It consists of a set-up procedure, a data alignment step and a background removal step. The set-up procedure uses a calibration standard to adjust the test data to a common reference standard. Because there could be significant differences in the pulling speed for the two data sets, the two data sets must be aligned in time (position). We developed a data alignment method based on the locations of the tube support plates. The background removal processing reduces slow varying signals due to liftoff changes and ID variations so that the flaw signals are enhanced.

4.1 Overview of Automatic Flaw Detection System

The automatic flaw detection system is accomplished by three major components - signal preprocessing, wavelet identification of flaw indications, and defect evaluation. In eddy current data analysis, the data preprocessing is a very important procedure for

overcoming the variations between "identical" probes and instruments as well as the variability in the material properties. Three steps are applied to preprocess the raw data sets. They are initial set-up procedure, data alignment, and background removal. The initial set-up procedure is to make sure that all data have the same signal analysis standard and interpretation by utilizing a calibration standard tube to establish the reference standard. For providing a very consistent comparison basis, alignment of data sequences is required in order to get rid of variation in pull speeds. This alignment algorithm is achieved by using characteristic features of tube support plates (TSP). The background removal is utilized to remove variations due to lift-off and other geometrical effects. Once the data sets are preprocessed, we apply a wavelet flaw identification technique to process the data and then characterize the noise and flaw signals.

The wavelet flaw identification technique was used to reduce noise and identify possible flaw indications. Due to multi-resolution and unique time-frequency localization properties of the wavelet transform, the flaw signals have specific characteristics in the wavelet domain. To fully utilize those characteristics to distinguished flaw indications from noise, a mixture of statistical and wavelet techniques was developed. Such a wavelet analysis method was accomplished by four main algorithms. They are the fast wavelet algorithm, extrema algorithm, denoising procedure, and transient detection algorithm. Through the wavelet analysis method, the locations of the possible flaw indications are identified. After this stage, an algorithm to make the final decision on all possible flaw indications is needed.

To further evaluate the possibilities of flaw indications, we invoked fuzzy logic to discriminate between true positives and false positives. A template matching technique and a

fuzzy inference system are utilized to classify the possible flaws. The template matching technique uses the signals of the artificial flaws as templates to match with possible flaw signals and execute a normalized complex crosscorrelation. Through this process, we obtain both phase and shape information which are placed into a fuzzy inference system for final decision making. Also, an estimation of the size (%TW) of the flaw is provided too.

4.2 Set-up Procedure

The initial set-up using a calibration standard is an important step before processing the raw data. It is used to overcome the variations between "identical" probes and instruments as well as the test material which affect probe impedance. This procedure also ensures that every set of test data has the same signal analysis standard and interpretation. The calibration standard is a tube of the same material and geometry as that of the test material, and also has the same electrical and magnetic properties. Many artificial defects are machined in the calibration standard tube to establish a reference for later data analysis.

There are three main steps in the set-up procedure. The first step sets rotation angles of the phase for the differential channels that will be used in later processing. The phase adjustment is based on a reference standard which sets the phase angle of a 100%TW OD flaw to be 40 degrees. The second step establishes the mixes by using the broached TSP in the calibration standard. The mixing process is used to suppress the unwanted tube support plate's signal so that the flaw signal masked by it can be enhanced and detected. The third step builds up the calibration curve for the differential channels and the mix channel. The

calibration curve is very important for determining the flaw type and estimating the size of flaw. A semi-automatic set-up procedure was developed to complete these three steps.

4.2.1 Phase rotation

The phase rotation step ensures that all the raw data have the same phase reference standard so that the phase analysis of all the data set is consistent. To provide the same phase analysis standard, a 100%TW OD flaw is used as a reference and the phase angle of this flaw is defined to be 40 degrees. We first calculate the original phase of the 100%TW OD flaw, then the phase adjustment can be achieved by subtracting the original phase from 40. Finally, phase adjustment is applied to both the data set and the calibration data after background removal. The implementation of the phase rotation setting is described as follows:

(1) Input the start point and end point of a window which contains the 100% TW OD flaw.

(2) Remove the DC mean which is the average of the data values in the window.

(3) Find the positions of the local maximum and the local minimum in the window.

(4) Calculate the phase angle between those two extrema points.

(5) Compute the phase difference between 40 degrees and the calculated phase angle.

(6) Record the phase adjustment.

(7) Repeat the steps (2) to (7) for all high frequency differential channels 600 kHz, 400 kHz, 200 kHz, and the mix channel.

Figure 4.1 and 4.2 illustrate the phase rotation process of several OD flaws before and after rotation setting. In Figure 4.2, we can see that the phase of 100%TW OD flaw is set to be 40 degrees.

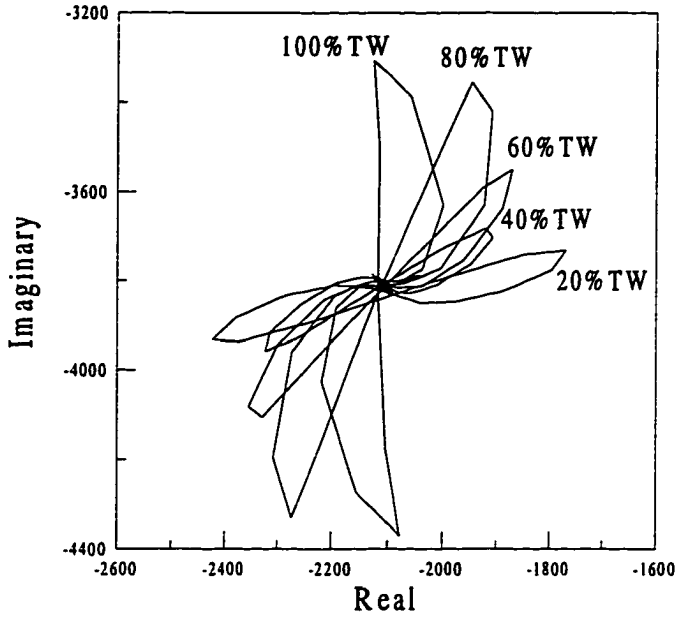

Figure 4.1 The Lissajous pattern of 100%TW, 80%TW, 60%TW, 40%TW, and 20%TW OD flaws before calibration.

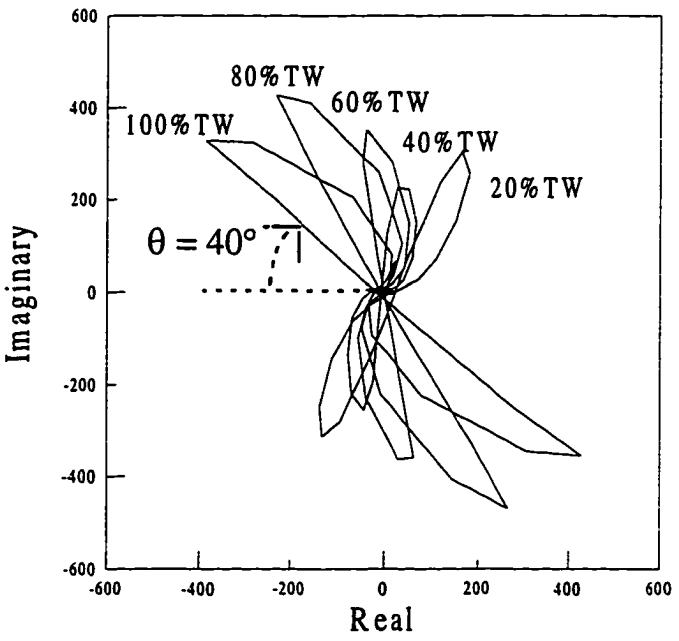

Figure 4.2 The Lissajous pattern of 100%TW, 80%TW, 60%TW, 40%TW, and 20%TW OD flaws after calibration.

4.2.2 Mixing

The concept of mixing is quite simple but the results of most currently available mixing algorithms are far from ideal. At this time, there is still no industrial standard mixing algorithm. Most companies use their own proprietary mixing algorithms. The mixing algorithm is very important because a large number of flaws occur near or within the tube support plate area and their signals are distorted by the TSPs. A successful mixing algorithm must be able to significantly suppress the unwanted tube support plate signals so that clean flaw signals can be obtained. To optimize a mixing algorithm, it takes many experiments to determine appropriate parameters for the algorithm. We expanded tremendous effort on evaluating various mixing algorithms in an attempt to achieve optimal results. Finally, we came up with an algorithm which gives satisfactory results. The mixing algorithm is described in the following paragraphs.

Mixing is a technique used to suppress unwanted signals in multiple frequency measurement data. It is based on the assumption that the signals from different channels can be represented by different linear combinations of several test variables. Through rotation and scaling, and subtraction of signals from different channels, we may obtain the wanted test variable while suppressing unwanted test variables. In its hardware implementation, the optimal rotation and scaling factors are reached by visual inspection of the residue signal. In the software implementation, it is usually assumed that the unwanted signal is much larger than the wanted signal, and thus the aim is to minimize the residue signal in the least-squares sense. This is actually a kind of adaptive filtering.

Suppose the signal at the higher frequency is the linear combination of the flaw signal and the unwanted signal, while the signal at the lower frequency is the unwanted signal only. The unwanted signal in the higher frequency is represented as scaled and rotated version of the signal in the lower frequency. Let $S_1(n)$ be the signal from the higher frequency, and $S_2(n)$ be the signal of the lower frequency. Reducing the scaling and rotation to a simple parameter, the enhanced flaw signal $S_3(\mathrm{n})$ can be represented as

$$S_3(n) = S_1(n) - D \cdot S_2(n), \tag{4.1}$$

where the complex mixing factor D can be derived by using the least mean-square method. Let

$$\varepsilon = \sum_n \left| S_1(n) - D \cdot S_2(n) \right|^2 \text{ and } \frac{\partial \varepsilon}{\partial D} = 0.$$

Carrying out the differentiation, we get

$$\frac{\partial \varepsilon}{\partial D} = 2 \cdot (-S_2^*(n)) \cdot \sum_n (S_1(n) - D \cdot S_2(n))$$

$$= 2 \cdot (\sum_n S_1(n) \cdot S_2^*(n) - D \cdot S_2(n) \cdot S_2^*(n)) = 0$$

The solution of the above equation gives

$$D = \frac{\sum_n S_1(n) \cdot S_2^*(n)}{\sum_n \left| S_2(n) \right|^2}. \tag{4.2}$$

Figures 4.3 to 4.5 illustrate the effect of mixing. Figure 4.3 shows the mixing results for tube support plate suppression using the broached TSP in the calibration standard. This data contains no flaw. Figure 4.4 displays the signal from OD flaws on the calibration standard tube in the 400 kHz channel and the mixed channel. We can see that the flaws'

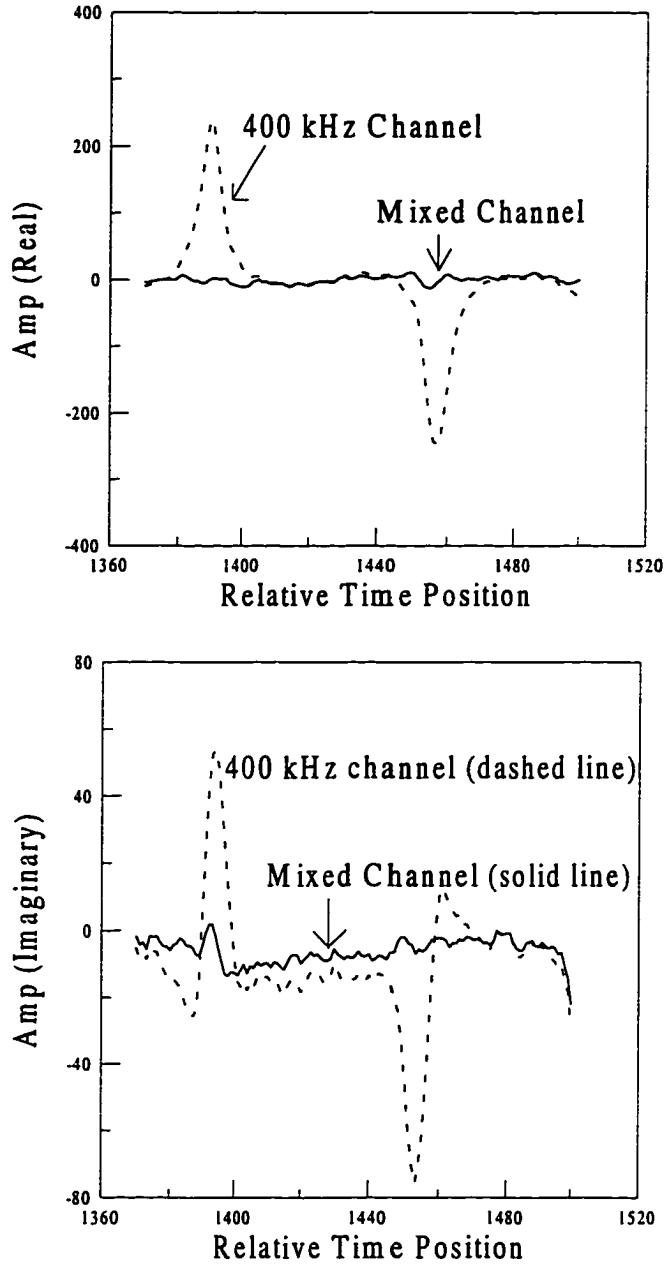

Figure 4.3 The signal from the broached TSP on the calibration tube in the 400 kHz channel and the mix channel. Top plot shows the real part and the bottom plot shows the imaginary part.

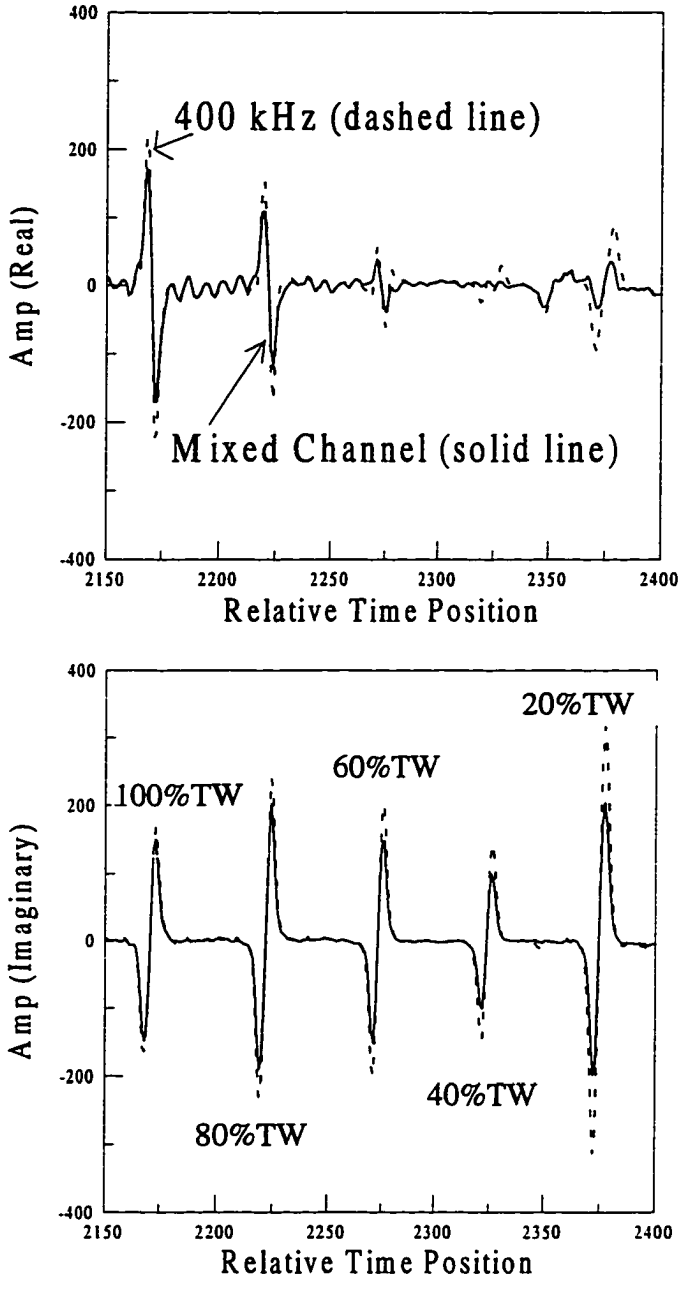

Figure 4.4 Signals of OD flaws on the calibration tube in the 400 kHz channel and the mix channel. The top picture is the real part and the bottom picture is the imaginary part.

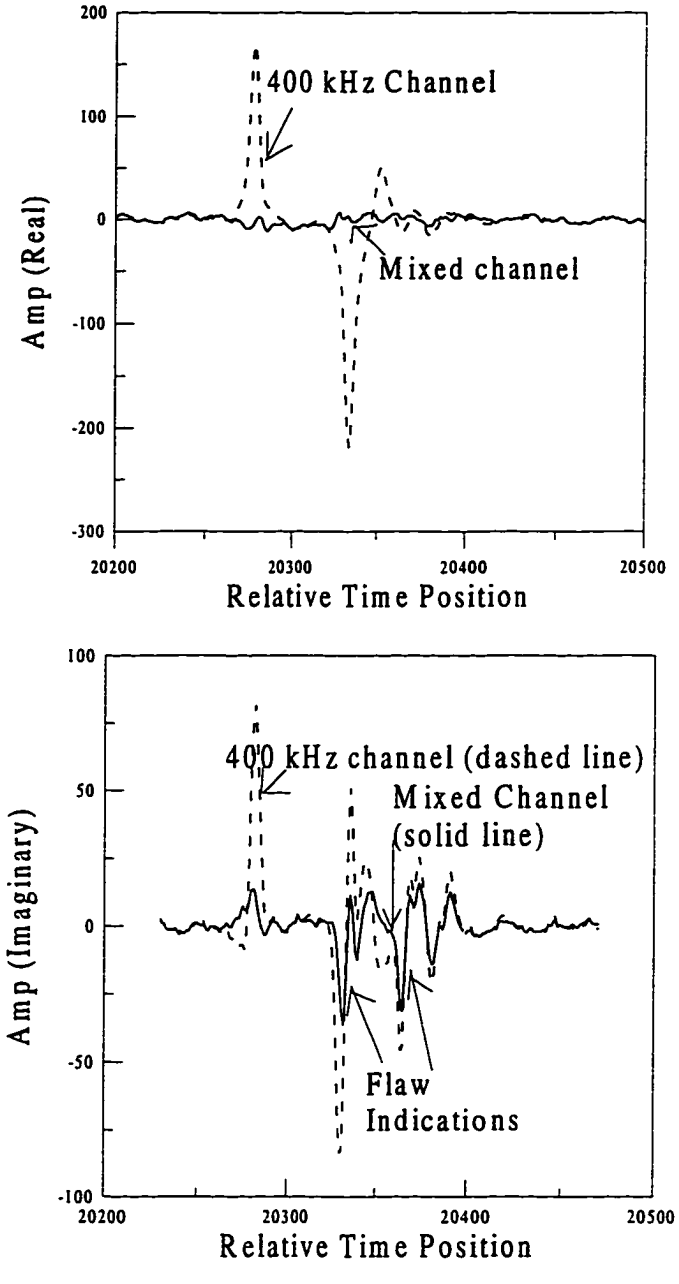

Figure 4.5 Example of the mixing process for suppressing TSP signals. The top plot is the real part and the bottom plot is the imaginary part. A 400/200 kHz mix was used. There is one flaw in the TSP region.

shapes are still preserved after the mixing process. Figure 4.5 illustrates the mixing results for real flaws on the TSP region. It is obvious that the unwanted TSP signal is suppressed and the flaw signals are enhanced.

4.2.3 Calibration curve

Building the calibration curve is an important step of the set-up procedure. In eddy current signal analysis, the calibration curve is a mapping function which maps the phase of a flaw indication to the depth of the flaw. Also it provides a criterion for determining whether an indication is a flaw indication or not. An indication is said to be a flaw indication if its phase angle falls in the calibration curve and its lissajous pattern satisfies certain criteria. A calibration curve is used for each of the basic frequencies and the mix channel. An example of calibration curve is shown in Fig. 4.6. Basically, the calibration curve can be divided into two regions according to the flaw type. In the first region, the phase angle is between 0 to 40 degrees, and the flaw type for this region is an inside diameter (ID) flaw. The calibration curve in this region is a straight line which is drawn from the point with 0 degree and 0%TW to the point with 40 degrees and 100%TW. For the second region, we use the phase of the 20%TW, 60%TW, and 100%TW OD flaws to build a second order polynomial calibration curve. The type of flaw in the second region is an outside diameter (OD) flaw. The second order polynomial calibration curve is built as follows: After the phase adjustment on the calibration data has been done by the phase rotation procedure, we locate the 20%TW and 60%TW OD flaw signals and obtain their phase angles. As we know, the phase angle of the

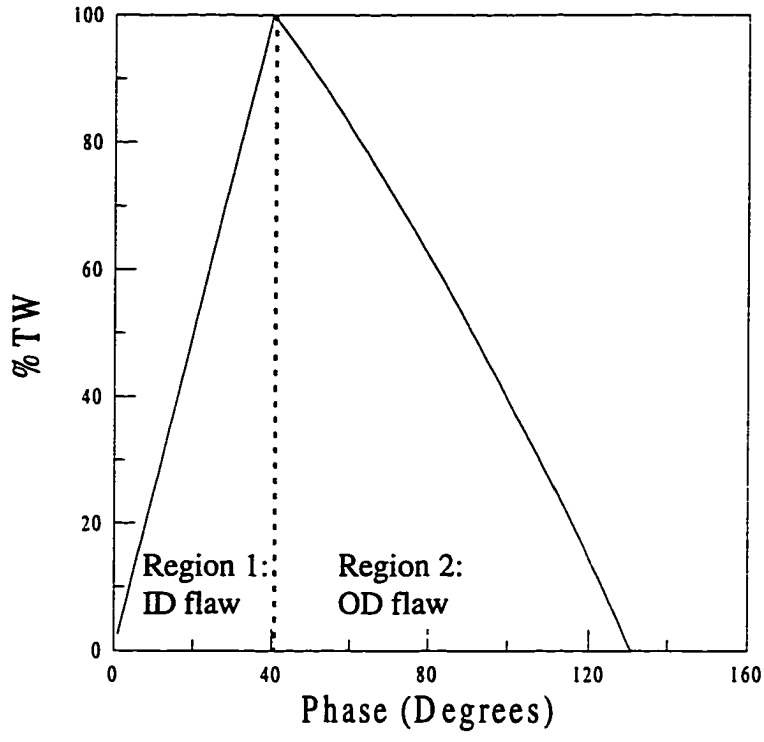

Figure 4.6 A calibration curve for the 400 kHz channel.

100%TW OD flaw is 40 degrees by definition. Since we know the phase angles of 100%TW, 60%TW and 20%TW OD flaws, a second order polynomial can be determined by using this three data points. The general form of a second order polynomial is given by

$$y = ax^2 + bx + c. \tag{4.3}$$

where y is the %TW and x is the phase angle. We substitute the three %TWs and their corresponding phase angles into above equation so that the coefficients of the polynomial can be solved. In addition to the three points determining the calibration curve, we can also use five data points (20%TW, 40%TW, 60%TW, 80%TW, and 100%TW) to fit a second order polynomial using a least-square method. However, the difference between a calibration curve fitted by three points method and a calibration curve fitted by five points method is very

small. An example of calibration curve fitting using three points method and five points method will be demonstrated below to show the difference between them. In general, the industries use three points method for its ease of calculation.

Table 4.1 shows the %TW and phase angles of OD flaws used for the calibration curve fitting. For the three points method, we use 20%TW, 60%TW, and 100%TW three data points to solve the coefficients of second order polynomial. The solved coefficients are shown on table 4.2 and its corresponding calibration curve is plotted as Fig. 4.7 (a). For the five points method, we use 20%TW, 40%TW, 60%TW, 80%TW, and 100%TW five data points to fit the second order polynomial using the least-square method. The calculated coefficients of the calibration curve are displayed on table 4.2. We plot the calibration curve as Fig. 4.7 (b). The difference $\Delta\varepsilon$ between the three point fitted calibration curve and five point fitted calibration curve is shown as Fig. 4.7 (c). We see that the maximum $\Delta\varepsilon$ is -0.6016%TW at phase angle 93° with 47.5047 %TW at three points method and 46.9031%TW at five points method. Obviously, the difference between two methods is small and acceptable. So we use the three points method to obtain the calibration curve.

Table 4.1 The data values for fitting calibration curve.

	100%TW	80%TW	60%TW	40%TW	20%TW
Phase (degrees)	40	62	82	99	115

Table 4.2 The coefficients of second order polynomial.

Method	Coefficients		
	a	b	c
Three points	-0.0035	-0.5299	126.7359
Five points	-0.0033	-0.5602	127.5434

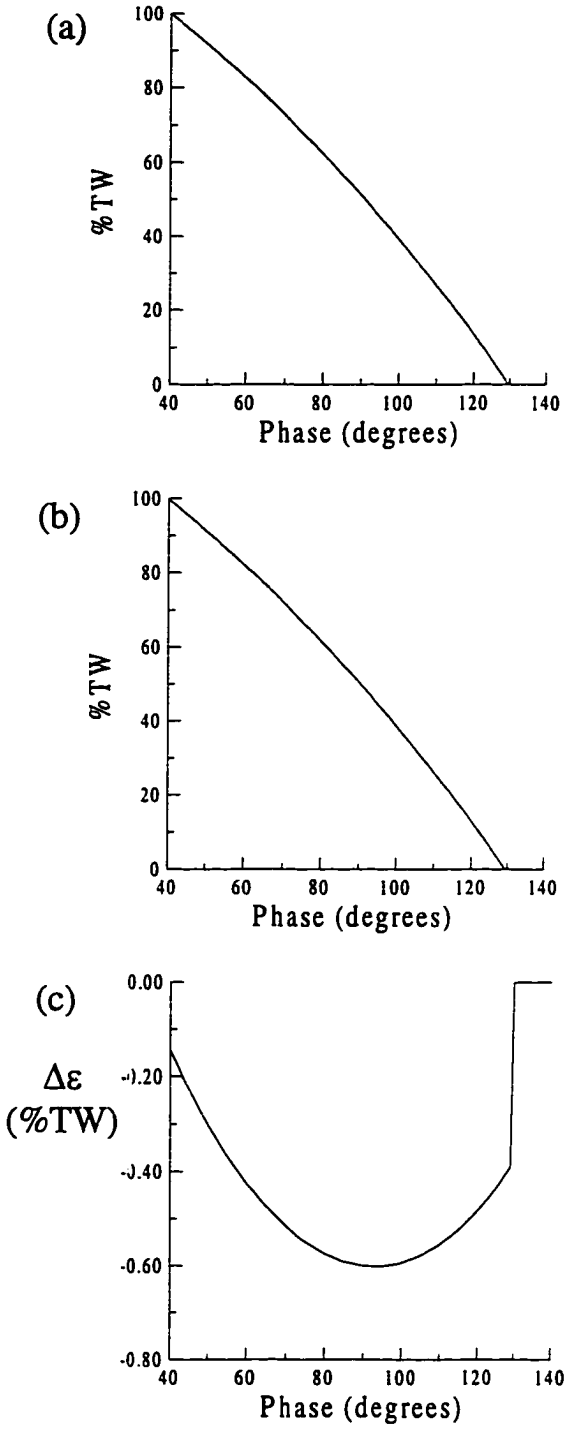

Figure 4.7 An example of calibration curve fitting using (a) three points method and (b) five points method. The difference Δε between (a) and (b) is shown in (c).

4.3 Automatic Data Alignment: Tube Support Plate Detection

After the set-up procedure, we apply the data alignment process to align the two data sets in time position. Comparison of two data sets of the same generator tube requires that one data set be calibrated against the other. Variations in pulling speeds change the relationship between sampling time and the corresponding location of the probe in the tube. To accomplish automatic alignment of two data sequences, the data must contain some type of reference information. In our work we used the signals from tube support plates (TSPs) as the reference. TSPs are used to support the heat exchanger tubes and to secure them in position. Since TSPs have fixed physical locations and they create strong signals, with the prior knowledge of the tube dimension and support plate width, the time position relationship between the two data sets can be compared at each support plate region by using the location (times) of a TSP's two peak signals. Then we can align the two data sets and establish the same time position correspondence for the two data sets.

The design of an automatic data alignment scheme is based on fundamental characteristics of TSP signals, such as amplitude, phase and time width. A TSP signal from a differential probe contains two peaks which have a phase difference of about π radians. The method we have developed for automatically locating the TSPs searches for a peak signal in the data sequence and then searches for a second peak near the first peak. When they are located we apply two criteria to check whether they correspond to a TSP. The first criterion is that the phase difference of the two peaks must be within some range. The second criterion is that the amplitudes of the two peaks must agree within a factor of about three. After the first TSP has been located, the search process is repeated for the next TSP, and so

on. The algorithm for TSP detection is applied on the 35kHz channel and is adjustable according to the tube dimension and the design of the steam generators. For a straight tube steam generator with fifteen tube support plates, the tube support plate detection algorithm consists of eight steps:

(1) Input the file names for year 1 and year 2 data sets. Duplicate the data sets and apply the TSP detection algorithm on the duplicated data sets only. Initiate the count of TSP to be zero.

(2) Find the null offset by calculating the mean of the data sets after excluding entry and exit data points. The excluded region contains about 10000 data points. The mean is then subtracted from each data point in the original data.

(3) Find the peak with the largest magnitude in the whole data set.

(4) Search the adjacent region of the peak excluding intermediate adjacent data points(The search window ranges from 30 data points to 100 data points away from the peak on both sides) and find the location with the largest magnitude in this window. The search region can be adjusted according to the plate width, sampling rate and the pulling speed of the probe.

(5) Check the magnitude ratio and phase angle difference between these two peaks. Two criteria were established for a TSP signal. The first one is that the phase angle difference θ must satisfy $|\theta - \pi| \leq \frac{\pi}{3}$ and the second one is that the magnitude ratio must be less or equal to 3, where magnitude ratio = larger magnitude/smaller magnitude.

(6) If the candidate peaks represent a TSP signal, we mark the positions of these two peaks and set the data value in the adjacent area of those peaks to be zero. The count for TSP

is incremented by 1. If TSP signal criteria are not met, set the data values in the adjacent area of the first peak to be zero (this is used to avoid deadlock). The count is unchanged.

(7) Repeat steps (5) to (8) till the count reaches 15.

(8) Sort the peak positions and output the sorted peak locations.

Once the TSPs are located on those two data sets, we start to align one data set to the other. The data alignment is done by using a linear interpolation method. Assume the pulling speed of the probe is almost constant between two adjacent tube support plates so that the data between the two TSP regions can be considered as uniformly sampled. However, due to variations in pulling speed for the two data set, the acquired data for the same tube obtained at different inspection time could be different. Therefore, there exists a piecewise linear mapping between the two data sets of the same tube obtained at different times. Based on this relationship, we have developed the following data alignment algorithm:

Assume that the data sequence of year 1 is $x(n)$ and the data sequence of year 2 is $s(j)$. Suppose that two adjacent TSP's peaks in the year 1 data set are $x(n1)$ and $x(n2)$ with corresponding peaks $s(j1)$ and $s(j2)$ in the year 2 data set. For a data point $\{x(n) | n1 < n < n2\}$, the aligned data point $s'(n)$ is given by

$$s'(n) = (l-m) \times s(m+1) + (1+m-l) \times s(m), \qquad l \in R,\ m \in Z \tag{4.4}$$

where $l = (j2 - j1) \cdot \dfrac{(n-n1)}{(n2-n1)}$, and m is the truncation of l. We also let $s'(n1) = s(j1)$ and $s'(n2) = s(j2)$. By using the same procedure on all the TSPs' peaks, the aligned data sequence is obtained.

Figure 4.7 and figure 4.8 illustrate the effect of data alignment. In Figure 4.7, we see that the locations of the TSPs in year 1 and year 2 are different. After the data alignment has been applied, the year 2 data is aligned to the year 1 data so that we can compare these two data sets based on the aligned time basis. The aligned results are shown in Figure 4.8. In Figure 4.8, the backgrounds of the two data sets are removed so that we can easily compare these two data sets.

4.4 Background Removal

The background removal is used to remove low frequency noise, such as lift-off noise. The background removal is achieved by moving a window with size 256 data points over the whole data set and fitting the data points in the window using a second order polynomial. The coefficients of the second order polynomial are obtained using a least-square criterion. Before the background is fitted, two preprocessing steps must be applied. The first step is to mask the interference data points. The second step is to mask the TSP regions. These two steps are used to avoid data points with large values affecting the background fitting. The equations for computing the coefficients of the polynomial using a least-square criterion is derived as below.

Assume the background of the raw data points is $\{f(x_i) |\ 1 \le i \le n, i \in Z\}$, where n is the window size. Suppose that the fitted background is an m order polynomial with the background points $\left\{\sum_{j=0}^{m} a_j x_i^j |\ 1 \le i \le n, i, j \in Z\right\}$. By using the least-square method, we know that

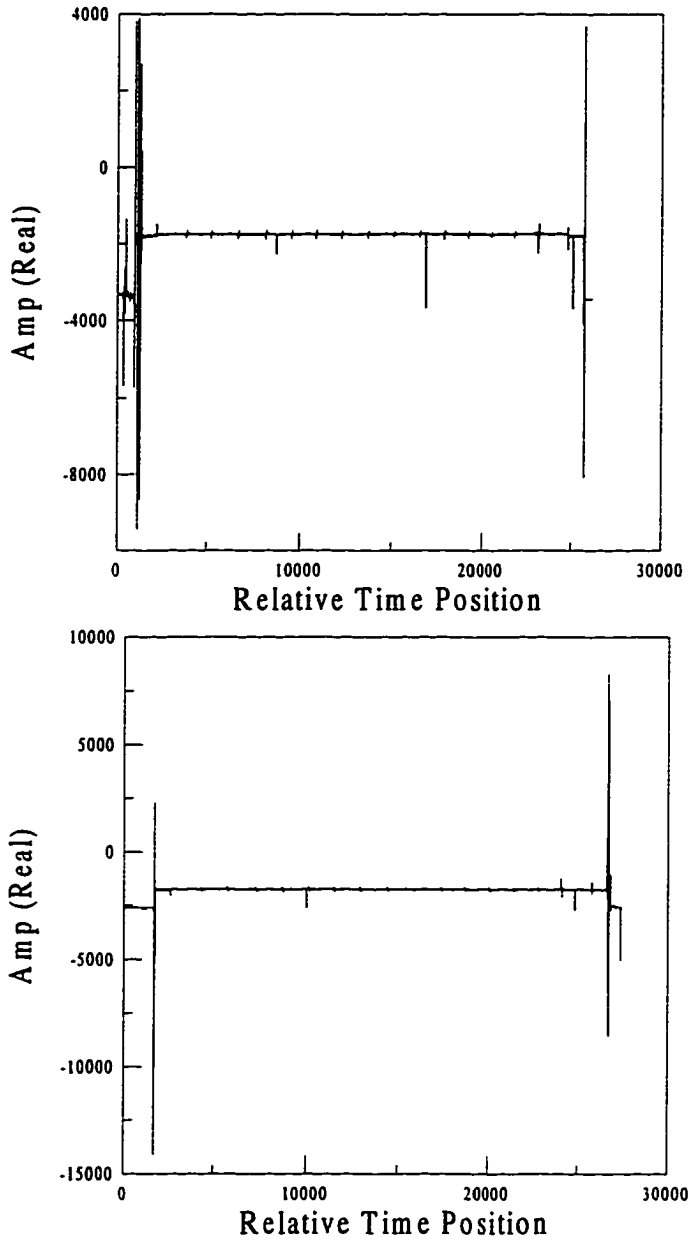

Figure 4.7 Real part of two raw data sets obtained from the same heat exchanger tube at different times. Top picture is year 1 data and the bottom picture is year 2 data. Due to variations in pulling speed, the relative time positions of tube support plates are different between year 1 and year 2.

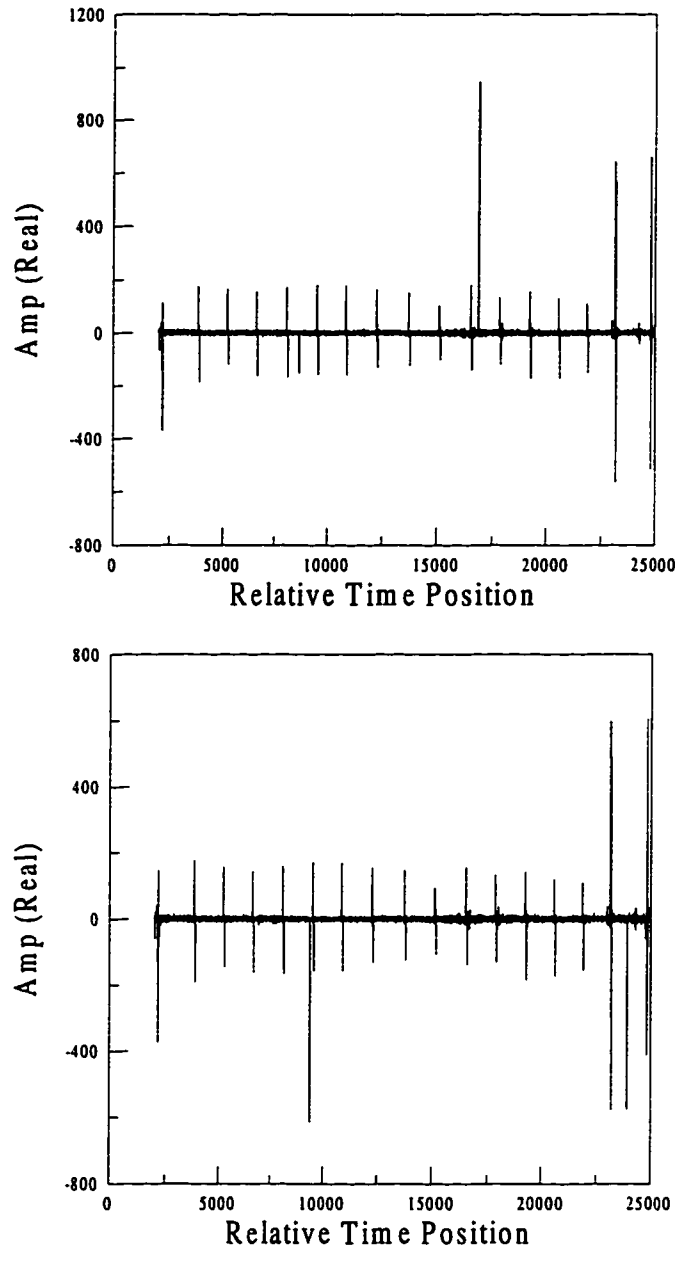

Figure 4.8 The result of data alignment after background removal. For the purpose of display, the entry and exit data points were truncated. Top picture is year 1 data and bottom picture is year 2 data. We used the tube support plates of year 1 data to be references and aligned the TSPs of year 2 data to the corresponding TSPs in year 1 data.

$$\varepsilon = \sum_{i=1}^{n} \left| f(x_i) - \sum_{j=0}^{m} a_j x_i^j \right|^2 \text{, and } \frac{\partial \varepsilon}{\partial a_l} = 0 \quad l = 0, \ldots, m.$$

Therefore we obtain a set of equations

$$\sum_{j=0}^{m} a_j \sum_{i=1}^{n} x_i^{j+l} = \sum_{i=1}^{n} f(x_i) x_i^l \qquad l = 0, \ldots, m \tag{4.5}$$

where m is the order of the polynomial and n is the length of the data record. The above linear equations can be inverted by LU decomposition algorithms, such as Gauss elimination algorithm [18]. The coefficients are then obtained by back substitution in the decomposed upper triangular matrix. After the coefficients for the polynomial are obtained, the background is removed from the signal by subtracting the polynomial from the data. Figure 4.9 illustrates the effect of the background removal using a second order polynomial. It is obvious that the background can be well fitted with the second order polynomial.

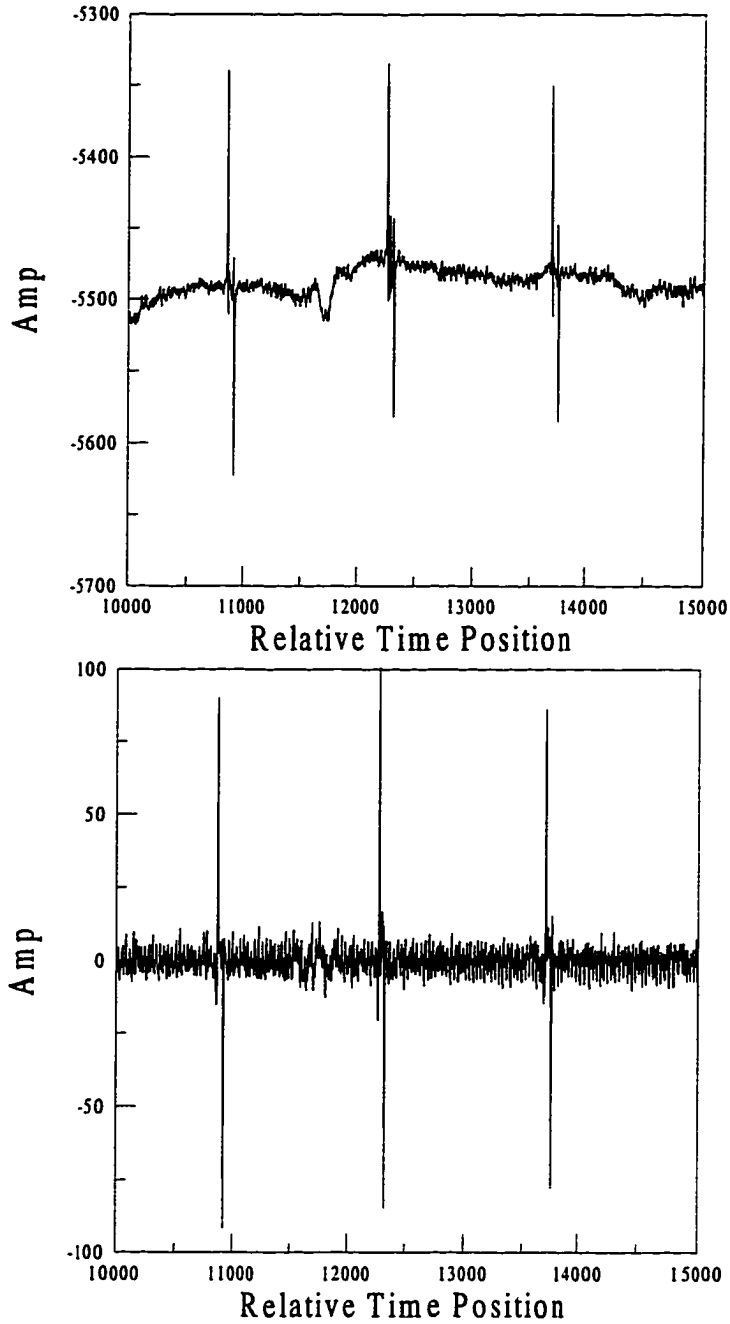

Figure 4.9 Result of background removal. Top plot is the original data sequence and the bottom plot is the data after background removal.

CHAPTER 5. WAVELET IDENTIFICATION OF FLAW INDICATIONS (STAGE #2 OF SYSTEM)

The applications of wavelets in the field of signal and image processing has been widely explored in the recent years. Due to the features of time-frequency and the multiresolution view of signal analysis, wavelets are very successfully applied in various research fields and show very promising results. Since the probe's to a flaw is localized in time makes it advantageous to utilize the time-frequency property and the multiresolution analysis of wavelets to characterize the flaw. So it turns out that the flaw has special characteristics in the wavelet domain. Based on these characteristics, a wavelet flaw detection algorithm was investigated and the results shows great potential in flaw detection. In this chapter, fundamental wavelet theory is introduced first. Emphasis is placed on the wavelet transform, multiresolution analysis , and the pyramidal algorithm. Then, based on wavelet theory, wavelet flaw detection algorithm is addressed. The algorithm consists of four main steps: fast wavelet transform, extrema algorithm, denoising procedure, and transient detection algorithm.

5.1 Wavelets Overview

Wavelets are the families of basis functions which are created by translation and dilation of a prototype function - the mother wavelet expressed as

$$\psi^{a,b}(x) = |a|^{-1/2}\psi(\frac{x-b}{a}), \tag{5.1}$$

where a, b are the scaling and translation indices, respectively [19-23]. Scaling of the wavelet function plays a special role in wavelet algorithms. It allows us to examine data at various resolutions or scales, so that both the global features and local features can be displayed and analyzed in the same time. This multiresolution of signal analysis is the essential component of the wavelet transform. In other words, we can observe the both general and detailed views of the signal simultaneously [24].

Wavelet analysis has advantages over traditional Fourier methods in analyzing data with sharp discontinuities by using basis functions which are created from the mother wavelet. Fine temporal analysis is achieved with contracted (high-frequency) versions of the wavelet, while fine frequency analysis uses dilated (low-frequency) versions. One may treat the wavelets as mathematical functions that divide data into frequency components, and then analyze each component with a resolution matched to its scale.

Wavelets have wide application in many fields such as image compression, speed discrimination, and de-noising noisy data etc. In this section, we will see how the wavelet technique is applied in our field. Through the wavelet transform, original signals are represented in terms of a wavelet expansion. Data operations are performed by using just the corresponding wavelet coefficients. By utilizing the flaw characteristics in the wavelet domain, the flaw indications can be identified and distinguished from the noise.

5.2 The Wavelet Transform

In the history of signal analysis, the invention of the Fourier transform plays a very important role that built up the foundation of modern signal analysis techniques. Especially, it provides a new way to view and analyze the signal in the frequency domain. The Fourier transform uses complex sinusoids for basis functions and works by translating a function in the time domain into a function in the frequency domain. The Fourier transform of a continuous time signal $x(t)$ is given by [25]

$$X_F(\omega) = \int_{-\infty}^{+\infty} e^{-j\omega t} x(t)dt \tag{5.2}$$

With this transform, the signal can be analyzed for its frequency content. However, due to the infinite extent of the basis functions, localized time information is spread out over the entire frequency domain. Also, the Fourier transform is not suitable for analyzing a nonperiodic signal because that the summation of the periodic functions, sine and cosine, does not accurately represent the signal. To solve such problems, the windowed Fourier transform (WFT) was addressed by introducing windowed complex sinusoids as basis functions[]. With the WFT, the input signal $x(t)$ is chopped up into sections, and each section is analyzed for its frequency content separately. The windowed Fourier transform of signal x(t) is given by [26]

$$X_{WF}(\omega,\tau) = \int_{-\infty}^{+\infty} g_{\omega,\tau}(t)x(t)dt \tag{5.3}$$

and the basis functions $g_{\omega,\tau}(t)$ are defined as

$$g_{\omega,\tau}(t) = e^{-j\omega t} g(t-\tau) \tag{5.4}$$

where $g(\cdot)$ is an appropriate window like a Gaussian. That is, $X_{WF}(\omega,\tau)$ is the Fourier transform of $x(t)$ windowed with $g(\cdot)$ shifted by τ. From the equation, we can easily see that the windowed Fourier transform provides information about signals simultaneously on both time and frequency. It maps a function of one variable (time) into a function of two variable (time and frequency). This results show the well known time-frequency localization property. Also, $X_{WF}(\omega,\tau)$ can be interpreted as the content of x with frequency ω near time τ.

The wavelet transform is similar to the windowed Fourier transform in the mathematical formula but with a few important differences. The wavelet transform formula is

$$X_W(a,b) = \int_{-\infty}^{+\infty} \psi_{a,b}(t) x(t) dt \tag{5.5}$$

and the basis functions $\psi_{a,b}(t)$ are defined as

$$\psi_{a,b}(t) = |a|^{-1/2} \psi(\frac{t-b}{a}) \tag{5.6}$$

where $\psi(t)$ is a single prototype wavelet called the "mother wavelet" or "analyzing wavelet", and a, b are the scaling and translation indices, respectively. The wavelet transform and windowed Fourier transform have another similarity for their basis functions localized in frequency. The most interesting dissimilarity between these two transforms lies in the shapes of the basis functions $g_{\omega,\tau}(t)$ and $\psi_{a,b}(t)$. Those functions $g_{\omega,\tau}$ all consist of the same envelope function g, translated to the proper time location, and filled in with higher frequency oscillations. All the $g_{\omega,\tau}$, regardless of the value of ω, have the same width. In

contrast, the $\psi_{a,b}$ have time-widths adapted to their frequency: high frequency $\psi_{a,b}$ are very narrow, while low frequency $\psi_{a,b}$ are much broader. By looking at the basis function coverage of the time-frequency plane, the time-frequency resolution differences between the windowed Fourier transform and the wavelet transform are easily understood. Figure 5.1 shows a windowed Fourier transform, where the window is simply a square wave. The square wave window truncates the sine or cosine function to fit a window of a particular width. Because a signal window is used for all the frequencies in the WFT, the resolution of the analysis is the same at all locations in the time-frequency plane.

For the wavelet transform, the windows will vary, and therefore, results in a family of basis functions, which make wavelets interesting and useful. From the theory of the uncertainty principle, it is not possible to have arbitrarily high resolution in both time and frequency. The lower bound for the time-bandwidth product of possible basis functions is given by $\Delta T \cdot \Delta\Omega \geq (1/4\pi)$, where $(\Delta T)^2$ and $(\Delta\Omega)^2$ are the variances of the absolute values of the functions and their Fourier transform, respectively [25]. However, one can trade resolution in time for resolution in frequency by varying the window used. Due to the variations in windows, the wavelet transform has such a special property that it has short high-frequency basis functions and long low-frequency ones. Figure 5.2 shows the coverage in the time-frequency plane with one wavelet function, the Daubechies wavelet. One thing needed to be emphasized is that the wavelet transforms do not have a single set of basis functions like the Fourier transform, which utilizes just the sine and cosine functions. Instead, wavelet transforms have an infinite set of possible basis functions. Thus, wavelet analysis

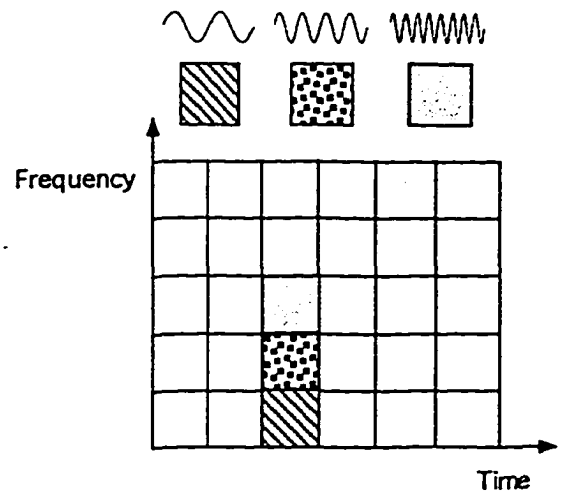

Figure 5.1 Fourier basis function, time-frequency tiles, and coverage of the time frequency plane

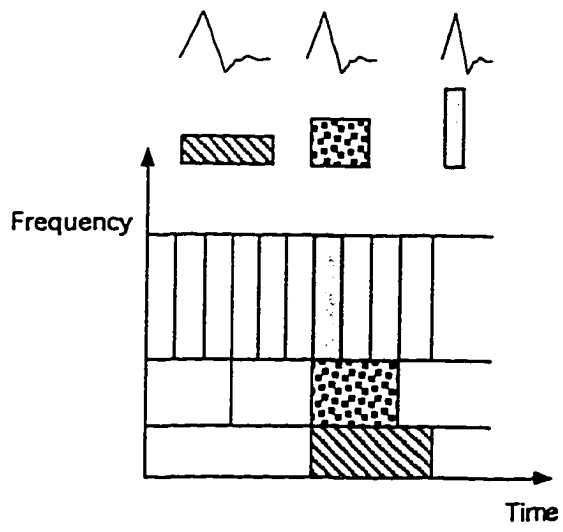

Figure 5.2 Daubechies wavelet basis function, time-frequency tiles, and the coverage of the time-frequency plane.

provides immediate access to information that can be obscured by other time-frequency methods such as Fourier analysis.

5.3 Orthonormal Wavelet Bases: Multiresolution Analysis

In applications of the wavelet transform, the wavelet transform in (5.5) is rarely used for its high redundancy with the continuous parameters (a,b) applied. Usually, the transform is evaluated on a discrete grid in the time-scale plane corresponding to a discrete set of continuous basis functions. This is performed by using a set of orthonormal basis functions. The approach is to design functions $\psi(\cdot)$ such that the set of translated and scaled versions of $\psi(\cdot)$ forms an orthonormal basis. The discretized translation and dilation parameters of the wavelet are described by:

$$\psi_{m,n}(t) = a_0^{-m/2} \cdot \psi(a_0^{-m} t - n b_0), \qquad m,n \in Z, \quad a_0 > 1, \quad b_0 \neq 0 \tag{5.7}$$

which corresponds to $a = a_0^m$ and $b = n a_0^m b_0$. Note that the translation step depends on the dilation. In signal processing, a typical selection of a_0 and b_0 is $a_0 = 2$ and $b_0 = 1$, which is the case for octave scales. One classic example is the Haar basis shown in Fig.5.3, where

$$\psi(t) = \begin{cases} 1 & 0 \le t < 1/2 \\ -1 & 1/2 \le t < 1 \\ 0 & \textit{otherwise.} \end{cases}$$

However, the Haar function is discontinuous and is not generally appropriate for signal processing. The most well known continuous set of basis functions is the Daubechies wavelets which are obtained from a compactly supported wavelet constructed by Daubechies [19]. A Daubechies wavelet with 4 coefficients is displayed in Fig.5.4.

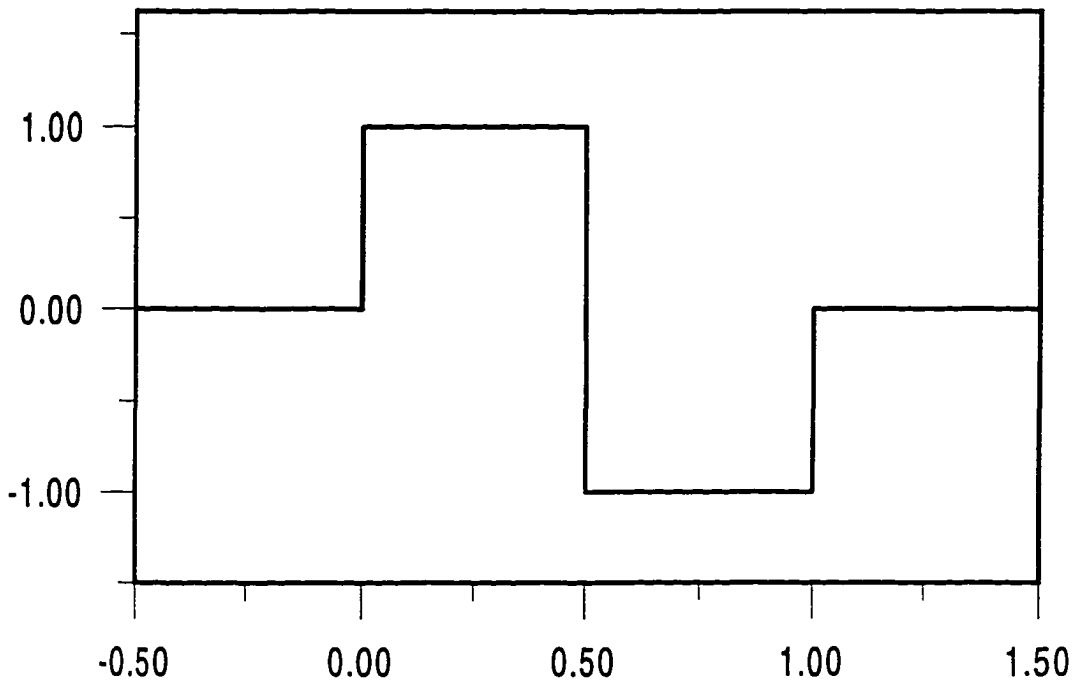

Figure 5.3 The Haar wavelet.

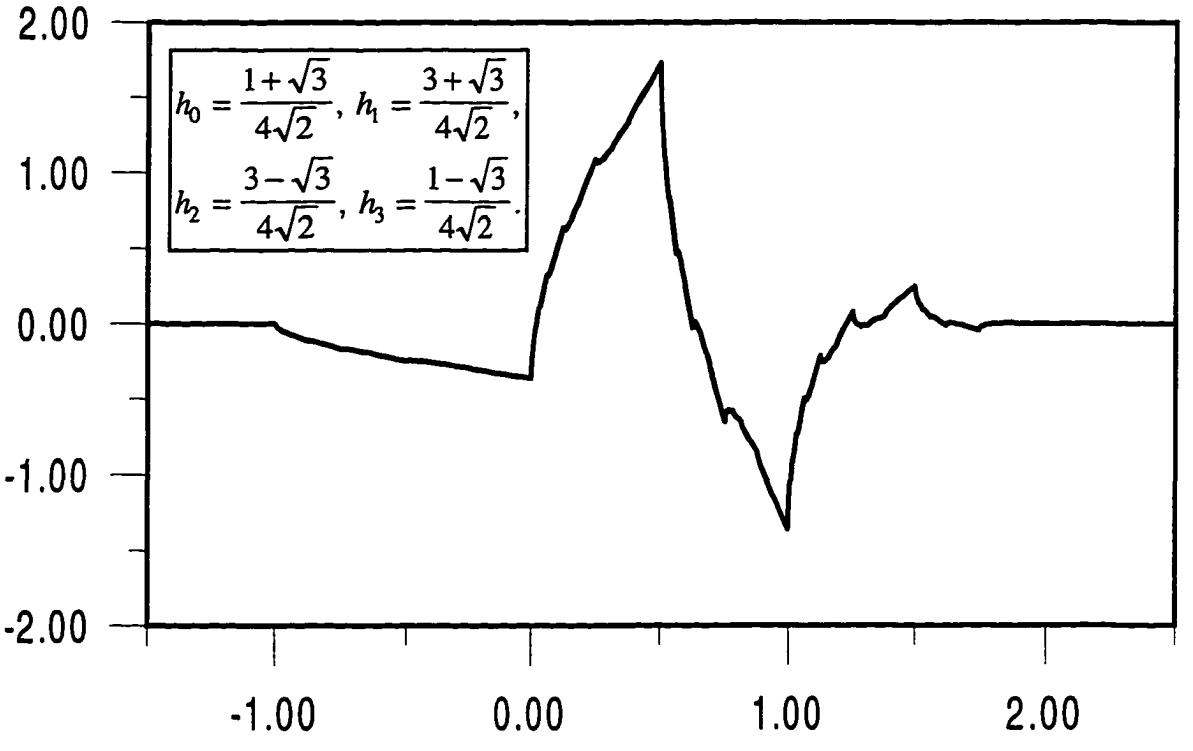

Figure 5.4 The Daubechies wavelet with four coefficients.

A fast method for performing discrete wavelet analysis based on the orthonormal wavelet bases is developed here. The method is called multiresolution analysis and was investigated by Mallat [27]. He used this to analyze information in images and demonstrated the usefulness of the application. The approach is to decompose the original image into an orthonormal set of Wavelet basis functions and then to further decompose the wavelets into multiscale (or multiresolution) and to provide a simple hierarchical framework for interpreting the image information. Through this decomposition, an orthogonal multiresolution representation, called a wavelet representation, is defined.

The scenario of the multiresolution approach is described as follows: An original version $f^0 = \{f_n^0\}_{n \in Z}$ of the signal is sampled at regular time intervals $\Delta t = \tau > 0$. f^0 is split into a "blurred" version f^1 at the coarser scale $\Delta t = 2\tau$ and a "detailed version " d^1 at scale $\Delta t = \tau$. This process is repeated, giving a sequence f^0, f^1, f^2, . . . of more and more blurred versions together with the details d^1, d^2, d^3, . . . removed at every scale ($\Delta t = 2^m \tau$ in f^m and d^{m-1}). Each d^m can be written as a superposition of wavelets of $\psi_{m,n}$. After N iterations, the original signal can be decomposed as

$$f^0 = f^N + d^1 + d^2 + \cdots + d^N .$$

The above scenario introduces the idea that a ladder of spaces $(V_j)_{j \in Z}$ represents successive resolution levels. Based on such an idea, a formal definition of multiresolution analysis can be described as follows:

A sequence of closed subspaces $\{V_j\}$, $j \in Z$ of $L^2(\mathbf{R})$ has the following properties [19] :

(1) $V_j \subset V_{j-1} \quad \forall j \in Z$

(2) $\bigcap_j V_j = \{0\}$, $\bigcup_j V_j$ is dense in L^2

(3) $f \in V_j \leftrightarrow f(2^j \cdot) \in V_0$

(4) $f \in V_0 \rightarrow f(\cdot - n) \in V_0$ for all $n \in Z$

When a ladder of spaces V_j satisfies the four properties above, together with

(5) $\exists \phi \in V_0$ such that the $\phi_{0,n}(x) = \phi(x-n)$ constitute an orthonormal basis for V_0,

then there exists ψ so that

$$\mathrm{Proj}_{V_{j-1}} f = \mathrm{Proj}_{V_j} f + \sum_{k \in Z} \langle f, \psi_{j,k} \rangle \psi_{j,k} . \tag{5.8}$$

(Proj_{V_j} is the orthogonal projection onto V_j.) The function ϕ (or $\phi_{0,0}$) is called a *scaling function* of the multiresolution analysis with $\phi_{j,k} = 2^{-j/2}\phi(2^{-j}x - k)$, and the $\psi_{j,k}(x) = 2^{-j/2}\psi(2^{-j}x - k)$ constitutes an automatic orthonormal basis.

The construction of ψ is derived from the scaling function ϕ. From (3) and (5) above, we know that $\phi \in V_0 \subset V_{-1}$, and $\phi_{-1,k}(x) = \sqrt{2}\phi(2x-k)$ constitute an orthonormal basis for V_{-1}. Then there exists a $c_k = \sqrt{2}\langle \phi, \phi_{-1,k} \rangle$ such that the scaling function satisfies the *dilation equation*

$$\phi(x) = \sum_k c_k \phi(2x-k). \tag{5.9}$$

For any scale j, the subspace V_j is generated by $\phi_{j,k} = 2^{-j/2}\phi(2^{-j}x - k)$. Since $V_j \subset V_{j-1}$, there exists a unique orthogonal complementary subspace W_j of V_j in V_{j-1}. That is

$$V_{j-1} = V_j \oplus W_j, \tag{5.10}$$

where $\oplus$ denotes an orthogonal sum. We can visualize this as shown in Fig 5.5. The subspace W_j is called " wavelet subspace" and is generated by $\psi_{j,k}(x) = 2^{-j/2}\psi(2^{-j}x - k)$. Based on this relationship, the mother wavelet ψ is derived from the corresponding scaling function as follows

$$\psi(x) = \sum_k (-1)^k c_{1-k}\phi(2x - k). \tag{5.11}$$

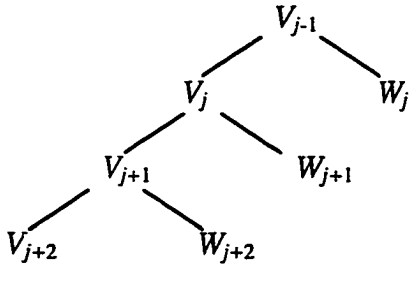

Figure 5.5 The wavelet tree for displaying the multiresolution aspect of space.

From the above discussion, we can conclude that the multiresolution analysis is implemented by using two functions, the scaling function ϕ and the mother wavelet ψ. By the scaled and shifted versions of these two functions, we have the multiresolution decomposition of $L^2(\mathbf{R})$ in which, for any scale j, V_j represents the smoothing part in resolution level j and W_j represents the details in resolution level j. The construction of the mother wavelet is derived from the scaling function. In general, given an orthonormal basis for V_0 made up of $\phi(x)$ and its integer translates, then, we can find coefficients c_k such that

$$\phi(x)=\sum_k c_k\phi(2x-k) \tag{5.12}$$

because $V_0 \subset V_{-1}$. Then

$$\psi(x)=\sum_k (-1)^k c_{1-k}\phi(2x-k) \tag{5.13}$$

and its integer translates form an orthonormal basis for W_0. So

$\left\{\psi_{j,k}(x)=2^{-j/2}\psi(2^{-j}x-k),\ j,\ k\in Z\right\}$, j, constitutes an orthonormal basis for $L^2(\mathbf{R})$. Thus, every function $f\in L^2$ can be written as

$$f(x)=\sum_{j,k}\left\langle f,\psi_{j,k}\right\rangle\psi_{j,k}\,. \tag{5.14}$$

Up to this point, we have introduced the concept of multiresolution analysis. However, how to produce suitable ϕ,ψ still needs to be explored. Here, the discussion is limited to fundamental theory. For detailed discussion on the construction of wavelets, one may refer to the books of Daubechies[19], Chui[20] and the papers by Strang[28], and Mallat[27].

The construction of wavelets is based on two sets of coefficients $\{h_k\}$, $\{g_k\}$ called *recursion coefficients* (note that the recursion coefficient h_k is actually equal to $c_k/\sqrt{2}$). In order to produce suitable ϕ and ψ, the recursion coefficients must satisfy

(1) $\sum_k h_{2k}=\sum_k h_{2k+1}=1/\sqrt{2}$, which implies $\sum_k h_k=\sqrt{2}$.

(2) $\sum_k g_{2k}=-\sum_k g_{2k+1}=(1/\sqrt{2})\cdot\alpha$, where $|\alpha|=1$. This implies $\sum_k g_k=0$.

(3) $\sum_k h_k \bar{h}_{k-2j} = \delta_{0j}$ for all j (orthonormality of translates of ϕ).

(4) $\sum_k g_k \bar{g}_{k-2j} = \delta_{0,j}$ for all j (orthonormality of translates of ψ).

(5) $\sum_k h_k \bar{g}_{k-2j} = 0$ for all j (orthonormality of translates of ϕ, ψ).

If the $\{h_k\}$ satisfy conditions (1) and (3), then the choice

$$g_k = (-1)^k h_{1-k}$$

will satisfy the rest.

A simple example using the Haar wavelet is given as following for helping understand the theory. Let V_0 be the space of L^2 piecewise constant spline functions. If we choose the scaling function ϕ to be

$$\phi(x) = \begin{cases} 1, & 0 \le x < 1, \\ 0 & otherwise, \end{cases}$$

Since $V_0 \subset V_{-1}$, and the $\phi_{-1,k}$ are an orthonormal basis in V_{-1}, we have

$$\phi = \sum_k h_k \phi_{-1,k} .$$

Then we know

$$\phi(x) = \chi_{[0,1]}(x) = \chi_{[0,1/2]}(x) + \chi_{[1/2,1]}(x) = \phi(2x) + \phi(2x-1) = \frac{1}{\sqrt{2}}\phi_{-1,0}(x) + \frac{1}{\sqrt{2}}\phi_{-1,1}(x),$$

where

$$\chi_{[a,b]}(x) = \begin{cases} 1 & a \le x < b, \\ 0 & otherwise. \end{cases}$$

So the recursion coefficients $\{h_k\}$ are obtained as

$$h_0 = h_1 = \frac{1}{\sqrt{2}}.$$

Consequently, $g_0 = \frac{1}{\sqrt{2}}$ and $g_1 = -\frac{1}{\sqrt{2}}$ that is

$$\psi(x) = \frac{1}{\sqrt{2}}\phi_{-1,0} - \frac{1}{\sqrt{2}}\phi_{-1,1} \text{ or } \psi(x) = \begin{cases} 1 & 0 \le x < 1/2 \\ -1 & 1/2 \le x < 1 \\ 0 & \textit{otherwise.} \end{cases}$$

Figure 5.6 shows the scaling function and the Haar wavelet.

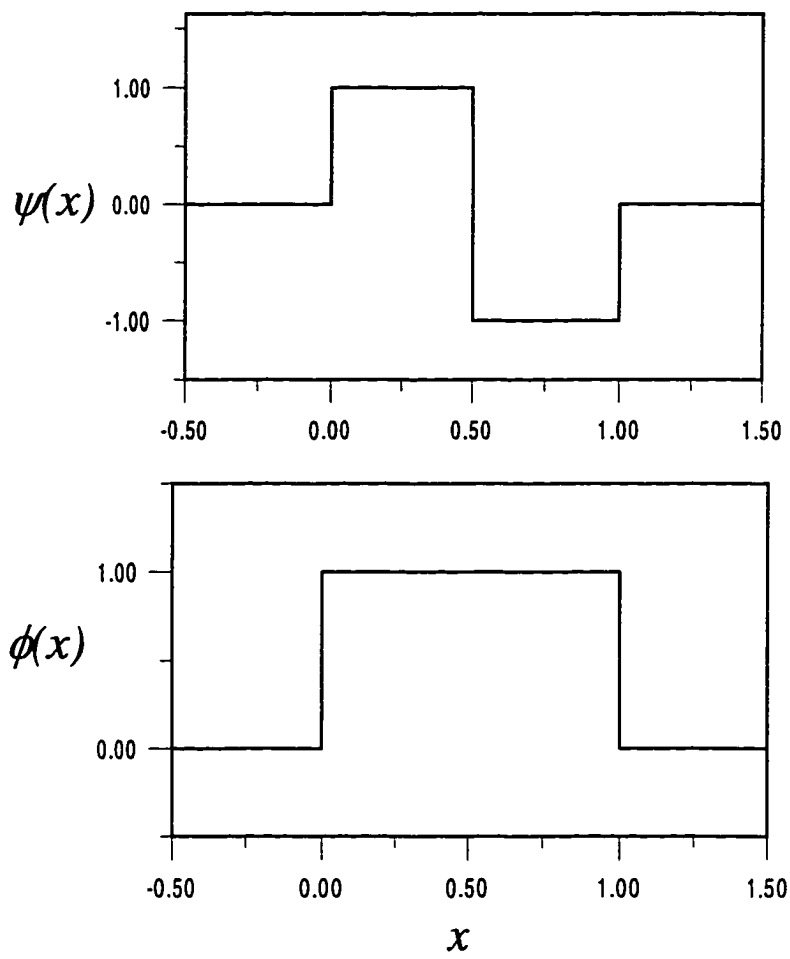

Figure 5.6 The Haar wavelet (top picture) and the box function (bottom picture).

5.4 Fast Wavelet Transform: Pyramidal Algorithm

In sections 5.1 to 5.3, we have introduced the concept of a wavelet transform and the idea of multiresolution analysis. In this section, we will discuss how to implement the wavelet transform with real data and how to apply multiresolution representations for analyzing the information content of signals. Actually, the main issue is how to decompose a signal into its wavelet coefficients and how to reconstruct the signal from coefficients. An algorithm called a " pyramidal algorithm" or " tree algorithm" will be discussed in this section [29]. The pyramidal algorithm is a fast discrete wavelet transform algorithm for orthonormal wavelets based on multiresolution decomposition. It has a computational complexity of $O(N \log_2 N)$. One may treat it like the fast Fourier transform (FFT) for the discrete Fourier transform.

Multiresolution analysis leads naturally to a hierarchical and fast scheme for the computation of the wavelet coefficients of a given function. In digital signal processing, the idea of orthonormal wavelet basis and multiresolution is closely related to a subband filtering scheme. In subband filtering, we can divide the whole spectrum (a linear space for band-limited finite-energy signals) into two parts by using a low-pass filter and a high-pass filter. We can repeat the same procedure for the first subband (the lower half of the spectrum) by using the scaled version of the same low pass and high pass filters. The whole spectrum can be divided into gradually smaller subbands by iteratively applying the above process. One can see that the above subband filtering scheme corresponds to the multiresolution decomposition of a linear space. Let V_0 be the whole space, then V_1 is the smoothing part of resolution 1 and W_1 is the details in resolution 1. V_1 is generated by the scaling function,

while W_1 is generated by the mother wavelet. Therefore, the scaling function is a low pass filter, while the mother wavelet is a high pass filter. For a digital signal, the low-pass filter and the high-pass filter can be realized by finite impulse response (FIR) filters. An FIR filter is also defined by a set of filter coefficients. In multiresolution analysis, the set of recursion coefficients $\{h_k\}$ is the FIR of the low-pass filter called H, and $\{g_k\}$ is the FIR of the high-pass filter called G. In signal processing contexts, H and G are called quadrature mirror filters.

The fast wavelet transform is implemented by convolutions of signals with quadrature mirror filters. We prove this as follows: From the previous section, we know that any function $f \in L^2$ can be written as

$$f(x) = \sum_{j,k} \langle f, \psi_{j,k} \rangle \psi_{j,k}(x), \tag{5.15}$$

where ψ is the mother wavelet. We can also write out partial decompositions. Assume the whole space is V_0 and for any $m \geq 1$, then

$$\begin{aligned} V_0 &= V_1 \oplus W_1 \\ &= V_2 \oplus W_2 \oplus W_1 \\ &\cdots \\ &= V_m \oplus W_m \oplus W_{m-1} \oplus \cdots \oplus W_1 \end{aligned}$$

For the same decomposition, taking any $f \in V_0$ we can write

$$f(x) = \sum_k \langle f, \phi_{0,k} \rangle \phi_{0,k}(x)$$

$$= \sum_k \langle f, \phi_{1,k} \rangle \phi_{1,k}(x) + \sum_k \langle f, \psi_{1,k} \rangle \psi_{1,k}(x)$$

...

$$= \sum_k \langle f, \phi_{m,k} \rangle \phi_{m,k}(x) + \sum_k \langle f, \psi_{m,k} \rangle \psi_{m,k}(x) + \cdots + \sum_k \langle f, \psi_{1,k} \rangle \psi_{1,k}(x)$$

Let

$$s_k^j = \langle f, \phi_{j,k} \rangle,$$

and

$$d_k^j = \langle f, \psi_{j,k} \rangle.$$

The original representation of $f \in V_0$ is then

$$f(x) = \sum_k s_k^0 \phi_{0,k}(x), \tag{5.16}$$

and the wavelet decomposition of f from level 0 to level m is

$$f(x) = \sum_k s_k^m \phi_{m,k}(x) + \sum_{j=0}^{m} \sum_k d_k^j \psi_{j,k}(x). \tag{5.17}$$

From the dilation equation, we know that

$$\phi_{0,0}(x) = \phi(x) = \sum_k c_k \phi(2x) = \sqrt{2} \sum_k h_k \phi(2x) = \sum_k h_k \phi_{-1,0}(x).$$

Generalizing the recursion formula, we get

$$\phi_{n,k}(x) = 2^{-n/2} \phi(2^{-n}x - k) = 2^{-n/2} \cdot 2^{-1/2} \sum_i h_i \phi(2 \cdot [2^{-n}x - k] - i)$$

$$= 2^{-(n-1)/2} \sum_i h_i \phi(2^{-(n-1)}x - 2k - i) = \sum_i h_i \phi_{n-1,2k+i}(x)$$

and likewise for ψ. So

$$\phi_{n,k}(x) = \sum_i h_i \phi_{n-1,2k+i} \tag{5.18}$$

and

$$\psi_{n,k}(x) = \sum_i g_i \psi_{n-1,2k+i} \tag{5.19}$$

Because

$$\langle \phi_{0,j}, \phi_{0,k} \rangle = \delta_{j,k}$$

$$\langle \psi_{0,j}, \psi_{0,k} \rangle = \delta_{j,k}$$

$$\langle \phi_{0,j}, \psi_{0,k} \rangle = 0$$

$$\langle \psi_{0,j}, \psi_{1,k} \rangle = 0$$

$$\langle \phi_{0,j}, \phi_{1,k} \rangle = \left\langle \phi_{0,j}, \sum_i h_i \phi_{0,2k+i} \right\rangle = \sum_i h_i \langle \phi_{0,j}, \phi_{0,2k+i} \rangle = \bar{h}_{j-2k}$$

$$\langle \phi_{0,j}, \psi_{1,k} \rangle = \left\langle \phi_{0,j}, \sum_i g_i \psi_{0,2k+i} \right\rangle = \sum_i g_i \langle \phi_{0,j}, \psi_{0,2k+i} \rangle = \bar{g}_{j-2k}$$

therefore

$$s_k^1 = \langle f, \phi_{1,k} \rangle = \left\langle \sum_j s_j^0 \phi_{0,j}, \phi_{1,k} \right\rangle = \sum_j s_j^0 \langle \phi_{0,j}, \phi_{1,k} \rangle = \sum_j \bar{h}_{j-2k} s_j^0 ,$$

That is, the $s_k^1 = \langle f, \phi_{1,k} \rangle$ are obtained by convolving the sequence $(s_j^0 = \langle f, \phi_{0,j} \rangle)_{j \in Z}$ with $(\bar{h}_{-j})_{j \in Z}$ and then retaining only the even samples. Similarly, we have

$$d_k^1 = \langle f, \psi_{1,k} \rangle = \left\langle \sum_j s_j^0 \phi_{0,j}, \psi_{1,k} \right\rangle = \sum_j s_j^0 \langle \phi_{0,j}, \psi_{1,k} \rangle = \sum_j \bar{g}_{j-2k} s_j^0$$

where $d_k^1 = \langle f, \psi_{1,k} \rangle$ are the wavelet coefficients of the level 1 (or resolution 1).

Using the notation $a = (a_j)_{j \in Z}$, $\bar{a} = (\bar{a}_{-j})_{j \in Z}$ and $(Ab)_k = \sum_j a_{2k-j} b_j$, we can rewrite the above two equations as

$$s^1 = \bar{H} s^0, \qquad d^1 = \bar{G} s^0.$$

The sequence $s^0 = (s_j^0)_{j \in Z}$ is convolved with filters H and G and the two resulting sequences are then subsampled. Therefore, s^0 is decomposed into a coarser approximation s^1 and the "detailed" d^1. Similarly, we can decompose s^1 into s^2 and d^2 such that

$$s^2 = \bar{H} s^1, \qquad d^2 = \bar{G} s^1.$$

Schematically, the decomposition can be represented as shown in Figure 5.7

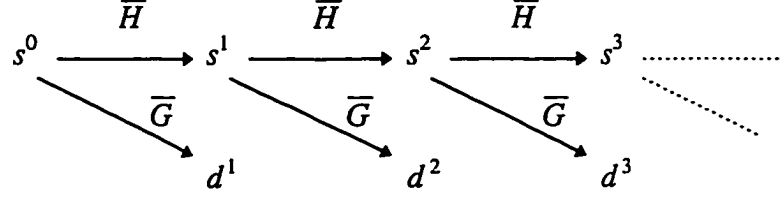

Figure 5.7 Schematic representation of decomposition.

If we stop the decomposition at level m, then we will decompose the information in s^0 into $d^1, d^2, d^3, \ldots, d^m$ and a final coarse approximation s^m. Since what we have done is a succession of orthogonal basis transformations, the inverse operation is just the reverse of the forward algorithm. Starting from the highest resolution, the inverse transform reconstructs the signal by composing its components in the subspaces of different resolution. Therefore,

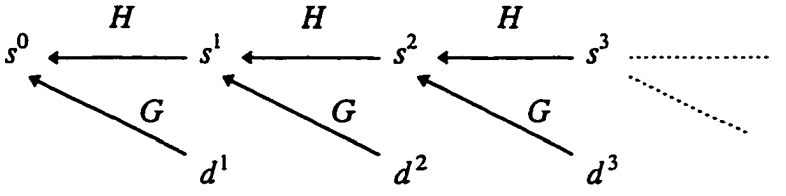

Figure 5.8 Schematic representation of reconstruction.

$$s^{m-1} = Hs^m + Gd^m,$$

where H is the inverse of $\overline{H}$ and G is the inverse of $\overline{G}$. Schematically, the reconstruction can be represented as shown in Figure 5.8

5.5 Wavelet Identification of Flaw Indications

In the previous section, we built a solid concept of wavelet theory. In this section, we will discuss the application of the wavelet analysis on the flaw detection of steam generator tubing data. The development of a wavelet flaw detection method is based on the characteristics of flaw signals and the noise in the wavelet domain. We utilize these characteristics to design a wavelet flaw detection algorithm for distinguishing the flaw signals from the noise in the wavelet domain. Through this detection algorithm, the positions of the possible flaw indications can be found, and then a further evaluation of these flaw candidates on the found positions can be performed on the raw data by using a template matching technique and a fuzzy inference system. In this section, we will introduce the characteristics of the flaw first. The ideas and design of the wavelet detection algorithm will be discussed next.

Lissajous patterns and phase are very important for the analysis of flaw signals. The signals of flaw indications detected by a differential bobbin probe are characterized by a shape like a figure "8" in a lissajous pattern [14]. By looking at the real and imaginary parts separately, the shape of a flaw indication is similar to the derivative of a gaussian function which is taken to be the defect property. The flaw signal is a transient signal because the response of probe decreases rapidly as the probe moves away from the indication. This property introduces the time localization characteristic of a flaw signal. Many types of degradation mechanisms can cause large variations in an eddy current signal. Additionally, there are many kinds of noise sources combined with the flaw signal, which makes the analysis more complex. Conventional frequency domain noise reduction techniques, such as bandpass filtering and smoothing, are not very successful in the processing of eddy current signals due to the fact the flaw signal is localized in time so that most of its frequency components overlap with the frequency components of the noise.

The wavelet transform offers a new direction for analyzing signals--especially those signals that are localized in both time and frequency. As we know, the multiresolution concept is the basic difference between wavelet analysis and conventional signal analysis techniques, such as the Fourier transform. The limitation of the Fourier transform is that its basis function is localized in the frequency domain, but not in the time domain. Therefore, it is only capable of separating signals which lie in different regions of the frequency domain. Since eddy current flaw signals are localized in the time domain and only partly localized in the frequency domain, it is impossible to fully separate them from the noise by using Fourier transform based techniques.

On the other hand, the multiresolution view of wavelet analysis gives us more information for analyzing eddy current signals . We can see that most of the electronic noise rapidly changes in the time domain. Probe liftoff causes a slow variation in the signal. As for the signals of flaw indications, they are smooth curves in a small time window. In the raw data, the flaw signals are usually combined with many other noises so it is hard to detect the signals. By applying the wavelet transform to the signal, we are able to separate the flaw signals and noise in the wavelet domain.

We selected Mallat's quadratic spline wavelet shown in Fig. 5.9 as the mother wavelet in our wavelet analysis. It is a not an orthogonal wavelet derived from a cubic spline but has three unique properties that make it the optimal choice for our task. First, it is a very smooth function so that it is rather efficient in approximating smooth signals. Second, it has a very compact support in the time domain to make it an efficient way in approximating time localized signals. Third, Mallat's wavelet has an antisymmetric shape that resembles an eddy

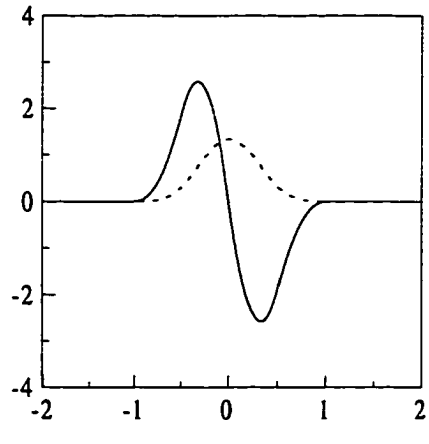

Figure 5.9 Mallat's quadratic spline wavelet (solid line). The dashed line is the smoothing function.

current flaw signal. Also, the wavelet transform using Mallat's wavelet has an equal number of data points at every resolution. This is desirable because the position information of the indication will remain in the transformed data at every resolution. The transformed data at different resolutions forms a new view of the original data which is called the wavelet domain. In the wavelet domain, the signal from a flaw indication has specific characteristics that can be used to separate it from noise and other unwanted signals. These characteristics are stated as follows:

(1) The wavelet transform coefficients of flaw indications at each resolution have larger amplitudes than most of the noise.

(2) The flaw indications have two antipolar local extrema that correspond to the two peaks of the flaw indications and this property appears on the first three resolutions of the imaginary part. Also, the two antipolar extrema will be positive on the first extrema and negative on the second extrema.

(3) The distance between two antipolar local extrema is within a certain time range related to the pulling speed.

Based upon these characteristics of the flaw indications, we have developed a wavelet flaw detection method. This method of detecting specific transients (flaw signals) in the background of noise combines statistics and wavelets. Nonparametric tests are implemented in the multiresolution framework of wavelet analysis. The statistical approach handles the noise while the wavelet transform provides time-frequency localization of the transients. This strategy makes it possible to access the signal's components in the data in the presence of significant noise.

The design of the wavelet flaw detection algorithm is mainly based on two ideas. The first one identifies the main characteristics of the noise component and the effects on the wavelet transform of the input signal. The second part deals with the detection of the significant transitions which distinguish the wavelet transform of a true flaw signal from the wavelet transform of noise. The wavelet flaw detection algorithm contains four main components: the fast wavelet transform, the extrema algorithm, the denoising procedure, and the transition detection algorithm. The fast wavelet transform carries out multiresolution analysis by decomposing signals by way of the Mallat's quadratic spline mother wavelet basis. The extrema algorithm detects the sharp variations of signals. At each wavelet resolution, we detect the local extrema where a change in the first derivative of the signal exists. The denoising procedure is accomplished by applying nonparametric tests (histogram with optimal threshold) to trim the list of wavelet components. The transient detection algorithm is based on the multiresolution analysis of the trimmed list of extrema. The purpose of this algorithm is to identify the possible indication signal's position. This algorithm is implemented by combing information in various resolutions and applying rules derived from test results to determine the possibility of a flaw signal. Then we may apply a template matching technique and a fuzzy inference system to test whether these candidate positions have indications.

5.5.1 Fast wavelet transform

Multiresolution analysis is a very effective way to analyze the information contents of signals. To obtain the multiresolution view of signals, a fast wavelet transform is performed

first on the preprocessed raw data. The filters we use are proposed by Mallat and Zhong [29]. Mallat's mother wavelet is not orthogonal but it has a small support. The advantages of Mallat's mother wavelet over other mother wavelets in this research are on the shape of the mother wavelet and the preservation of position information at each resolution. Mallat's wavelet has an antisymmetric shape that resembles the eddy current flaw signal sensed differential bobbin coils. This allows the transformed coefficients to characterize flaw signals. Unlike the pyramidal algorithm which uses orthogonal wavelet bases with downsampling by 2 at each decomposition process, the wavelet transform using Mallat's non-orthogonal wavelet has an equal number of data points at every resolution. This is a very desirable property because the position information of an indication will remain in the transformed data at every resolution.

Mallat's mother wavelet $\psi(x)$ is characterized by three discrete filters H, G, and K which are used for the fast wavelet transform computation. The finite impulse response of these filters is given in Table 5.1[29].

Table 5.1 Finite impulse response of the filters H, G, and K that correspond to the quadratic spline wavelet of Fig. 5.9.

n	H	G	K
-3			0.0078125
-2			0.0546875
-1	0.125		0.171875
0	0.375	-2.0	-0.171875
1	0.375	2.0	-0.054685
2	0.125		-0.0078125
3			

The algorithm based on these filters for computing the discrete wavelet transform is described as follows:

Let $\psi_{2^j}(x)$ represent the dilation of $\psi(x)$ by a factor 2^j. The wavelet transform of $f(x)$ at the scale 2^j and at the position x is defined by the convolution product

$$W_{2^j} f(x) = f * \psi_{2^j}(x).$$

The smoothing part of the decomposition process is defined by

$$S_{2^j} f(x) = f * \phi_{2^j},$$

where S_{2^j} is the smoothing operator. Suppose the original signal is a discrete sequence. We denote the operators by $S^d_{2^j}$ and $W^d_{2^j}$ by a discrete signal $S^d_1 f$. Let H_j, G_j, and K_j be the discrete filters obtained by putting $2^j - 1$ zeros between each of the coefficients of the filters H, G, and K. Then at each scale 2^j, we decompose $S^d_{2^j} f$ into $S^d_{2^{j+1}} f$ and $W^d_{2^{j+1}} f$. So the algorithm is

$j = 0$

while ($j < J$)

$$W^d_{2^{j+1}} f = \frac{1}{\lambda_j} \cdot S^d_{2^j} f * G_j$$

$$S^d_{2^{j+1}} f = S^d_{2^j} f * H_j$$

$$j = j + 1$$

end of while.

The λ_j is a normalization coefficient for the quadratic wavelet. The values of λ_j that correspond to the filters of Table 5.1 are given in Table 5.2 [29].

Table 5.2 Normalization coefficients λ_j for the quadratic wavelet. For $j > 5$, $\lambda_j = 1$.

J	λ_j
1	1.50
2	1.12
3	1.03
4	1.01
5	1.00

In numerical applications, the original discrete signal D has a finite number N of nonzero values: $D = (d_n)_{1 \le n \le N}$. To solve the boundary problem, Mallat uses the same periodization technique as in a cosine transform. He assumes that the original signal has a period of $2N$ samples, he extends it with a symmetry for $N < n \le 2N$: $d_n = d_{2N+1-n}$. By periodizing the signal with a symmetry, we avoid creating a discontinuity at the boundaries. In the fast wavelet algorithm, the convolutions must take into account this periodization. As for the inverse transform, it reconstructs $S^d_{2^{j-1}} f$ from $S^d_{2^j} f$ and $W^d_{2^j} f$. The reconstruction algorithm is

$j = J$

while $(j > 0)$

$$S^d_{2^{j-1}} f = \lambda_j \cdot W^d_{2^j} f * K_{j-1} + S^d_{2^j} f * \tilde{H}_{j-1}$$

$$j = j - 1$$

end of while.

$\tilde{H}_{j-1}$ is the complex conjugate filter of H_{j-1}.

The fast wavelet transform is obtained by moving a window of width 256 data points through the preprocessed data. The overlap between two adjacent windows is used to avoid the discontinuity of a flaw at its border. We apply the fast wavelet transform to data collected at frequencies of 200 kHz, 400 kHz, and 600 kHz to regions outside the TSPs. For the TSP regions, only the mix channel is applied. From our preliminary tests, we found that the first three resolutions are the most significant for discriminating flaws against noise. Resolutions that are higher than third contain more global (or low frequency) information so that the local information such as that for a flaw is not retained. The characteristics of a flaw in the wavelet domain do not show up on higher resolutions. Therefore, execution of the fast algorithm is for the first three resolutions only. Figure 5.10 shows plots of the first three resolutions of the wavelet transform using Mallet's mother wavelet. Figure 5.11 shows plots of the third resolution and fourth resolution of the wavelet transform. We can see that the shape variations of the original data signals are retained on the third resolution but do not show up on the fourth resolution. In the fourth resolution, we can only see a large scale smooth function which corresponds to the global information.

5.5.2 Extrema algorithm

A lot of information is obtained from the wavelet transform. However, very little information in the wavelet transformed data is of interest. A useful approach is needed to extract the meaningful information corresponding to the flaw signal from the transformed data. As we mentioned before, the signal for a narrow crack is a transient signal which has an

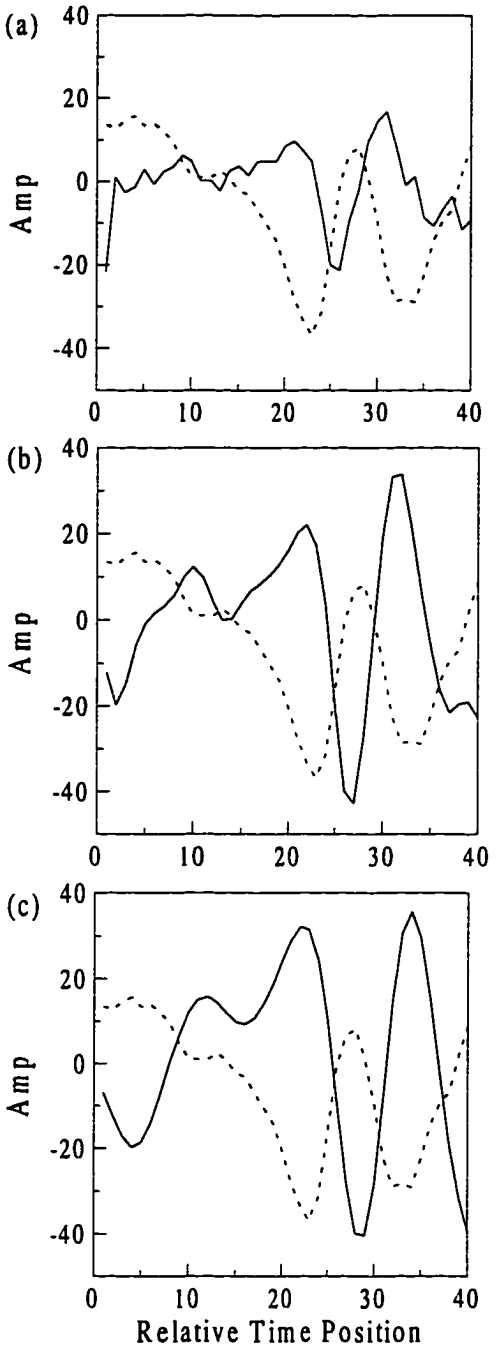

Figure 5.10 Plots of the first three resolutions of the wavelet transform using Mallat's mother wavelet. The dotted lines represent the original data. The solid lines are the wavelet coefficients. (a) , (b) and (c) correspond to resolution 1, 2, and 3 respectively.

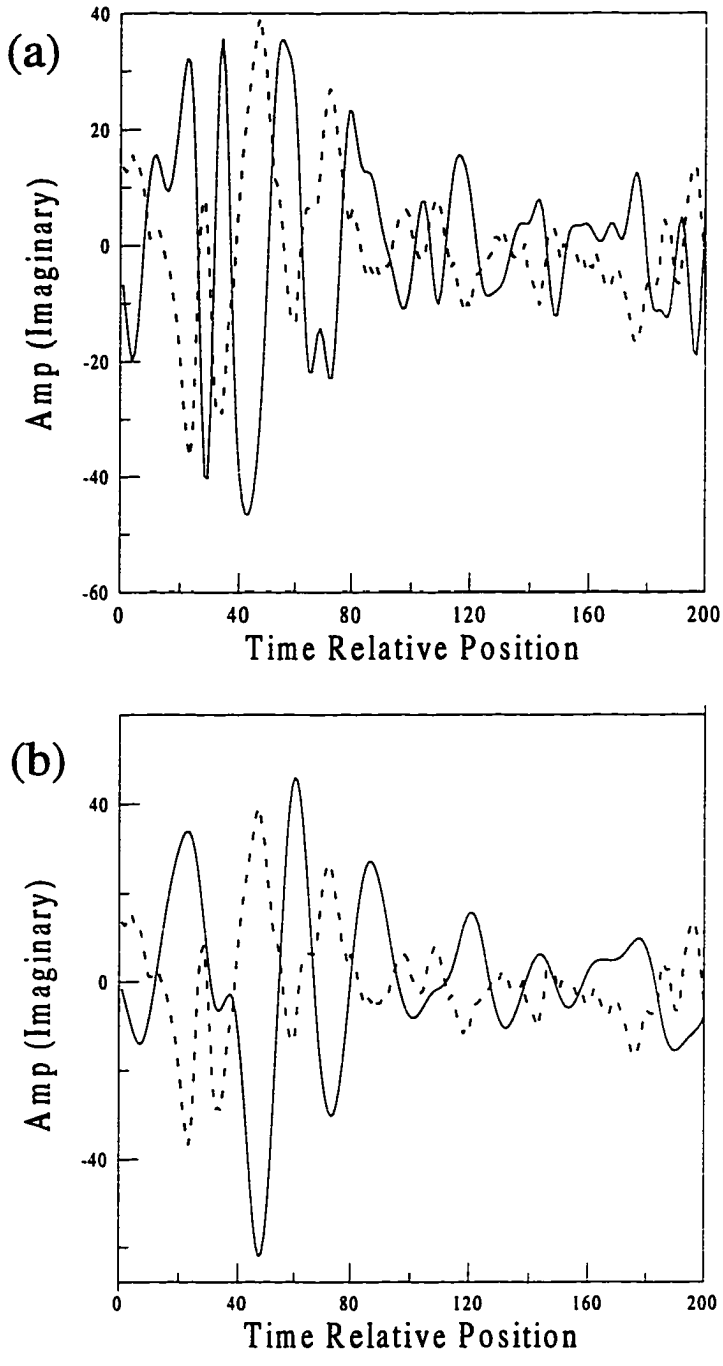

Figure 5.11 Plots of the third resolution and fourth resolution of the wavelet transform. The dotted lines represent the original data. The solid lines represent the wavelet coefficients. (a) and (b) correspond to resolution 3 and 4.

antisymmetric shape with two peaks on the differential frequency channel. In the wavelet domain, such an antisymmetric shape would cause two shape variation points with larger amplitudes than two adjacent points. Those shape variation points are actually the local extrema showing up on the first three resolutions. Therefore, we can utilize the extrema as the feature for extracting the flaw information in the wavelet domain and also for removing redundancy. Fig. 5.12 shows an example of the shape variation points in the original data and their corresponding local extrema.

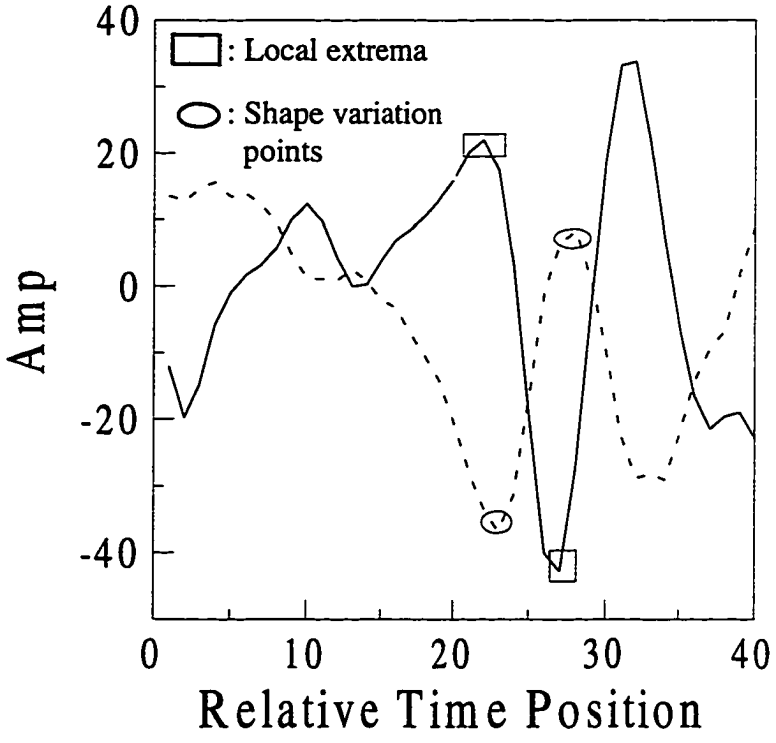

Figure 5.12 Shape variation points and their corresponding local extrema. The dotted line is the original data and the solid line is the wavelet coefficients on resolution 2.

The extrema are defined as the points with larger absolute wavelet coefficients than their two neighbor points. We implement the extrema algorithm by moving a three-point window through the data and marking the central point if it is an extremum. Then we keep the marked central points and set the other wavelet values to zero. This process is applied independently to all three resolutions in the wavelet domain. Fig 5.13 shows the results after applying (a) the wavelet transform and (b) the extrema algorithm in resolution 1. The dotted lines are the original data, while the solid lines are processing results.

5.5.3 Denoising procedure

Even though the extrema algorithm removes much of the redundancy and extracts the shape variation information, we still keep some extra extrema corresponding to noise or other sources. In [31], Carmona proposed a statistical (histogram) approach to remove the noise component of the signal. He assumes that the distribution of noise is known. A data sequence with no transient (flaw) signal is used to estimate the variance of this sequence. Based on the distribution and the variance of the noise, one can generate simulated noise samples. After the wavelet transform is computed, the extrema representation of the data is obtained. Then we construct, for each resolution $j = 1, \ldots, J$, a histogram H_j. Suppose that a level of significance α is chosen and $h_j(\alpha)$ is the $100(1-\alpha)$ percentile computed from the histogram H_j. We trim the list of extrema of the wavelet transform by deleting the extrema with smaller absolute values than $h_j(\alpha)$. The main idea is that the trimmed extrema are suspected to be the results of the noise component of the signal.

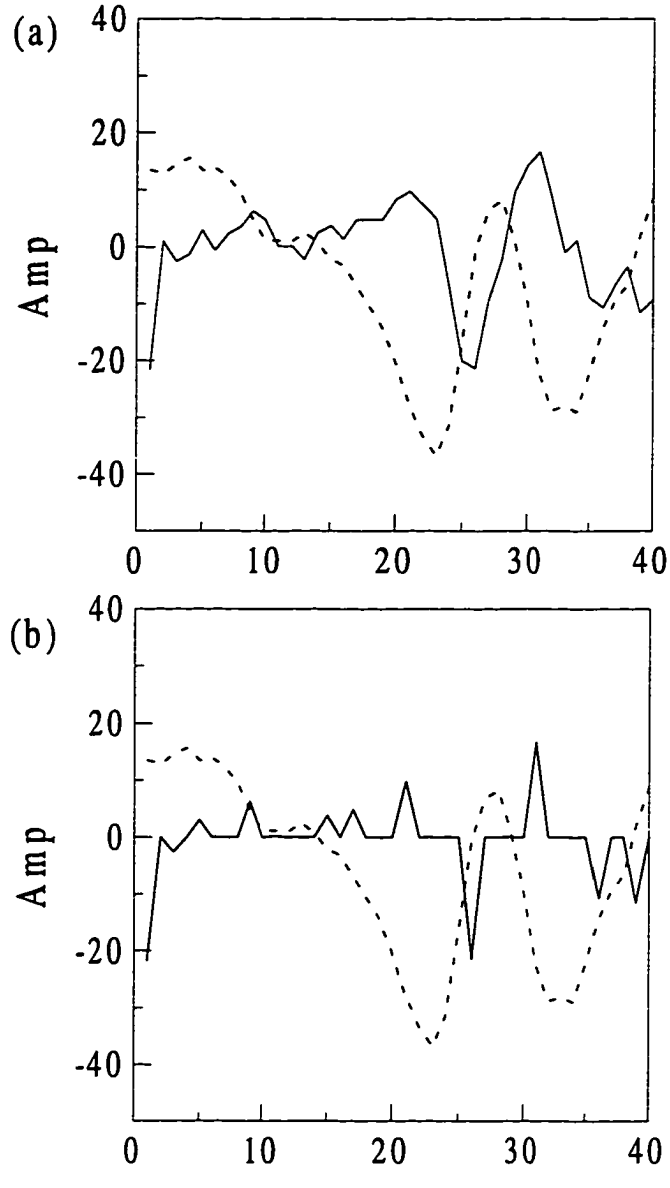

Figure 5.13 Results after applying (a) the wavelet transform (same as Fig. 5.10(a)) and (b) the extrema algorithm to part (a). The dotted lines are the original data, while the solid lines are the processing results.

We made some preliminary calculations using Carmona's idea. A window of width 256 data points were moved through the whole preprocessed data set. The histogram analysis of extrema was implemented on each window after the fast wavelet transform and the extrema algorithm were applied. We found that the optimal value of α was difficult to choose because the variations of noises in the tubing data are large. In addition to examining the noise component of the signal, we also studied the extrema corresponding to the flaw signal. We found that the absolute extreme values corresponding to the flaw signals have one common property: They are larger than some particular threshold. But for the extrema from the noise, most of them are smaller than a threshold. Therefore, we use a different approach to remove the noise component by trimming the list of extrema by an threshold value obtained from the transient (flaw) component for each resolution. The threshold value is obtained from experience. A series of real data sets with known flaws was tested. We analyzed the values of extrema caused by the flaws and chose the smallest one to be the reference value. The threshold value was selected as a value smaller or equal to the reference value. Fig. 5.14 shows the results of the denoising procedure in the 400 kHz differential channel. They are obtained by trimming the list of extrema with the threshold values 5, 8, and 8, which correspond to the resolution level 1, 2, and 3, respectively.

5.5.4 Transient detection algorithm

The original purpose of the transient detection algorithm was to find pairs of antipolar peaks on the first three resolutions in wavelet domain individually. Then we checked

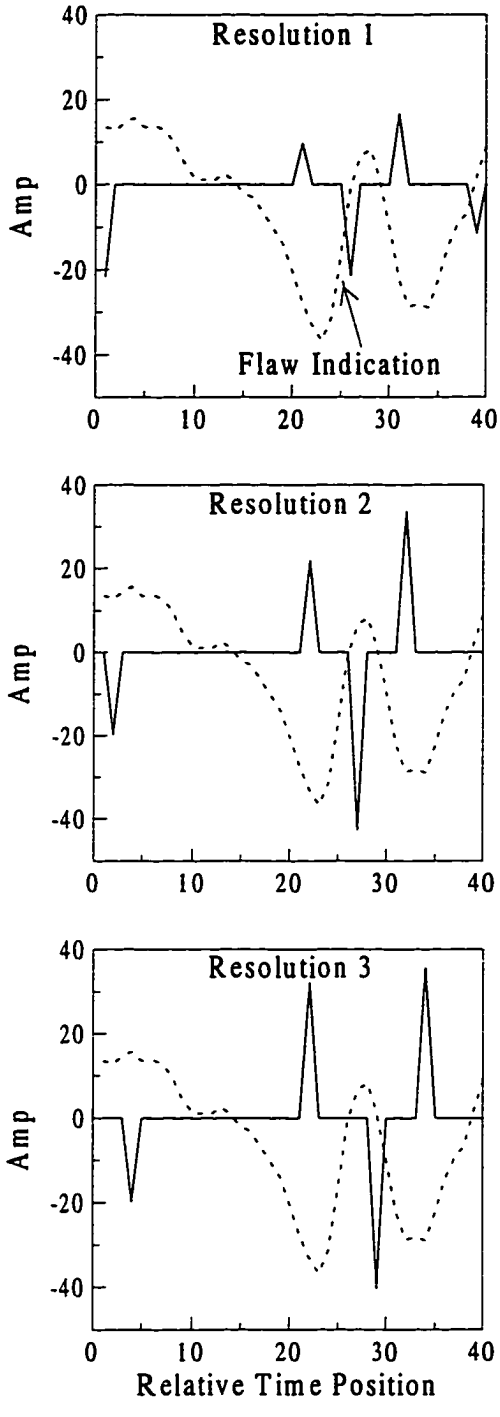

Figure 5.14 Plots of the first three resolutions after applying the denoising procedure in a 400 kHz differential channel. The input to the procedure was the output of the extrema algorithm

whether the antipolar peaks show up on all three resolutions at about the same location. We also checked that the distance between those antipolar peaks is within some specified range. From our preliminary tests, we learned that some antipolar peaks will be paired incorrectly by the transient detection algorithm. Such a situation results in an incorrect judgment of the checking-pairs of antipolar peaks showing up on all three resolutions at about the same location. This suggested that the transient detection algorithm needed to be modified. The redesigned transient detection algorithm should be able to locate the antipolar peaks and identify the positions on first three resolution simultaneously. Based on this objective, we have redesigned the algorithm as follows:

Identify the positions of sign changes on the wavelet coefficients of the second resolution and only keep the positions having signs opposite to the original data value.

(1) Search for negative wavelet coefficients which are near the identified sign-change position with a search window of size 4.

(2) Check the other two resolutions at the identified sign-change position to see whether there are negative peaks showing up too. (The search with range of 4 toward lower position at first resolution and toward higher position at third resolution. Also, the sign of original data value must be opposite to the wavelet coefficient's on the third resolution.) Mark the position if it meets the above conditions.

(3) Repeat step 3 for each near-by negative wavelet coefficient.

(4) Choose the negative antipolar peak by selecting the peak with the largest amplitude of the wavelet coefficients to see if there is more than one marked point. Go to step 10 if there is no negative antipolar peak.

(5) Find the near-by positive wavelet coefficients. (The search range is from the upper three data points to a minimized range. We obtain the minimized range by choosing the minimum between 15 data points and the distance of the negative-marked position and the preceding identified positive sign-change position.)

(6) Repeat steps 3~4 for each found positive wavelet coefficient.

(7) Repeat step 5 for getting the positive antipolar peak. Go to step 10 if there is no positive antipolar peak.

(8) Record the positions of the pair of antipolar peaks if they both exist.

(9) Repeat steps 2~9 for the succeeding negative sign change positions.

In this modification, one thing must be pointed out. It is that we not only check the signs of the wavelet coefficients on the first three resolutions, but also check the signs of the original data values at step (1). Due to the opposite-sign characteristic of an original data value and its corresponding wavelet coefficients, applying this procedure in the transient detection algorithm can eliminate many redundancies which cause false positives. In here, we also want to emphasis that the parameters used in the algorithm are obtained from many "trial and error" experiences. It means that we might need to modify the parameters according to specific flaw types. Fig 5.15 shows the flaw detection result after applying the transient detection algorithm on Fig. 5.14.

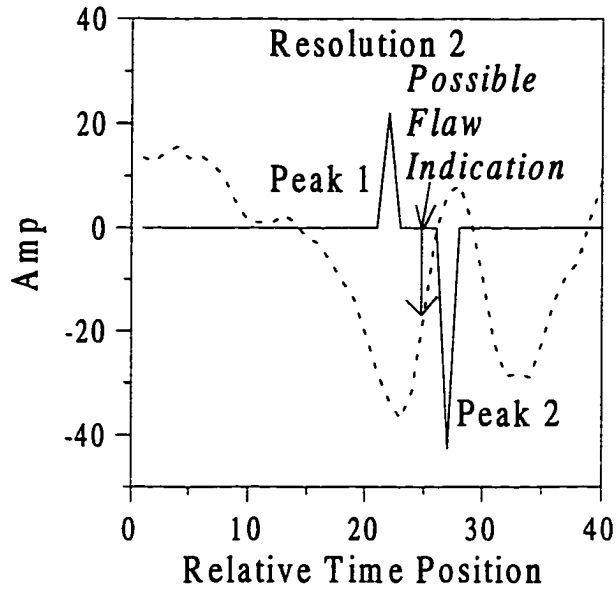

Figure 5.15 Flaw detection result of Fig 5.14 after applying the transient detection algorithm. The arrows show the estimated location of a flaw.

5.5.5 Auxiliary algorithm for wavelet detection algorithm in TSP region

In the wavelet detection algorithm, the identification of possible flaws is based on the wavelet coefficients of the first three resolutions. This idea is applicable outside the TSP region but it must be modified within the TSP region. In the TSP area, we apply the mixing algorithm to suppress the unwanted TSP signals and to reveal the masked flaw signals if a flaw exits within the TSP region. However, the mixing algorithm uses the least mean-square method so that the unwanted TSP signals are not removed, but just suppressed. The residuals of the suppressed TSP signals are still there and their shapes might resemble the shape of a true flaw. For the wavelet detection algorithm, a residual might be judged to be a "false flaw" due to this shape similarity. To solve such a problem, we studied the characteristics of both

flaws within the TSP region and the residuals of the suppressed TSP signals. Two conclusions can be drawn. First, the true flaw in the TSP region must have an anti-symmetric shape, but the two peaks' values might be similar or differ greatly. Second, the residuals of suppressed TSP signals might have an anti-symmetry shape too, but one of the peak's values will be very small compared to the large value of the other peak. Based on the above two conclusions, we used an auxiliary algorithm to judge whether the identified possible flaw is a true flaw or not.

Two major criteria, amplitude ratio and amplitude threshold, were used in the auxiliary algorithm. The auxiliary algorithm is described as follows:

(1) Find the possible flaw center whose first differential value is a local maximum: This is accomplished by applying the first differential method on the original data value within the region between two antipolar peaks detected by the wavelet detection algorithm.

(2) Search for two "real" antipolar peaks in the original data set: These two antipolar peaks are defined as the two nearest local extrema of the possible flaw center (positive peak on the higher position and negative peak on the lower position).

(3) Calculate the amplitude ratio of the peaks: The amplitude ratio is defined as

ratio = larger peak's amplitude/smaller peak's amplitude.

(4) Compare the amplitude ratio with a *ratio threshold* and also compare the smaller peak's amplitude with an *amplitude threshold*: A possible flaw should have amplitude ratio larger than ratio threshold and also its smaller peak's amplitude is larger than amplitude threshold too. In our work ratio threshold was about 10 and amplitude threshold was 8.

CHAPTER 6. DEFECT EVALUATION

(STAGE #3 OF SYSTEM)

6.1 Introduction

After applying the wavelet analysis method, an algorithm is still necessary to make the final decision regarding possible flaw indications for discriminating between true positives and false positives. A template matching technique and a fuzzy inference (logic) system were investigated to achieve this goal. The template matching technique provides useful information for characterizing the flaw indications. However, due to noise and interference, this information may not be accurate and the boundary between a flaw and a nonflaw is fuzzy. This suggests the possibility of applying the theory of fuzzy logic to this classification problem. A fuzzy inference system is applied to the output of template matching to make the decisions on whether or not an indication is indeed a flaw. We also use the fuzzy inference system to estimate the size (or more precisely, the percentage of through-wall penetration) of the flaw.

In this chapter, we first introduce the fundamentals of a fuzzy logic system, which include fuzzy sets, fuzzy logic and a fuzzy logic system. This discussion provides a basic understanding of a fuzzy logic system and how it is applied in our research. Then we discuss the template matching technique which originated from the theory of signal detection theory for radar systems. The template matching technique provides the input features (signal shape and phase) of the fuzzy inference system. Finally, the fuzzy inference system itself is

introduced, and the design of a membership function and the fuzzy rules are discussed in detail.

6.2 Fundamentals of Fuzzy Logic System

In recent years, research on fuzzy logic has been active in a number of application areas such as industrial process control [32], medical diagnosis [33], signal processing [34] and so on. The applications of fuzzy logic are implemented as fuzzy logic systems which are established based on fuzzy sets and fuzzy logic. The main advantage of a fuzzy logic system is that it can simultaneously handle numerical data and linguistic knowledge. Usually, one can treat a fuzzy logic system as a transformation that is a nonlinear mapping from an input space to an output space. In practice, a fuzzy logic system consists of a set of input variables that are related to a set of output variables through a set of rules. Each variable is described by a set of membership functions or fuzzy sets, each of which provides a quantitative relationship between the actual value of the variable and the linguistic description used in the rules. In this section, a general introduction to the theory of fuzzy sets and fuzzy logic is given. The elements and construction of the fuzzy inference system are also discussed.

6.2.1 Fuzzy sets

In [35], Lotfi A. Zadeh first introduced the theory of fuzzy sets, which are sets with boundaries that are not precise but, rather, fuzzy. This theory introduces a whole new concept that everything is not a matter of affirmation, but a matter of a degree. It offers a way to treat the vagueness of many phenomena and provides a new approach to handle

linguistic knowledge. The concept of fuzzy sets is an extension of the classical (crisp) sets. Before the fuzzy set is introduced, a crisp set is defined. This is because a crisp set is a very basic concept and has a connection with fuzzy sets. Typically, a fuzzy set is a generalization of a crisp set [36].

A crisp set A is defined in such a way so as to separate the individuals in a given universe of discourse (which provides the set of allowable values for a variable) into two groups: members (those that certainly belong to the set) and nonmembers (those that certainly do not). Alternatively, we can introduce a zero-one *membership function* (also called a characteristic function, discrimination function, or indicator function) for A, denoted $\mu_A(x)$, such that $A \Rightarrow \mu_A(x) = 1$ if $x \in A$ and $A \Rightarrow \mu_A(x) = 0$ if $x \notin A$.

In contract to the crisp set, a fuzzy set F can be defined mathematically by assigning to each possible individual in the universe of discourse a value representing its grade of membership in the fuzzy set. This grade corresponds to the degree to which that individual is similar with the concept represented by the fuzzy set. A formal definition abstracted from Kandel [37] goes as follows.

A fuzzy set F is a subset of the universe of discourse X that admits partial membership. The fuzzy set F is defined as the ordered pair

$$F = \{x, \mu_F(x)\}, \tag{6.1}$$

where $x \in X$ and $0 \leq \mu_F(x) \leq 1$. The membership function $\mu_F(x)$ describes the degree to which the object x belongs to the set F, where $\mu_F(x) = 0$ represents no membership, and $\mu_F(x) = 1$ represents full membership.

As an example, let X represent the height of all men. The subset F of X that represents those men whose height is medium, is a fuzzy set with the membership function shown in Fig. 6.1. The most commonly used shapes for membership functions are triangular, trapezoidal, piecewise linear and Gaussian. However, the design of a membership function is very flexible. It can be chosen based on the user's experience. Even more, membership functions have been designed using optimization procedures [38]. The *support* of a fuzzy set F is the crisp set of all points x in X such that $\mu_F(x) > 0$. The element x in X at which $\mu_F = 0.5$, is called the *crossover point.* A fuzzy set whose support is a single point in X with $\mu_F = 1.0$ is called a *fuzzy singleton.*

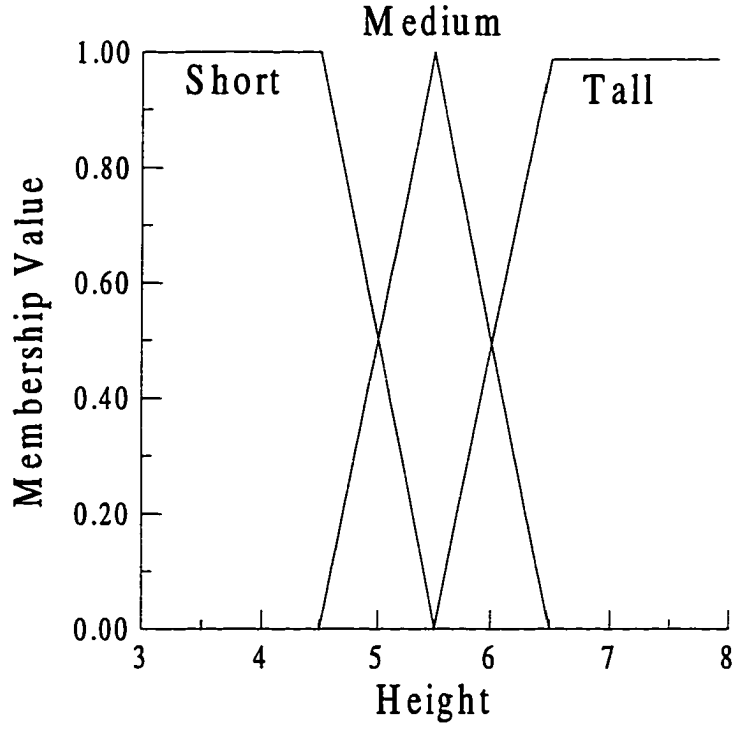

Figure 6.1 Membership functions for X(height) = { short men, medium men, tall men }.

The operations on fuzzy sets are extensions of those used for traditional sets. These operations include *comparison, containment, intersection, union, and complement.* In addition to these operations, there are more specific operations which are described following [39, 40]. Assuming X is the universe of discourse, $A \in X$ and $B \in X$, these operations are defined as follows.

Comparison: Is $A = B$?

$$A = B \text{ iff } \mu_A(x) = \mu_B(x) \qquad \forall x \in X \tag{6.2}$$

Containment: Is $A \subset B$?

$$A \subset B \text{ iff } \mu_A(x) < \mu_B(x) \qquad \forall x \in X \tag{6.3}$$

Union: The union of two fuzzy sets A and B, $A \cup B$, is found by combining the membership functions of A and B. It is defined as

$$\mu_{A \cup B}(x) = \max(\mu_A(x), \mu_B(x)) \qquad \forall x \in X \tag{6.4}$$

Intersection: The intersection of two fuzzy sets A and B, $A \cap B$, is found by combining the membership functions of A and B and is defined as

$$\mu_{A \cap B}(x) = \min(\mu_A(x), \mu_B(x)) \qquad \forall x \in X. \tag{6.5}$$

Complement: The complement of fuzzy set A, $\overline{A}$, is defined as

$$\mu_{\overline{A}}(x) = 1 - \mu_A(x) \qquad \forall x \in X. \tag{6.6}$$

Cartesian Product: If $A_1, \cdots, A_n$ are fuzzy sets in $X_1, \cdots, X_n$, respectively, the Cartesian product of $A_1, \cdots, A_n$ is a fuzzy set in the product space $X_1 \times \cdots \times X_n$ with the membership function

$$\mu_{A_1 \times \cdots \times A_n}(x_1, x_2, \cdots, x_n) = \min\{\mu_{A_1}(x_1), \cdots, \mu_{A_n}(x_n)\} \tag{6.7}$$

or

$$\mu_{A_1\times\cdots\times A_n}(x_1, x_2, \cdots, x_n) = \mu_{A_1}(x_1)\cdot\mu_{A_2}(x_2)\cdots\mu_{A_n}(x_n). \tag{6.8}$$

Fuzzy Relation: An n-ary fuzzy relation is a fuzzy set in $X_1 \times \cdots \times X_n$ and is expressed as

$$R_{X_1\times\cdots\times X_n} = \{((x_1, \cdots, x_n), \tag{6.9}$$

$$\mu_R(x_1, \cdots, x_n) | (x_1, \cdots, x_n) \in X_1\times\cdots\times X_n\}.$$

Sup-Star Compositions: If R and S are fuzzy relations in $U \times V$ and $V \times W$, respectively, associated with the fuzzy relation R is its membership function $\mu_R(x, y)$, where $\mu_R(x, y) \in [0, 1]$ and associated with fuzzy relation S is its membership function $\mu_S(y, z)$, where $\mu_S(y, z) \in [0, 1]$. The composition of R and S is a fuzzy relation denoted by $R \circ S$ and the *sup-star* composition of R and S is defined by

$$\mu_{R\circ S} = \sup_{y\in V}[\mu_R(x, y) \star \mu_s(y, z)], \tag{6.10}$$

where $\star$ is the min or product operator.

The use of fuzzy sets provides a basis for a systematic way to manipulate vague and imprecise concepts. In particular, one can employ fuzzy sets to represent linguistic variables. A linguistic variable can be regarded as a variable whose values are defined in linguistic terms. It is characterized by a quintuple (x, $T(x)$, X, G, M) in which x is the name of variable; $T(x)$ is the term sets, that is, the set of names of the linguistic values x can assume in the universe of discourse X ; G is a syntactic rule for generating the names of values of x; and M is a semantic rule for associating with each value its meaning. For instance, if speed is interpreted as a linguistic variable, then its term set T (speed) could be

T (speed) = { slow, moderate, fast, very slow, $\cdots$ }

where each term in T(speed) is characterized by a fuzzy set in a universe of discourse X = [0, 100].

6.2.2 Fuzzy logic

Fuzzy logic, which is based on the concepts of linguistic variables and fuzzy sets, is much closer in spirit to human thinking and natural language than traditional logic. It provides an effective way to capture the approximate, inexact nature of the real world. A reality of fuzzy logic is the rules which are often written using linguistic expressions in the form of IF-THEN statements. The rules play a very important role in the fuzzy logic system. Here, we first introduce classical logic and then fuzzy logic. This is because fuzzy logic is an extension of classical logic. Some basic concepts of classical, two-valued logic are briefly reviewed in the following. These concepts include propositions, negation, conjunction, disjunction, implication, and equivalence.

Propositions: A proposition, also called *statement*, is a declarative sentence that is logically either *true* (T) denoted by 1 or *false* (F) denoted by 0. The sets T_2={0, 1} is called *truth value* set for the proposition. Usually, we uses letters, p, q, r, $\cdots$, to represent propositions. *Compound propositions* consists of two or more simple propositions joined by one or more logical connectives presented in Table 6.1 [36].

Negation: Negation or denial of p, denoted $\bar{p}$ (read *not p*) is true when p is false and *vice versa*, hence

$$\bar{p} = 1 - p . \tag{6.11}$$

Table 6.1 Logical connectives.

Not	–
and	∨
or	∧
if . . . then	→
if and only if	↔

Conjunction: Conjunction of p and q, denoted $p \wedge q$ (read p *and* q) is true when p and q are both true;

$$p \wedge q = \min(p, q). \tag{6.12}$$

Disjunction: Disjunction of p and q, denoted $p \vee q$ (read p *or* q) is true when p or q is true or both p and q are true.

$$p \vee q = \max(p, q). \tag{6.13}$$

Implication (Conditional proposition): The proposition p implies q, denoted $p \rightarrow q$ (also read *if* p *then* q) is true except when p is true and q is false; p and q are called *premise* (*antecedent*) and *conclusion* (*consequent*), corresponding;

$$p \rightarrow q = \min(1, 1 + q - p). \tag{6.14}$$

Equivalence (Biconditional proposition): The proposition p *if and only if* q, denoted $p \leftrightarrow q$ (also read p *iff* q) is true when p and q are both true or both are false;

$$p \leftrightarrow q = 1 - |p - q|. \tag{6.15}$$

In traditional propositional logic there are two very important inference rules, *Modus Ponens* and *Modus Tollens* [40].

Modus Ponens----Premise 1: "x is A"; *Premise 2*: "IF x is A Then y is B"; *Consequence*: "y is B." Modus Ponens is associated with the implication " A implies B" [$A \rightarrow B$]. In terms of propositions p and q, Modus Ponens is expressed as $(p \wedge (p \rightarrow q)) \rightarrow q$.

Modus Tollens----Premise 1: " y is not B"; *Premise 2*: " IF x is A THEN y is B"; *Consequence*: " x is not A." In terms of propositions p and q, Modus Tollens is expressed as $(\overline{q} \wedge (p \rightarrow q)) \rightarrow \overline{p}$.

As in the extension of crisp set theory to fuzzy set theory, the extension of classic logic to fuzzy logic is made by replacing the bivalent membership functions of classical logic with fuzzy membership functions. Therefore, the IF-THEN statement "IF x is A, THEN y is B," where $x \in X$ and $y \in Y$, has a membership function $\mu_{A \rightarrow B}(x, y)$ where $\mu_{A \rightarrow B}(x, y) \in [0, 1]$. Note that $\mu_{A \rightarrow B}(x, y)$ measures the degree of truth of the implication relation between x and y. In addition, the Modus Ponens and Modus Tollens is extended to Generalized Modus Ponens (GMP) and Generalized Modus Tollens (GMT) [40]:

GMP----Premise 1: "x is A^*"; *Premise 2*: "IF x is A THEN y is B"; *Consequence*: "y is B^*."

GMT----Premise 1: "y is B^*"; *Premise 2*: "IF x is A THEN y is B"; *Consequence*: " x is A^*."

Compare Modus Ponens and the Generalized Modus Ponens to see the differences, fuzzy set A^* is not necessarily the same as rule antecedent fuzzy set A, and fuzzy set B^* is not necessarily the same as rule consequent B. Typically, we introduce fuzzy sets A, A^*, B, B^* via linguistic variables x, y instead of crisps sets in the traditional logic. The Generalized

Modus Ponens is a fuzzy composition where the first fuzzy relation is merely the fuzzy set, A^*. Consequently, $\mu_{B^*}(y)$ is obtained from the sup-start composition:

$$\mu_{B^*}(y) = \sup_{x \in A^*} [\mu_{A^*}(x) \star \mu_{A \to B}(x, y)]. \tag{6.16}$$

6.2.3 Fuzzy logic system

In this section, we consider a fuzzy logic system whose basic configuration is shown in Fig. 6.2. There are four principle elements in such a fuzzy logic system: fuzzifier, fuzzy rule base, fuzzy inference engine, and defuzzifier. We consider a multi-input, single-output fuzzy logic system: $U \subset R^n \to R$. A multi-output system can always be separated into a group of single-output system.

The *fuzzifier* performs a mapping from the observed crisp space $U \subset R^n$ to a fuzzy set defined in U, where the fuzzy set defined in U is characterized by the membership function $\mu_F: U \to [0, 1]$, and is labelled by the linguistic variable F such as " short," "medium," "tall," or "very tall." The most widely used fuzzifier is the singleton fuzzifier, i.e., $\mu_{A^*}(x') = 1$ for $x = x'$ and $\mu_{A^*}(x') = 0$ for all other $x \in U$ with $x \neq x'$.

The *Fuzzy rule base* consists of a set of linguistic rules in the form of " IF a set of conditions are satisfied, THEN a set of consequences are inferred."[39] It is a fuzzy conditional statement in which the antecedent is a condition in its application domain and the consequence is a control action for the system under control. Basically, the fuzzy rule base provides a convenient way for expressing control policy and domain knowledge. In general, the fuzzy rule base consists of N rules in the following form:

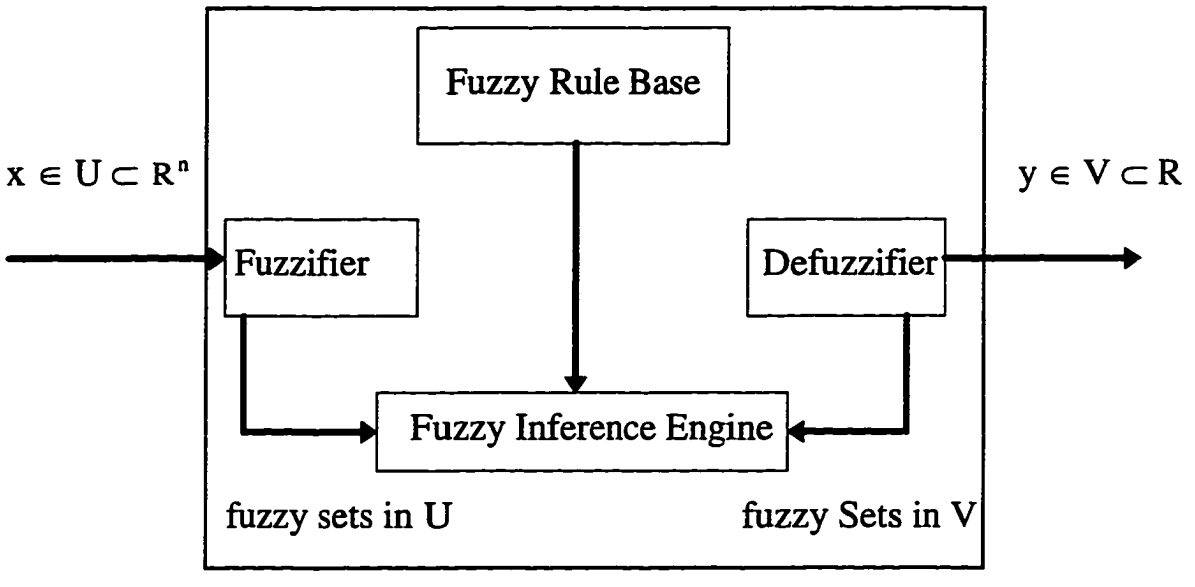

Figure 6.2 Basic configuration of fuzzy logic system.

$$R_j: IF\ x_1 \text{ is } A_1^j \text{ and } x_2 \text{ is } A_2^j \text{ and } \cdots \text{ and } x_n \text{ is } A_n^j,$$

$$THEN\ z \text{ is } B^j,$$

where $j = 1, 2, \cdots, N$, $x_i (i = 1, 2, \cdots, n)$ are the input variables to the fuzzy system, z is the output variable of the fuzzy system , and A_i^j and B^j are linguistic terms characterized by fuzzy membership function $\mu_{A_i^j}(x_i)$ and $\mu_{B^j}(z)$, respectively. Each R_j can be viewed as a *fuzzy implication* $A_1^j \times \cdots \times A_n^j \rightarrow B^j$, which is a fuzzy set in $U \times R$ with $\mu_{A_1^j \times \cdots \times A_n^j \rightarrow B^j}(\mathbf{x}, z) = \mu_{A_1^j}(x_1) \star \cdots \star \mu_{A_n^j}(x_n) \star \mu_{B^j}(z)$, and the most commonly used operation for "$\star$" are "product" and "min"[39].

The fuzzy inference engine is decision making logic that employs fuzzy rules from the fuzzy rule base to determine a mapping from the fuzzy sets in the input space U to the fuzzy

set in the output space R. Let A_x be an arbitrary fuzzy set in U; then each R_j determines a fuzzy set $A_x \circ R_j$ in R based on the sup-star composition [40]:

$$\mu_{B'}(z) = \mu_{A_x \circ R_j}(z) = \sup_{\mathbf{x} \in U} [\mu_{A_x}(\mathbf{x}) \star \mu_{A_1' \times \cdots \times A_n' \to B'}(\mathbf{x}, z)] \tag{6.17}$$

The *defuzzifier* performs a mapping from the fuzzy sets $A_x \circ R_j$ in R to a crisp point in $z \in R$. This mapping may be chosen as weighted average centroid defuzzifier [41]:

$$z = \frac{\sum_{j=1}^{N} w_j \mu_{A_x \circ R_j}(w_j)}{\sum_{j=1}^{N} \mu_{A_x \circ R_j}(w_j)} \tag{6.18}$$

where w_j is the point in R at which $\mu_{B'}(z)$ achieves its maximum value (usually, we assume that $\mu_{B'}(w_j) = 1$).

6.3 Template Matching Technique

From the knowledge of human experts, we learn that the shape and phase information of indications are the basis for judging a flaw indication. In order to make the final decision on a possible flaw indication detected by the wavelet detection algorithm, a technique which can provide both the shape and phase information is needed. To achieve this objective, we developed a template matching technique. The original idea for the template matching technique came from the concept of a calibration standard. On a calibration standard tube, lots of artificial flaws are machined to provide a reference standard. We use the signals from the artificial flaws in the calibration tube as the templates. For a signal from a true flaw indication, it should have characteristics similar to one or more of the templates. To measure

the similarity between the flaw signal and the various templates, the complex correlation coefficient was calculated between each template and a candidate flaw signal, since it is an efficient way to provide a quantitative measurement. In our research, we chose the 100%TW, 80%TW, 60%TW, 40%TW, and 20%TW OD flaws to be templates.

The template matching technique performs a normalized crosscorrelation between the template and a possible flaw signal. The normalized cross correlation between the template signal $\{T_n\}$ and the flaw signal $\{F_n\}$ is defined as

$$\rho = \frac{\sum_n F_n T_n^*}{\left[\sum_n |F_n|^2 \sum_n |T_n|^2\right]^{1/2}}, \tag{6.19}$$

where $\{F_n\}$ must be aligned to compensate for the pulling speed difference between the calibration data and the inspection data. The alignment is based on the two antipolar peaks of a differential eddy current signal. The shape similarity is defined as the magnitude of the complex cross correlation coefficient ρ. It ranges from 0 to 1. The phase similarity is defined as the phase angle of the complex coefficient ρ. For example, suppose that ρ is equal to $a+ib$. Then, the shape similarity of this case is $\sqrt{a^2+b^2}$, while the phase similarity is $Cos^{-1}(\frac{a}{\sqrt{a^2+b^2}})$. For each template, a fuzzy membership function is used to map the phase angle to a phase similarity which has a value from 0 to 1. The shape of the membership function is different for every template.

The template matching technique consists of three steps: template setting, indication matching, and normalized crosscorrelation. The template setting step is used to build up the

template. The indication matching step accomplishes the time alignment between a possible flaw indication and the templates to remove differences in the pulling speeds. From the normalized crosscorrelation, we can obtain the phase difference between the template and the indication. Furthermore, we obtain a measurement of the shape similarity between the test data and the template from the cross correlation.

The template setting step is described as follows:

(1) Input the start and end locations of the templates.

(2) Calculate the mean in the window which is the average from the start to the end data points. The mean is then subtracted from each data point in the window.

(3) Calculate the magnitude of each data point in the window and find the peak with the largest magnitude.

(4) Search the second largest peak whose phase difference with the largest peak is also larger than $\frac{2\pi}{3}$.

(5) Sort these two peaks in time order. Let peak1 be the first peak and peak2 be the second peak in time order.

(6) Calculate the center point by summing the positions of two peaks and dividing the sum by 2.

(7) Find the boundary point of the template within the window between the peak2 point and the end point. The boundary point of the template is defined as the point whose magnitude is closest to one fifth of the magnitude of the peak2.

(8) Time scale the template to a new length of 127 data points and store the scaled template. The scaling is performed by using a linear interpolation method

described in section 4.3. The center point of the template is set to be the center point of the scaled template, while the boundary point of the template is set to be the end point of the scaled template. Note that we just copy the right half part of the template into the new window. The left part of the window is duplicated from the right half part of the template with inverted data values.

(9) Normalize the scaled template.

After the templates are set, we match the possible flaw indication with each template. The indication matching is accomplished by using the linear interpolation method. The details are described as follows:

(1) An approximate flaw indication location is obtained using the wavelet flaw detection algorithm. In a window centered at the approximate location, search for the two largest peaks and record their locations.

(2) Calculate the center point of the two peaks.

(3) Calculate the mean of the data values of the two antipolar peaks.

(4) Remove the offset of the data in the window by subtracting the mean obtained in (3) from the original data.

(5) Time scale the data in the window so that its two peaks match with those of the template.

After the data is matched with the template, a normalized crosscorrelation is then performed and the amplitude similarity and phase similarity are computed.

6.4 Fuzzy Inference System

6.4.1 Input and output of the system

The fuzzy inference system (FIS) includes two subsystems. One is used for flaw decision making and the other one is used to estimate the flaw size. They have two groups of inputs. The first group contains phase differences obtained from the template matching technique. Each phase difference input denotes the angular difference of the lissajous pattern of the test signal and the lissajous pattern of a particular template. Five templates were used at each frequency channel. In this project, three frequency channels, 200 kHz and 400 kHz and 600 kHz, are used Those templates are the signals from the 20%, 40%, 60%, 80%, 100% through-wall (TW) artificial outside-diameter flaws. The second group of inputs contains shape similarities obtained from the magnitude of the normalized complex crosscorrelations.

The output of the first fuzzy inference subsystem is the decision on whether a signal is a flaw signal, or not. The output of the second fuzzy inference system is the %TW penetration of the flaw, if the signal is classified as a flaw signal. The shape similarity inputs have a range from 0 to 1, since it is the absolute value of the normalized crosscorrelation. The phase inputs have a range from -180 degrees to 180 degrees. For each template, a fuzzy membership function is used to map the phase difference into a phase similarity which has a value from 0 to 1. The shape of the membership function is different for every template.

6.4.2 Block diagram of the system

The decision rules of the fuzzy classification subsystem are based on the following observations regarding the eddy current flaw signal: first, a flaw signal should have a shape similar to a template, thus its shape similarity should be close to 1. Because the five templates have similar shape, it follows that the five shape similarity inputs should all be high for a flaw signal. Second, at least one of the five phase difference inputs must be small for a signal to be qualified as a flaw signal, which is due to the fact that the five templates construct a sparse but complete grid in the percent through-wall space. Any flaw signal must have a phase similar to one or two templates.

The construction of the percent through-wall fuzzy inference system is based on the relationship between the phase of the signal and the percent through-wall penetration of the flaw. This relationship is a nonlinear mapping function and usually can only be decided experimentally. The only information about this function is contained in the five sample points given by the five templates. Since a fuzzy system with centroid defuzzification is a universal approximator, we can build an approximation of this function by using a fuzzy system and the information obtained from the five templates The fuzzy inference system is shown in Fig. 6.3.

6.4.3 Membership functions and learning

The membership functions used in this system are modified asymmetric trapezoidal fuzzy membership functions. The actual shape of the membership functions for the five shape similarity inputs were learned by using the distribution of the training data set in the

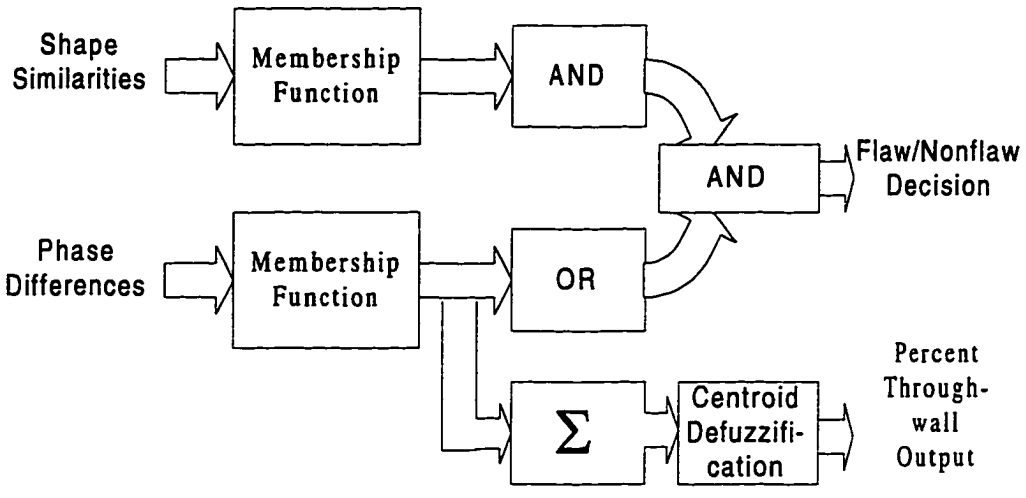

Figure 6.3 Block diagram of fuzzy inference system.

input feature space. Consider the shape similarity membership function shown in Fig. 6.4. Shape similarities are marked along the abscissa. The Os and Xs marked on the abscissa represent shape similarities for flaws and nonflaws, respectively. These values are obtained experimentally from data analyzed by experts. Os represent "called" flaws while Xs represent nonflaws. The shape similarity input is divided into three region. For region 1, where there are only flaw samples, the membership function has a value of 1. For region 3, where there are only nonflaw samples, the membership function has a value from 0.5 to 0. In region 2 where there are both flaw samples and nonflaw samples, the value of the membership function changes linearly from 1 to 0.5. To create the membership function, three reference points is used. The first reference point $R1$, which has the smallest shape similarity value as $S1$ of Os in region 1, is assigned to be the boundary point between region 1 and region 2 with membership value 1. The second reference point $R2$, which has the smallest shape similarity value as $S2$ of Os in region 2, is assigned to be the boundary point

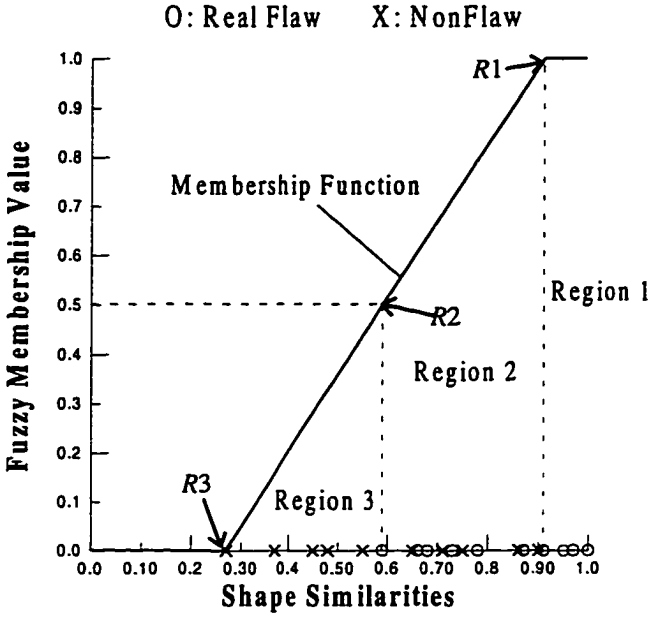

Figure 6. 4 Membership function of one shape similarity input.

between region 2 and region 3 with the membership value 0.5. A linear line is drawn from R1 through R2 till the axis of shape similarity. The cross point of linear line and the axis of shape similarity is defined as the third reference points $R3$ with the shape similarity value $S3$ and membership value zero. We express the membership function M as following equation

$$M(S) = \begin{cases} 1 & \text{if } S \geq S1 \\ \dfrac{S - S3}{S1 - S3} & \text{if } S1 > S \geq S3 \text{ with } S3 = S1 - 2(S1 - S2), \\ 0 & \text{if } S < S3 \end{cases} \quad (6.20)$$

where S is the input value of shape similarity.

The membership functions for the phase inputs have a triangular shape, which is a special case of the trapezoidal membership function. The shape of the input and output membership functions of the percent through-wall subsystem were established by using the calibration curve. In Figure 6.5, we show the input membership function of 40%TW

template. The top picture is the calibration curve. In this curve, the phase angles of 20%, 40%, 60%, 80%, 100% TW templates are 115°, 99°, 82°, 62°, and 40°, respectively. These were determined from the "standard" tubes. The triangle lying below the calibration curve is the input membership function of 40%TW template. Note that the horizontal axis of membership function is phase difference between the flaw candidate and the template. The input membership function of a template is obtained as follows: The triangle membership function is created by using three points: center, right boundary and left boundary points. The center point, which corresponds to the phase angle of the template, has 0 degrees in the axis of the phase difference. The right boundary point is defined as the phase difference between the template and its right adjacent template, while the left boundary point is defined

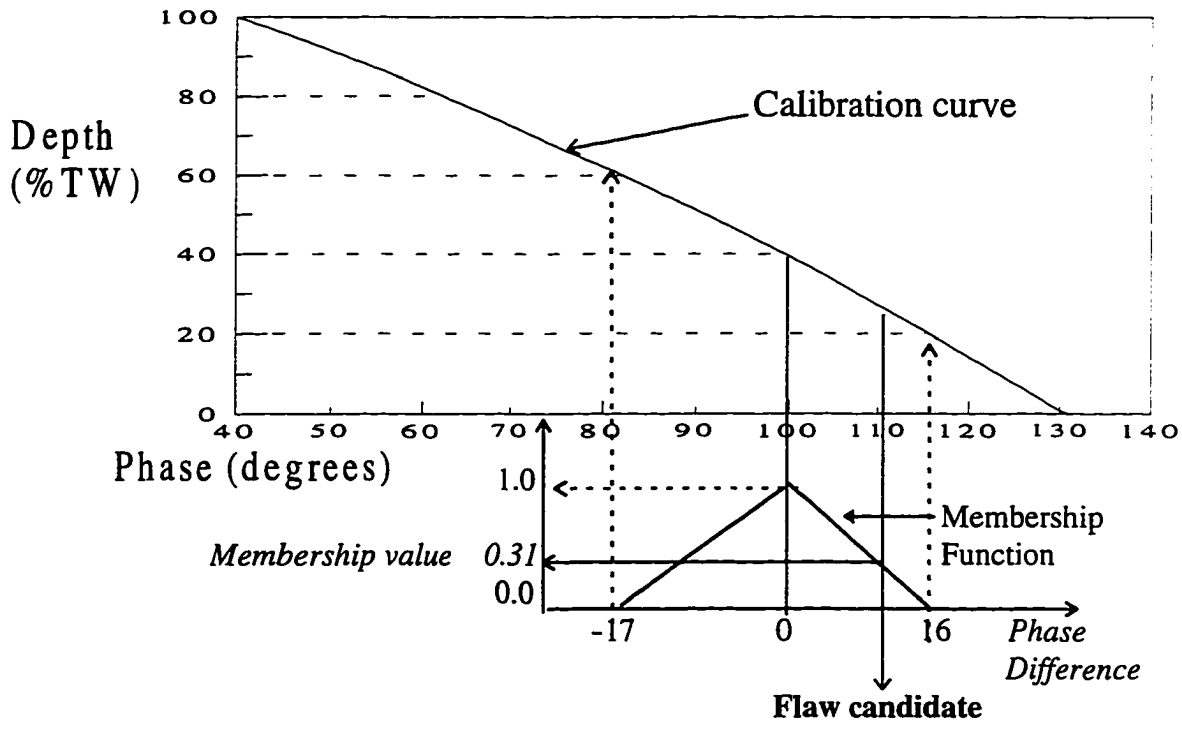

Figure 6.5 The input membership function for phase of 40%TW template.

as the phase difference between the template and its left adjacent template. Then we assign the center point with membership value 1.0 and the two boundary points with a membership value 0.0. As the point between the center and two boundary points, the value of the membership function changes linearly from 1 to 0.0. The membership value of point, which is outside the two boundary points, is set to be zero.

In this case of 40%TW template with phase angle 99°, its right adjacent template is 20%TW template with phase angle 115° and its left adjacent template is 60%TW template with phase angle 82°. The right boundary point is the difference between 115° and 99°, while the right boundary point is the difference between the 82°and 99°. Therefore, the values of center point, right boundary point and left boundary point in axis of phase difference are then 0, 16 and -17, respectively. We obtain the triangle membership function of 40 %TW template displayed in the bottom of Fig. 6.5. Suppose that a flaw candidate has phase angle 110. The phase difference between the flaw candidate and the 40 %TW template is 11. Through the membership function, we obtain the membership value 0.31.

The output membership function for phase of 40%TW template is shown in Fig 6.6. The creation of the output membership function is similar to the creation way of the input membership function. The horizontal axis of output membership function is depth (%TW). The triangular shape membership function is used. We define the center point as the %TW of the template itself. The right boundary point is the %TW of the right adjacent template, while the left boundary point is the %TW of the left adjacent template. Then we assign the membership value same as what we did in the input membership function.

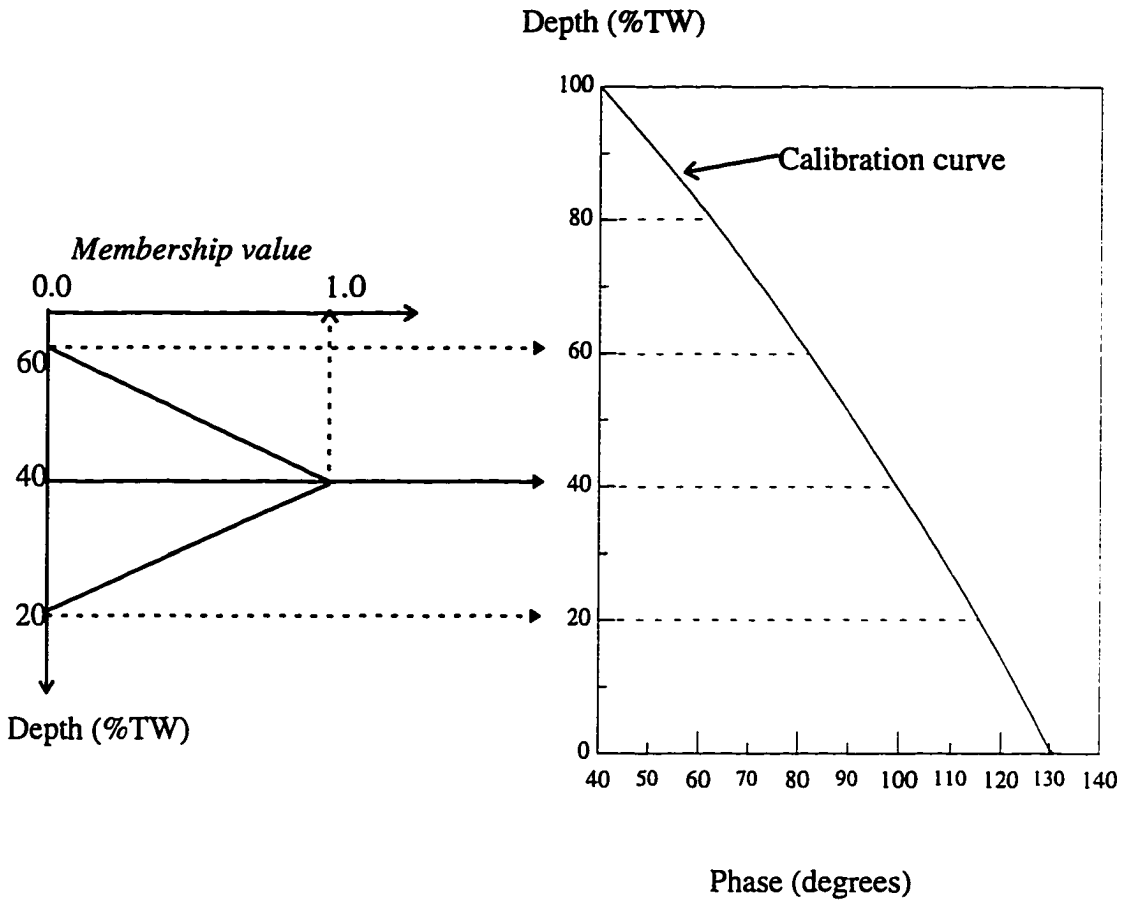

Figure 6.6 The output membership function for phase of 40% TW template.

An example of the membership functions for all inputs and outputs in the 400 kHz frequency channel is shown in Fig. 6.7. The input and output membership functions are drawn along axis. Note that the 100% TW template doesn't have an equal triangular membership function but a half equal triangular membership function. This is due to the satisfaction of the boundary condition of the calibration curve. An OD flaw must have a phase angle larger or equal to 40°. For different frequency channel, it will have different calibration curve so that the membership function would be changed according to the

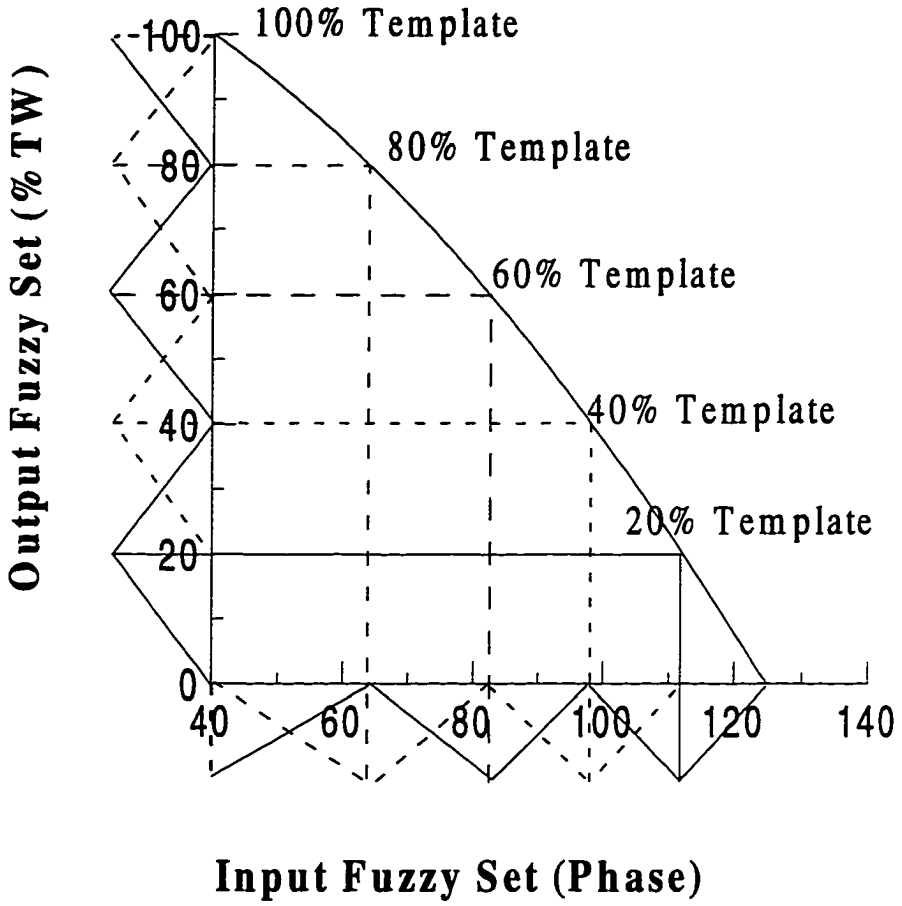

Figure 6.7 The membership functions of all inputs and outputs for an 400 kHz channel.

calibration curve. However, the shape and the design of the membership function are the same for different frequency channel.

6.4.4 Implementation of fuzzy inference system

In this section, we discuss how to implement the fuzzy inference system. According to the block diagram of Fig. 6.3, we have two subsystems in the fuzzy inference system. In subsystem 1, we make a flaw/nonflaw decision based on the output membership value (which is defined as an output membership value larger than 0.5). In subsystem 2, we calculate the

%TW if the possible flaw indication is judged to be a true flaw indication. The procedure for computing the outputs of the fuzzy system is described as follows:

(1) Fuzzy inputs: The inputs (shape similarities and the phase differences) from the template matching technique are fuzzifed. We map the inputs to be the membership values of each of the appropriate fuzzy sets (templates) via its corresponding membership function.

(2) Apply fuzzy operator: For the shape similarity part, we apply the minimum operator to obtain one shape output membership value. For the phase difference part, we apply the maximum operator to obtain one phase output membership value.

(3) Apply implication (or Inference) method: For the subsystem 1, we use the minimum implication method. The output membership value is the minimum of the shape output and the phase output in step 2.

(4) Make flaw/nonflaw decision: for regions outside the TSP, steps 1 to 3 are applied on three differential channels. If the output membership value of the 400 kHz channel is larger than 0.5 and the output membership values of the 200 kHz and/or 600 kHz are larger than 0.5, we conclude that possible flaw indication is a true flaw. If the output membership value of the 400 kHz channel is smaller than 0.5, we conclude that the indication is a nonflaw. There is one special case: an indication having a shape similar to the templates but having a phase that is not within the phase range of the calibration curve. Such an indication is called nonqualified indication (NQI). In such a case, we use the output of the phase subsystem and the output of the shape subsystem to make the final decision. We define an indication as NQI if it has an output shape membership value

larger than 0.8 at 400 kHz and 200 kHz and 600 kHz channels, while its output phase membership value is smaller than 0.5 in all the frequency channels.

(5) Calculate %TW: If an indication is judged to be a flaw, we calculate the %TW of the indication on the main testing frequency channel (400 kHz channel). The calculation of %TW is formulated as following

$$\%\text{TW} = \sum_{i=1}^{5} (\text{Phase of template } i \times \text{Membership value of template } i)$$

where $i = 1, 2, 3, 4, 5$ corresponds to 100%, 80%, 60%, 40%, and 20% TW templates.

An example of the fuzzy inference system on an 400 kHz frequency channel is shown on Fig. 6.8. In this example, templates No. 1, 2, 3, 4, and 5 correspond to the %TWs of 100%, 80%, 60%, 40%, and 20%, respectively. The inputs are obtained from the template matching technique. The output is one membership value. Note that we use three frequency channels to make the flaw decision. If it is a flaw, we calculate the percent through-wall on the 400 kHz frequency channel only.

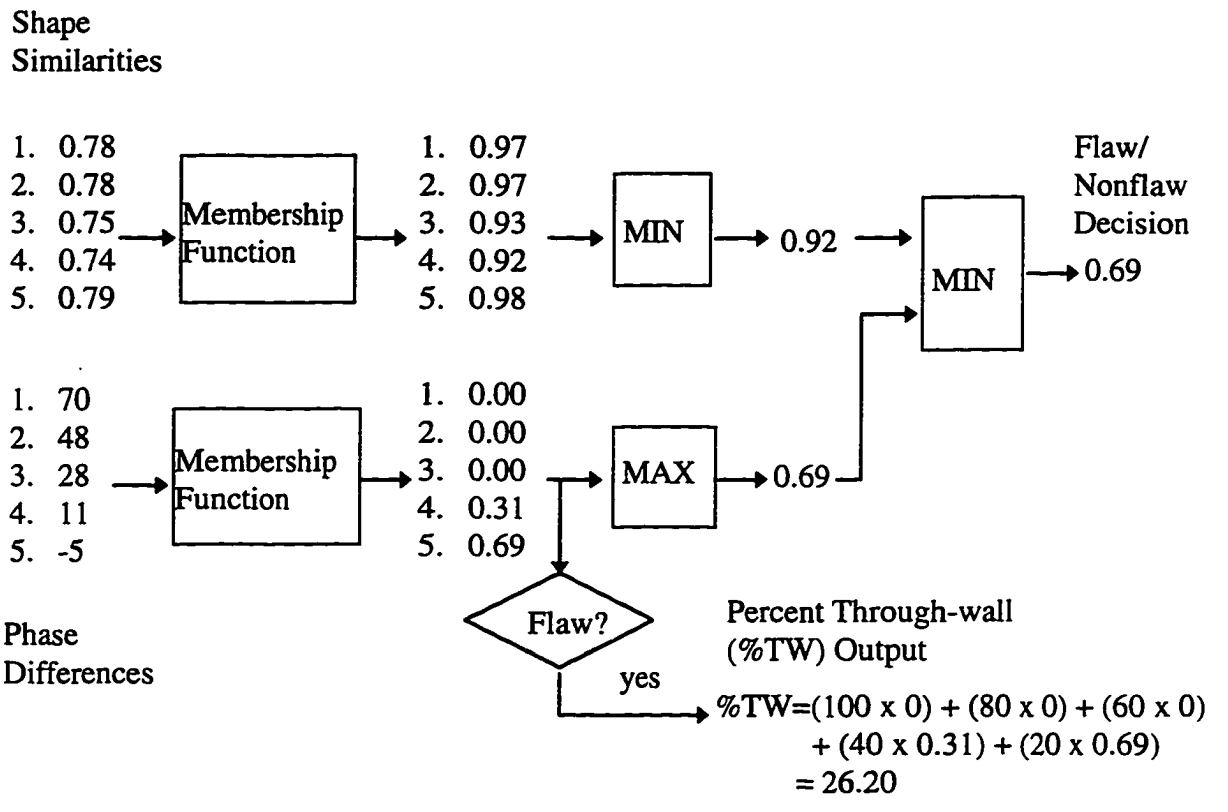

Figure 6.8 An example of the fuzzy inference system on an 400 kHz frequency channel.

CHAPTER 7. RESULTS AND DISCUSSION

We developed an eddy current signal processing system for automatic eddy current data analysis and flaw characterization by comparison with the judgment of a human expert. In addition to the development of the detection system, a great deal of effort was devoted to testing in order to obtain a mature and optimized automatic detection system. By doing such tests, we wished to evaluate the detection capability and the strengths and weaknesses of our flaw detection system. A rigorous testing of the eddy current signal processing system was therefore accomplished. Also, from the test results we gained a deeper understanding of the flaw characteristics and typical noise, which provided us with very practical knowledge for defining future research directions of this project and gave us a clear and long-standing motivation to achieve our goal. In this chapter, we first describe the processing procedures of the automatic detection system so that one can understand how the system is operated. The results of the tests of the processing procedures are shown next. Detailed tables of the testing results are attached as an appendix. A discussion of the testing results follows.

7.1 Processing Procedures of the Automatic Flaw Detection System

A software package has been developed for automatic analysis of data collected in steam generator tubing by eddy-current measurement. This program is automatic in the sense that, when given a raw set of eddy-current data, the package undertakes a multitude of analysis procedures and identifies possible candidate indications, including locations, with no

interaction from an operator other than initiating execution of the package. The goal of the package is to provide an accurate, consistent and efficient automatic data analysis package to aid the human analysts. The human interaction with the software package has been minimized to a few input parameters : input file name, year type, leg type, and the locations of templates and TSP. After the input parameters are given to the system, the computer can provide independent analysis results which can be compared to the results of traditional human analysis. The processing procedures for this package are described in details as follows:

(1) Data Input: the input parameters include data file names, calibration data file names, data year type (old/new), leg type (inlet/outlet), locations (start and end positions) of templates, and locations (start and end positions) of broached TSP in each calibration tube.

(2) Configuration setting: all the data sets are set to be inlet type and the data headers are removed. The inlet setting is to ensure that the processing of data sets refers to the same time direction. If the input data is outlet type, we reverse the time order of data and flip the data values. The input data consists of two parts. One is the data header which records inspection information such as test frequency, probe type and so on. The other part is the acquired raw data which are the recorded impedance responses of the probe in the tube. To process the data, we have to decode the data header first.

(3) Initial setup: three steps need to be carried out in this procedure. These steps include phase rotation, mixing, and calibration curve setup. Note that we apply these three steps to the calibration data. The phase rotation factors and the mixing factors are recorded so that they can be applied on the preprocessed raw data later.

(4) TSP detection: the TSPs of each of the data sets are detected by using the TSP detection algorithm. The positions of detected TSPs are output to the computer screen for further evaluation to verify proper operation of the TSP detection algorithm.

(5) Data alignment: the data points of the new data set are aligned to the old data set by aligning corresponding tube support plate signals and interpolating the data so that the same number of data points exist between corresponding tube support plates.

(6) Background removal: the backgrounds of the old data set and the new data set are fitted by using a second order polynomial fitting method. Then the fitted backgrounds are subtracted from the raw data. This is used to eliminate the variation in signal background due to probe lift-off, variation in tube wall thickness, etc. The phase rotation factor is then applied to the background removed raw data. The mix channel is also established at this time.

(7) Wavelet flaw detection: the wavelet flaw detection algorithm is used to identify candidate flaws. It consists of four routines: fast wavelet transform, extrema algorithm, denoising procedure and transient identification algorithm. There are some adjustable parameters in the denoising procedure and the transient detection algorithm. For the denoising procedure, the values of the denoising thresholds vary according to the test frequency and the resolution level in the wavelet domain. In the transient detection algorithm, the parameters define the range of acceptable distance between two antipolar peaks. We set the lowest distance to be 3 and the greatest distance to be 15. In the region outside TSP, the wavelet detection algorithm is applied to the imaginary part of the preprocessed data of three differential channels (the 200, 400, and 600 kHz channels). For

the TSP region, the algorithm is applied to the imaginary part of the mix channel. We output the positions of the detected possible flaw indications onto the screen.

(8) Multiple frequency analysis: this process is used to reduce the number of false calls made by the wavelet flaw detection algorithm. From expert knowledge, we learned that a real flaw should show up on 400 kHz, and 200 kHz and/or 600 kHz frequency channels. Therefore, we apply this rule in our algorithm. However, this rule applies only for regions outside the TSP. For regions inside the TSP, we use the auxiliary algorithm (described in section 5.5.5) to reduce the number of false calls.

(9) Template matching technique: this technique is used to provide phase and shape features for the subsequent fuzzy inference system to evaluate the flaw candidates. The positions of the flaw candidates are inputs to this process. The templates are created first and then each candidate flaw signal is matched to the templates. A normalized crosscorrelation between the candidate flaw signal and each template is performed to obtain two parameters: shape similarity and the phase difference. Note that the template matching technique is applied on three high frequency channels in the region outside TSP and on the mix channel in the TSP region. Five templates are used for each frequency channel.

(10) Fuzzy inference system: the fuzzy inference system combines all the shape and phase information obtained from the template matching technique and output membership values for decision making. First, we assign the membership values to the shape and phase similarities obtained from the template matching procedure. Then the membership values are combined according to fuzzy rules created in this process.

(11) Detection criteria: This procedure is used to determine whether a candidate flaw is a true flaw or not. Different criteria are applied according to the locations of the candidate flaws. For regions outside TSP, if the output membership value at 400 kHz is larger than 0.5 and the output membership values at 200 kHz and/or 600 kHz are larger or equal to 0.5, the indication is considered a true flaw. If the output membership value at 400 kHz is equal to 0.5 and the output membership values of 200 kHz and/or 600 kHz are larger or equal to 0.5, the indication is said to be a non-qualified indication (NQI). Any memberships values other than above those defined above are judged to be nonflaws. For the TSP region, if the output membership value of the mix channel is larger than 0.5, then the indication is a true flaw. If the output membership value is equal to 0.5, it is a non-qualified indication.

7.2 Results of Testing

To evaluate the performance and determine the strengths and weaknesses of the automatic detection system, a rigorous testing procedure was performed. 100 heat-exchanger tubes (183 data sets) were tested by using the processing procedures in section 7.1. The test samples were provided by Framatome and were also evaluated by human inspectors. The parameters for the denoising procedure are listed in Table 7.1 A summary of test results is listed in Table 7.2 and Table 7.3. Details of the test results are given in the appendix.

The definition of each key word in Tables 7.2 and 7.3 is listed below:

1. Wavelet = The test results after applying wavelet detection algorithm and multiple frequency analysis.

Table 7.1 Denoising threshold values applied on the testing.

	Denoising threshold value		
	200 kHz Channel	400 kHz Channel	600 kHz Channel
Resolution 1	2.0	4.0	6.5
Resolution 2	2.5	8.0	10.0
Resolution 3	4.0	8.0	12.0

2. FIS = The test results after applying fuzzy inference system and detection criteria.

3. Human Analysis = The analysis results of human inspectors.

4. Missed Call = Indications called by human inspectors but not identified by the FIS.

5. Out. TSP = Indications located outside TSP region.

6. In. TSP = Indications located inside TSP region.

7. T = True positive indications called by human inspectors.

8. NQI = Non-qualified indication given by human inspector.

9. F = False positive indications not called by human inspectors.

10. T* = Possible true positive indications not called by human inspector.

Table 7.2 Summary of test results on true flaw indications.

	Wavelet				FIS				Human Analysis				Missed Call			
	Out. TSP		In. TSP		Out. TSP		In. TSP		Out. TSP		In. TSP		Out. TSP		In. TSP	
	T	NQI	T	NQI	T	NQI	T	NQI	T	NQI	T	NQI	T	NQI	T	NQI
Total No.	89	21	58	24	82	15	57	21	96	27	64	27	14	12	7	6
Sum	**192**				**175**				**214**				**39**			

Table 7.3 Summary of test results on nonflaw indications.

	Wavelet				FIS			
	Out. TSP		In. TSP		Out. TSP		In. TSP	
	F	T*	F	T*	F	T*	F	T*
Total No.	**1022**	**17**	**213**	**3**	**259**	**13**	**131**	**3**

7.3 Discussion

The evaluation of the testing is based on the results of human analysis. Although the results of human analysis is not guaranteed as 100% correct, its reliability is very high for an analysis obtained from experienced experts. So we still use the results of human analysis as a reference and compare our test results with them. Table 7.2 shows the summary of test results on true flaw indications. We categorize our test results according to the test processes (wavelet and FIS), flaw location (outside TSP and inside TSP) and flaw type (true flaw indication and non-qualified indication). The two columns, *human analysis* and *missed call,* in table 7.2 are provided for comparison and reference. In table 7.2, we see that the human inspectors identified 214 flaws in the 183 data sets. The wavelet detection algorithm found 192 flaws among the 214 flaws so that it can detect *90.1%* of the flaws identified by human inspectors. After the FIS system was applied, most of the flaws called by the wavelet detection algorithm and identified by human inspectors were confirmed by the FIS system. The FIS detected 175 flaws among the 214 flaws so we obtain *the successful detection rate* as *81.8%.*

Table 7.3 illustrates the effect of FIS for reducing false calls. The wavelet detection algorithm totally found 1022 false calls in regions outside the TSPs on the 183 data sets. Through the use of FIS, the false calls are reduced to be 259. Only one quarter of the false

calls are retained. The effect of FIS on reducing false calls is significant although some true flaws identified by wavelet detection system were dropped by FIS too. Note that a special symbol T* is used in table 7.3. In our preliminary tests, we found some indications which were originally not called by the human inspector. To further identify these indications, they were reviewed again by an expert. Some of these indications were determined to be true flaws. For these missed true flaw, we use T* to denote them.

To gain a deeper understanding of the weakness of the system, we traced and analyzed all the missed calls. Some limitations of the wavelet detection algorithm and the weaknesses in the design of the automatic flaw detection algorithm were discovered. However, based on the test results, the overall performance of the system is still satisfying. The *CPU execution time* of the program for two data sets is about *2:00 minutes on DEC 5000*. Usually each data set contains 25000 data points.

An example of comparing two data sets is described as below to demonstrate the system's capability on the data comparison : In tables 7.4 and 7.5, we show the test results of year 1 and year 2 data sets which are inspected from the same tube over different time. Four possible flaw indications (A, B, C, and D) were identified by the wavelet detection algorithm in table 7.4. Through the use of FIS, the system outputs each flaw candidate's time *position*, physical *location* and their *membership* value on each test frequency. If the flaw candidate is determined to be a flaw according to the detection criteria, the %TW of the flaw candidate is calculated. In this case, only flaw candidate B is identified and judged to be NQI. *Computer* and *Human* in table 7.4 are used to denote the results of our detection system and human analysis. The symbol $\surd$ on Computer indicates that the flaw candidate is identified to be a

Table 7.4 The test results of year 1 data set for comparing two data sets inspected from same tube.

Flaw	Position	Location	Membership				%TW	Computer	Human
			400 kHz	600 kHz	200 kHz	Mix			
A	22025	14 th TSP 2.06	0.56	0.00	0.00				
B	23067	14 th TSP 30.73	0.50	0.00	0.59		NQI	√	√
C	23153	15 th TSP -1.89	0.00	0.00	0.00				
D	23172	15 th -1.37	0.00	0.00	0.00				

Table 7.5 The test results of year2 data set.

Flaw	Position	Location	Membership				%TW	Computer	Human
			400 kHz	600 kHz	200 kHz	Mix			
B	23071	14 th TSP 30.84	0.60	0.63	0.61		28	√	√
D	23175	15 th TSP -1.29	0.00	0.00	0.00				

flaw by the flaw detection system, while the symbol √ in the Human column indicates the flaw candidate is a true flaw identified by a human inspector. In table 7.5, two flaw candidates (B and D) were found and flaw candidate B was identified to be flaw. By comparing the detected flaw on year 1 and year 2 data sets, we see that flaw B shows both on year 1 and year 2 data sets. Also the flaw grows from an NQI to be 28%TW.

To understand the detection probability of our automatic flaw detection system, we further analyzed the distributions of flaws identified by human inspectors and then analyzed how many flaws called by human inspector are identified by our system. So we can obtain a histogram of the detection probability. The analysis of a flaw's distribution is based on the

flaw's depth (or %TW). We divide the %TW of the flaws into 14 regions. The relationship between the %TW of flaw and region is defined by the following equation:

$$Flaw's\ Region = \begin{cases} i & if\ 5\times(i-1) < \%TW\ of\ flaw \le 5\times i,\ 1 \le i \le 12, \\ 13 & if\ 60 < \%TW\ of\ flaw \le 100, \\ 14 & if\ flaw\ is\ NQI. \end{cases}$$

According to the flaw's region, the results of the analysis on *Human* (which denotes the flaws identified by human inspector) and *System* (which denotes the flaws identified by automatic flaw detection system) are shown in table 7.6. A histogram of detection probability based on the analysis results is obtained and shown as Fig. 7.1. In Fig. 7.1, we only use the flaws belonging to region 1 through region 13 (or 0%TW to 100%TW) for showing the relationship between the flaw's depth (or %TW) and the detection probability of our system. Note that the NQI type flaw is not used in the histogram. The detection probability vs. %TW is calculated from following equation:

$$Detection\ probability\ from\ region\ 13\ (or\ 100\ \%TW)\ to\ region\ i\ (or\ 5\times i\ \%TW)$$

$$= \frac{\sum_{n=i}^{13} total\ no.\ of\ flaws\ in\ Region\ n\ of\ System}{\sum_{n=i}^{13} total\ no.\ of\ flaws\ in\ Region\ n\ of\ Human}.$$

Table 7.6 The analysis results of flaw distribution.

	Region													
	1	2	3	4	5	6	7	8	9	10	11	12	13	14
Human	9	19	13	23	14	27	18	15	8	6	2	1	4	55
System	5	13	13	23	12	23	17	14	7	6	2	1	4	38

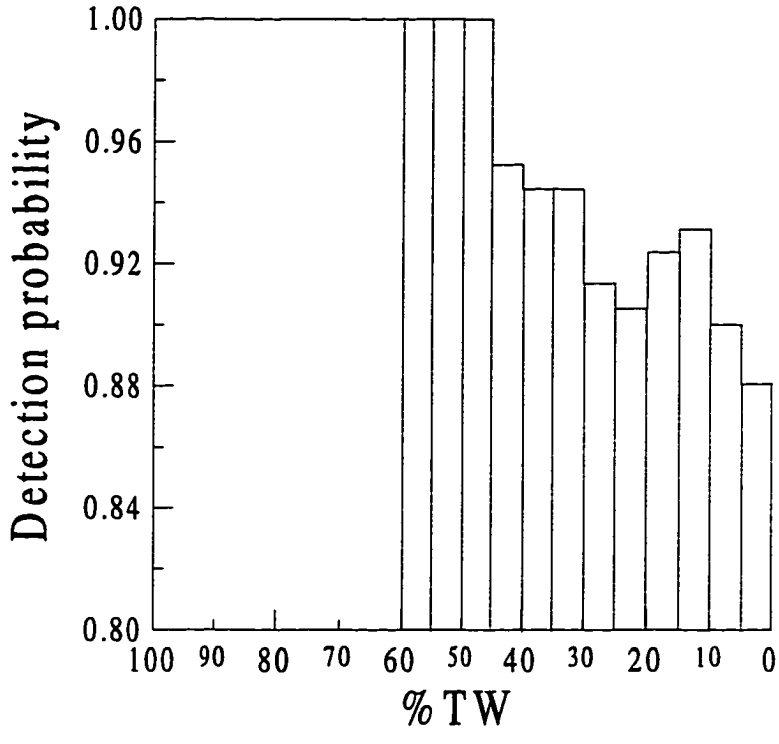

Figure 7.1 The histogram of detection probability.

In Fig. 7.1, we see the detection probability drops in the regions from 45%TW to 20%TW but increases again from 20%TW to 10%TW. This is due to not adequate test samples so that the flaw distribution is not uniform and the detection probability is not monotonically decreasing. However, from table 7.6 and Fig. 7.1, we see that the system can achieve detection probability above 0.91 for flaw's depth larger than 10%TW. For flaw depth below 10%TW or NQI type flaw, the detection probability drops. This is desirable for tiny flaws and many other reasons. Detailed reasons for the missed calls are studied and summarized as follows: There are three major reasons for the misses caused by the wavelet detection algorithm.

(1) Inconsistency in human analysis

This includes flaw indications which were called by the human inspector but not called by the detection system. Also, these flaws may have been called in the previous year's data but not called later by human inspectors. This type of flaw indication may be very small in magnitude and distorted in shape. In the wavelet domain, they don't satisfy the criteria of the transient detection algorithm. That is due to the fact that the flaw doesn't show up on all the first three resolutions in the wavelet domain. Due to the denoising procedure applied before the transient detection algorithm, the antipolar peaks of these flaws may be removed owing to their small wavelet coefficients. Another possibility is that the flaw is just a nonflaw signal distorted by noise and has a shape similar to a flaw.

(2) Limitations of the wavelet detection system

There are two major limitations of the wavelet detection system. The first one is that the shape of the mother wavelet is not effective for analyzing some types of flaw. The second limitation comes from incomplete removal of background signals in the data. This issue is further discussed in the next section.

(3) Difficulties at TSP regions

In the TSP regions, we use the auxiliary algorithm discussed in section 5.5.5 to help reduce the number of false positives. However, a tradeoff must be made between the probability of detection and the number of false positives. Several true flaws were dropped by the special criteria because one of the two peak's amplitude was below the amplitude threshold. This distortion in a flaw signal is due to the less-than-ideal suppression of the tube support signal by the mixing algorithm. To solve this problem, some other features (such as

phase information) could be added to improve the probability of detection of small flaws and to allow the amplitude threshold to be lowered.

As for the flaws called by the wavelet detection algorithm but dropped by the fuzzy inference system, there are three major reasons:

(1) Limitations of the background removal algorithm

Since the background removal algorithm used in template matching can not ideally remove the DC offset in the data, the template matching technique tends to find the wrong peaks in the data. This results in wrong phase and shape information provided to the fuzzy inference system so that the fuzzy inference system misjudges some real flaws to be false positives. A further discussion about the DC offset problem is given in the next section.

(2) Inconsistency of multiple channel information

In the fuzzy inference system, we required that the output membership values must be larger than 0.5 on two or three frequency channels for a true flaw indication. Due to noise and residual background signal, the template matching technique may find wrong peak locations for a flaw indication. The result is that a true flaw indication may have just one channel with output membership value larger than 0.5. In such a case, we might attach a special warning message to the output results of the fuzzy inference system if there is only one channel having output membership value larger than 0.5

(3) Uncertainties in NQI calls

In the fuzzy inference system, an NQI type flaw is defined as an indication having an output shape membership value larger than 0.8 but the phase membership value is smaller than 0.5 on two or three frequency channels simultaneously. To avoid the possibility of

creating a lot of false positives, we do not want to change this rule. Therefore, there are a lot of uncertainties in NQI calls.

7.4 Limitations of the Wavelet Flaw Detection System

From the test results, we found two major limitations of the wavelet detection algorithm. One is the natural limitation on the shape of the mother wavelet and the other one is the limitation of the background removal algorithm. During the test, we found that one special type of flaw, code-named "WAR"(*wear*), cannot be detected by the wavelet detection system. The *wear* type flaw is caused by the mechanical wear of the tube (fretting) and most of these appear in TSP regions. This type of flaw signal has a very irregular shape and is very different from ordinary OD flaw signals, which have a shape similar to the Mallat mother wavelet. The wear type flaw has a larger amplitude and a longer time width in the mix channel. For a human's eye, it is very easy to discriminate such flaws from normal data. However, our automatic flaw detection system utilizes the shape similarity between the Mallat mother wavelet and the differential flaw signal to identify potential flaws. This means that a flaw can be ignored if the flaw doesn't have a shape similar to the Mallat mother wavelet. To solve this type of problem, another algorithm aimed specifically to this type of flaw needs to be investigated. This can be done by looking into a larger scale of wavelet resolution or using other features to characterize such type of flaws.

The other limitation comes from the fact that, due to noise interference signals, the background (or DC) removal is not always performed very well. As a human being, we can easily filter out the background signal under various data conditions. However, it is not very

easy to develop an automatic processing routine to eliminate all the background signals under various noise conditions. Among our failed cases, there was an example of a triple flaw combination as shown in Fig. 7.2 and missed by the wavelet detection algorithm. Due to the superimposition of the three flaw signals, two of the flaw signals have a DC offset caused by the third flaw signal, which is the strongest among the three. In the wavelet detection algorithm, we assume that the background of the data is perfectly removed so that the wavelet detection algorithm can transform the preprocessed data into the wavelet domain without distortion. However, in this case, two of the flaws had less than ideal flaw shapes since they have one larger peak and one smaller peak due to the effect of the background signal. The result is that the smaller peak is treated as noise by the wavelet detection algorithm for its smaller wavelet coefficients. We need to add some other features to further improve the probability of detection for such multiple flaws so that this type of flaw will not be dropped by the wavelet detection algorithm.

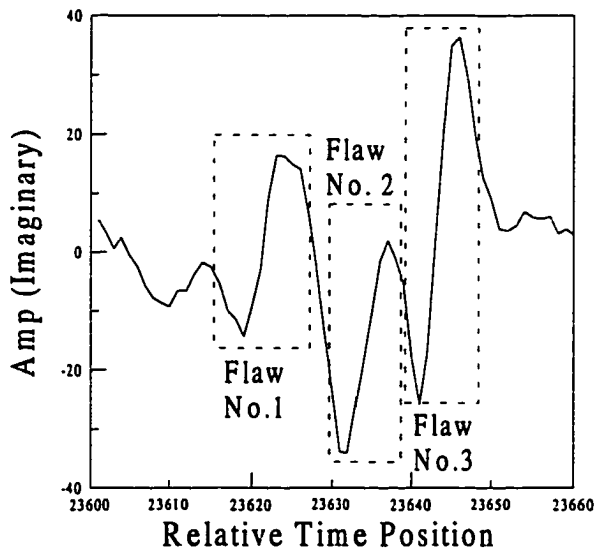

Figure 7.2 A triple flaw combination illustrating the limitation of background removal.

CHAPTER 8. SUMMARY AND FUTURE WORK

In this chapter we summarize the research work presented in this dissertation. Future research directions are proposed for improving the performance of the system and increasing the capability of the system.

8.1 Summary of the Research

A new approach, based on wavelet analysis followed by a fuzzy logic classifier, for automatic flaw detection using eddy current steam generator tubing data was investigated. The automatic flaw detection system consists of three stages: signal preprocessing, wavelet identification of flaw indications, and defect evaluation. To provide consistent and reliable analysis results, a signal preprocessing procedure was developed. It consists of three steps: set-up procedure, data alignment, and background removal. The set-up procedure uses a calibration standard to adjust the test data to a common reference standard. The data alignment procedure aligns two data sets to provide a comparison basis in time. The background removal removes slowly varying signals due to liftoff changes and tube inside diameter variations.

In stage 2, a wavelet flaw detection algorithm is used to detect possible flaw indications. Flaw signals and noise have different characteristics in the wavelet domain. Based on these characteristics, we designed the wavelet flaw detection algorithm to distinguish the flaw signal from noise. Four procedures were used to accomplish the detection task. These procedures include fast wavelet transform, extrema algorithm,

denoising procedure, and transient detection algorithm. The fast wavelet transform carries out multiresolution analysis by decomposing signals using Mallat's quadratic spline mother wavelet. The extrema algorithm extracts local extrema which correspond to sharp variation signals to remove redundancy. The denoising procedure trims the list of extrema for filter out noise components. The transient detection algorithm combines information in various resolutions and applies rules derived from the characteristics of flaw signals in the wavelet domain to detect possible flaw indications.

In stage 3, a fuzzy evaluation system is used to further evaluate the flaw candidates and to make final decisions. The fuzzy evaluation system consists of two parts: the template matching technique and the fuzzy inference system. The template matching technique provides shape and phase features for the fuzzy inference system by crosscorrelating the flaw candidates with the templates obtained from the calibration standard. The fuzzy inference system combines all the features and applies fuzzy rules abstracted from expert knowledge to determine whether or not a flaw indication is a true indication.

A rigorous test of the eddy current automatic flaw detection system was performed to evaluate the capability and reliability of the system. From the test results, we assessed the strengths and the limitations of the system. We concluded that the eddy current automatic flaw detection system holds great promise for automatically detecting flaw indications and offering a comparison between two data sets collected from the same tube at different times.

8.2 Future Work

The general problem of automatic eddy current data analysis for steam generator tube inspection is a very complex problem due to the variability of the noise and interference signals under different inspection conditions. The diffusive nature of the eddy current technique brings further difficulties in the data analysis task as many unwanted signals from probe wobble and dents have similar shape to the defect signal. Although our testing results have shown the potential of the automatic flaw detection system, a practical and reliable industrial solution requires further research and development in this area.

One area that merits further study is advanced signal processing techniques to further reduce noise and unwanted signals. In our early research we have applied some simple signal processing techniques, such as polynomial background removal and median filtering to remove both slowly varying and fast varying signals. However, those traditional signal processing techniques are inefficient when the noise or unwanted signals have similar shape and time width as the flaw signal. To deal with this problem, we need to study some new techniques that may be able to further improve the signal-to-noise ratio of the inspection data. Several such techniques are the spline smoothing [42], principal component analysis [43-46], and autoregressive moving average time series analysis.

Another goal of future research is to improve the mixing algorithm. Because most defects occur at or near the support plate structure, the performance of the mixing algorithm is critical to the quality of the data analysis. Because eddy current phenomena are highly nonlinear, the combined signal of the defect and the support plate structure is very complex. Our previous experience with the linear mixing algorithm and simple nonlinear mixing

algorithms has shown that these methods cannot provide satisfying results in some cases. One important problem associated with these methods is that, as the generator becomes old, the support plate structure itself changes due to wear and deposits. The structural change of the support plates changes the signature of the support plate signal. However, such changes cannot be correctly predicted by using traditional mixing methods. One possible approach is to use a neural network to model the complex nonlinear mapping from the support plate signal in a low frequency channel to the support plate signal in a high frequency channel. It is hoped that the neural network model would give a better representation of such nonlinear mapping and thus give a better predicted support plate signal.

The third area for future work is to integrate new processing techniques and more expert knowledge into an expert system which is based on the fuzzy inference system. Such integration requires comprehensive tests and comparisons of the techniques under study and the optimization of processing parameters according to inspection instrument and data quality. The major component of the expert system is the fuzzy inference system. To make it easy to use, the expert system should provide knowledge-based inference routines and learning algorithms to generate the optimal processing parameters in various stages of processing such as the denoising threshold in wavelet detection algorithm.

APPENDIX A: TEST RESULTS OF STEAM GENERATOR UNITS A AND B OF OCONEE

In this appendix, Details of the test results of steam generator units A & B of Oconee are described in Table A and B, respectively. The definition of each key word in Table A and B is listed below:

1. Wavelet = The test results after applying wavelet detection algorithm and multiple frequency analysis.
2. FIS = The test results after applying fuzzy inference system and detection criteria.
3. Human Analysis = The analysis results of human inspectors.
4. Missed Call = Indications called by human inspectors but not identified by the FIS.
5. Out. TSP = Indications located outside TSP region.
6. In. TSP = Indications located inside TSP region.
7. T = True positive indications called by human inspectors.
8. NQI = Non-qualified indication given by human inspector.
9. F = False positive indications not called by human inspectors.
10. T* = Possible true positive indications not called by human inspector.

Table A Test results of steam generator unit A of Oconee

	Wavelet				FIS				Human Analysis				Missed Call			
	Out. TSP		In. TSP		Out. TSP		In. TSP		Out. TSP		In. TSP		Out. TSP		In. TSP	
Tube No.	T	NQI	T	NQI	T	NQI	T	NQI	T	NQI	T	NQI	T	NQI	T	NQI
001i002	1	0	0	0	1	0	0	0	1	0	0	0	0	0	0	0
001h002	1	0	0	0	1	0	0	0	1	0	0	0	0	0	0	0
003i011	1	1	0	0	1	1	0	0	1	1	0	0	0	0	0	0
003h011	1	0	0	0	1	0	0	0	1	0	0	0	0	0	0	0
004i012	0	0	0	1	0	0	0	1	0	0	0	1	0	0	0	0
004h012	0	0	0	0	0	0	0	0	0	0	1	0	0	0	1	0
005i002	0	0	0	0	0	0	0	0	1*	0	0	0	1*	0	0	0
005h002	2	0	0	0	2	0	0	0	2	0	0	0	0	0	0	0
009o062	0	1	0	0	0	0	0	0	0	1	0	0	0	1	0	0
009h062	2	1	1	0	2	1	1	0	2	1	1	0	0	0	0	0
014o037	1	0	0	0	1	0	0	0	1	0	0	0	0	0	0	0
014h037	1	0	0	0	1	0	0	0	1	0	0	0	0	0	0	0
017i006	0	0	0	2	0	0	0	2	0	0	0	2	0	0	0	0
017h006	0	0	2	0	0	0	2	0	0	0	2	0	0	0	0	0
024i044	0	0	1	0	0	0	1	0	0	0	1	0	0	0	0	0
024h044	0	0	1	0	0	0	1	0	0	0	1	0	0	0	0	0
025o001	1	1	0	0	1	1	0	0	1	1	0	0	0	0	0	0
025h001	2	0	1	0	2	0	1	0	2	0	1	0	0	0	0	0
026i001	0	1	0	0	0	1	0	0	0	1	0	0	0	0	0	0
026h001	1	0	0	0	1	0	0	0	1	0	0	0	0	0	0	0
026o002	0	0	0	0	0	0	0	0	0	0	0	0	0	0	0	0
026h002	1	0	1	0	1	0	1	0	1	0	1	0	0	0	0	0
Subtotal No. 1	**15**	**5**	**7**	**3**	**15**	**4**	**7**	**3**	**16**	**5**	**8**	**3**	**1**	**1**	**1**	**0**

Table A (continued)

	Wavelet				FIS				
	Out. TSP		In. TSP		Out. TSP		In. TSP		
Tube No.	F	T*	F	T*	F	T*	F	T*	NOTE
001i002	3	0	0	0	0	0	0	0	
001h002	1	0	0	0	0	0	0	0	
003i011	16	0	2	0	3	0	1	0	
003h011	10	0	2	0	2*	0	1	0	* called on 92 as NQI but not called on 94
004i012	8	0	0	0	0	0	0	0	
004h012	9	0	3	0	3	0	2	0	Missed flaw found by Wavelet Algorithm
									but dropped by the TSP's Amp. criterion
005i002	4	2*	1	0	1	2	0	0	1* not called on 94, 2* called on 94
005h002	3	0	1	0	1	0	0	0	
009o062	8	3	3	1	3	0	0	1	
009h062	6	5	2	0	2	5	1	0	
014o037	2	0	5	0	1	0	5	0	One false positive shows on 92 & 94
014h037	5	0	1	0	2	0	0	0	and locates on 6 th TSP 1.6
017i006	12	0	1	0	2	0	1	0	One false positive shows on 92 & 94
017h006	3	0	1	0	0	0	0	0	and locates on 6 th TSP 2.84
024i044	36	0	3	0	3	0	3	0	
024h044	13	0	1	0	1	0	0	0	
025o001	6	1	1	0	0	1	1	0	
025h001	0	1	1	0	0	0	1	0	
026i001	4	0	2	0	1	0	1	0	
026h001	0	0	0	0	0	0	0	0	
026o002	3	1	2	0	0	1	2	0	
026h002	0	0	0	0	0	0	0	0	
Subtotal No. 1	**152**	**13**	**32**	**1**	**25**	**9**	**17**	**1**	

Table A (continued)

	Wavelet				FIS				Human Analysis				Missed Call			
	Out. TSP		In. TSP		Out. TSP		In. TSP		Out. TSP		In. TSP		Out. TSP		In. TSP	
Tube No.	T	NQI	T	NQI	T	NQI	T	NQI	T	NQI	T	NQI	T	NQI	T	NQI
029i001	1	0	0	0	1	0	0	0	1	0	0	0	0	0	0	0
029h001	1	0	0	0	1	0	0	0	1	0	0	0	0	0	0	0
030i001	0	1	0	0	0	1	0	0	0	1	0	0	0	0	0	0
030h001	1	0	0	0	0	0	0	0	1	0	0	0	1	0	0	0
031o099	0	0	0	1	0	0	0	1	0	0	0	1	0	0	0	0
031h099	0	0	1	0	0	0	1	0	0	0	1	0	0	0	0	0
032i003	0	0	0	1	0	0	0	1	0	0	0	1	0	0	0	0
032h003	0	0	1	0	0	0	1	0	0	0	1	0	0	0	0	0
037o113	1	0	0	0	1	0	0	0	1	0	0	0	0	0	0	0
037h113	1	0	0	0	1	0	0	0	1	0	0	0	0	0	0	0
038o114	0	0	1	0	0	0	1	0	0	0	1	0	0	0	0	0
038h114																
045i004	1	0	0	0	1	0	0	0	1	0	0	0	0	0	0	0
045h004	1	0	0	0	1	0	0	0	1	0	0	0	0	0	0	0
045o116	0	0	1	0	0	0	1	0	0	0	1	0	0	0	0	0
045h116	0	0	1	0	0	0	1	0	0	0	1	0	0	0	0	0
048o031	0	0	0	0	0	0	0	0	0	0	0	1	0	0	0	1
048h031	0	0	1	0	0	0	1	0	0	0	1	0	0	0	0	0
051i002																
055i005	0	0	0	1	0	0	0	1	0	0	0	1	0	0	0	0
055h005	0	0	0	0	0	0	0	0	0	0	1	0	0	0	1	0
Subtotal No. 2	**7**	**1**	**6**	**3**	**6**	**1**	**6**	**3**	**7**	**1**	**7**	**4**	**1**	**0**	**1**	**1**

Table A (continued)

	Wavelet				FIS				
	Out. TSP		In. TSP		Out. TSP		In. TSP		
Tube No.	**F**	**T***	**F**	**T***	**F**	**T***	**F**	**T***	**NOTE**
029i001	5	0	0	0	0	0	0	0	10 th TSP 8.1
029h001	3	0	1	0	1	0	0	0	
030i001	5	0	1	0	1	0	0	0	One false positive shows on 92 & 94
030h001	1	0	0	0	0	0	0	0	and locates on 10 th TSP 6.6
031o099	4	0	1	0	2	0	1	0	
031h099	1	0	1	0	0	0	1	0	
032i003	12	0	1	0	6	0	1	0	5 th TSP 17.1
032h003	3	0	0	0	1	0	0	0	
037o113	3	0	0	0	1	0	0	0	
037h113	0	0	0	0	0	0	0	0	
038o114	7	0	0	1	2	0	0	1	
038h114									TSP detection error
045i004	22	0	4	0	4	0	4	0	
045h004	22	0	2	0	4	0	2	0	
045o116	4	0	0	0	0	0	0	0	
045h116	10	0	0	0	2	0	0	0	
048o031	6	0	2	0	1	0	1	0	7 th TSP 5.0
048h031	7	0	2	0	2	0	0	0	
051i002									TSP detection error
055i005	3	0	1	0	1	0	0	0	
055h005	2	0	0	0	0	0	0	0	
Subtotal No. 2	**120**	**0**	**16**	**1**	**28**	**0**	**10**	**1**	

Table A (continued)

	Wavelet				FIS				Human Analysis				Missed Call			
	Out. TSP		In. TSP		Out. TSP		In. TSP		Out. TSP		In. TSP		Out. TSP		In. TSP	
Tube No.	T	NQI	T	NQI	T	NQI	T	NQI	T	NQI	T	NQI	T	NQI	T	NQI
063i003	1	0	0	0	1	0	0	0	1	0	0	0	0	0	0	0
063h003	1	0	0	0	1	0	0	0	1	0	0	0	0	0	0	0
068i014	0	0	0	1	0	0	0	1	0	0	0	1	0	0	0	0
068h014	0	0	1	0	0	0	1	0	0	0	1	0	0	0	0	0
078o101	1	0	0	0	1	0	0	0	1	0	0	0	0	0	0	0
078h101	1	0	0	0	1	0	0	0	1	0	0	0	0	0	0	0
080c032	2	0	0	0	1	0	0	0	2	0	0	0	1	0	0	0
081 007																
084o118	0	0	0	1	0	0	0	1	0	0	0	1	0	0	0	0
084h118	0	0	1	0	0	0	1	0	0	0	1	0	0	0	0	0
086o127	0	0	1	0	0	0	1	0	0	0	1	0	0	0	0	0
086c127	0	0	1	0	0	0	1	0	0	0	1	0	0	0	0	0
087o126	1	0	0	0	1	0	0	0	1	0	0	0	0	0	0	0
087c126	1	0	0	0	1	0	0	0	1	0	0	0	0	0	0	0
089 121																
090o120	0	0	0	1	0	0	0	1	0	0	0	1	0	0	0	0
090h120	0	0	0	1	0	0	0	1	0	0	0	1	0	0	0	0
091o119	0	0	1	0	0	0	1	0	0	0	1	0	0	0	0	0
091c119	0	0	1	0	0	0	1	0	0	0	1	0	0	0	0	0
091o124	1	0	0	0	1	0	0	0	1	0	0	0	0	0	0	0
091c124	1	0	0	0	1	0	0	0	1	0	0	0	0	0	0	0
Subtotal No. 3	**10**	**0**	**6**	**4**	**9**	**0**	**6**	**4**	**10**	**0**	**6**	**4**	**1**	**0**	**0**	**0**

Table A (continued)

	Wavelet				FIS				
	Out. TSP		In. TSP		Out. TSP		In. TSP		
Tube No.	**F**	**T***	**F**	**T***	**F**	**T***	**F**	**T***	**NOTE**
063i003	10	0	1	0	4	0	0	0	
063h003	4	0	5	0	1	0	4	0	
068i014	2	0	1	0	1	0	1	0	
068h014	3	0	0	0	0	0	0	0	
078o101	1	0	0	0	0	0	0	0	
078h101	0	0	0	0	0	0	0	0	
080c032	14	0	2	0	4	0	0	0	
081 007									TSP detection error for incomplete data
084o118	2	0	1	0	0	0	1	0	
084h118	3	0	0	0	0	0	0	0	
086o127	13	0	0	0	1	0	0	0	
086c127	1	0	5	0	0	0	4	0	
087o126	0	0	0	0	0	0	0	0	
087c126	1	0	4	0	0	0	2	0	
089 121									Data oscillation likes as sinusoidal
090o120	2	0	0	0	0	0	0	0	
090h120	3	0	0	0	1	0	0	0	
091o119	2	0	0	0	0	0	0	0	6 th TSP 22.5
091c119	5	0	3	0	3	0	2	0	
091o124	2	0	0	0	2	0	0	0	
091c124	3	0	2	0	1	0	1	0	
Subtotal No. 3	**71**	**0**	**24**	**0**	**18**	**0**	**15**	**0**	

Table A (continued)

	Wavelet				FIS				Human Analysis				Missed Call			
	Out. TSP		In. TSP		Out. TSP		In. TSP		Out. TSP		In. TSP		Out. TSP		In. TSP	
Tube No.	T	NQI	T	NQI	T	NQI	T	NQI	T	NQI	T	NQI	T	NQI	T	NQI
092i002	0	0	1	0	0	0	1	0	0	0	1	0	0	0	0	0
092c002	0	0	1	0	0	0	1	0	0	0	1	0	0	0	0	0
094i002	0	0	0	1	0	0	0	1	0	0	0	1	0	0	0	0
094c002	0	0	0	1	0	0	0	1	0	0	0	1	0	0	0	0
098o122	0	0	0	0	0	0	0	0	1	0	0	0	1	0	0	0
098c122	0	0	0	0	0	0	0	0	1	0	0	0	1	0	0	0
098 126																
115o112	0	0	0	1	0	0	0	0	0	0	0	1	0	0	0	1
115h112	0	0	1	0	0	0	1	0	0	0	1	0	0	0	0	0
116i095	0	0	1	0	0	0	1	0	0	0	1	0	0	0	0	0
116h095	0	0	1	0	0	0	1	0	0	0	1	0	0	0	0	0
127i005	0	0	0	1	0	0	0	1	0	0	0	1	0	0	0	0
127c005	0	0	1	0	0	0	1	0	0	0	1	0	0	0	0	0
130i001	1	0	0	0	1	0	0	0	1	0	0	0	0	0	0	0
130c001	2	0	0	0	2	0	0	0	2	0	0	0	0	0	0	0
130i002	1	0	0	0	1	0	0	0	1	0	0	0	0	0	0	0
130c002	1	0	0	0	1	0	0	0	1	0	0	0	0	0	0	0
130i009	1	0	0	0	1	0	0	0	1	0	0	0	0	0	0	0
130c009	1	0	0	0	1	0	0	0	1	0	0	0	0	0	0	0
135o081	0	0	1	0	0	0	1	0	0	0	1	0	0	0	0	0
135h081	0	0	1	0	0	0	1	0	0	0	1	0	0	0	0	0
Subtotal No. 4	**7**	**0**	**8**	**4**	**7**	**0**	**8**	**3**	**9**	**0**	**8**	**4**	**2**	**0**	**0**	**1**

Table A (continued)

	Wavelet				FIS				
	Out. TSP		In. TSP		Out. TSP		In. TSP		
Tube No.	**F**	**T***	**F**	**T***	**F**	**T***	**F**	**T***	**NOTE**
092i002	2	0	1	0	1	0	1	0	
092c002	15	0	0	0	2	0	0	0	TSP detection error
094i002	16	0	2	0	2	0	2	0	
094c002	3	0	2	0	2	0	0	0	
098o122	1	0	0	0	0	0	0	0	True flaw' voltage is small. (0.18 on 92
098c122	0	0	0	0	0	0	0	0	and 0.31 on 94)
098 126									TSP detection error
115o112	2	0	1	0	1	0	0	0	
115h112	0	0	0	0	0	0	0	0	
116i095	0	0	0	0	0	0	0	0	
116h095	0	0	0	0	0	0	0	0	
127i005	2	0	0	0	0	0	0	0	
127c005	2	0	1	0	1	0	1	0	
130i001	5	1*	3	0	4	1	1	0	* called on 94 but not called on 92
130c001	6	0	0	0	4	0	0	0	
									(at 10 th TSP 12.0)
130i002	1*	0	0	0	0	0	0	0	* shows both on 92 & 94 but not called
130c002	3	0	0	0	2	0	0	0	Flaw called on 92 is different with flaw
									called on 94.
130i009	6	0	2	0	0	0	2	0	
130c009	7	0	1	0	3	0	1	0	
135o081	5	0	1	0	2	0	1	0	False positives show on 92 & 94
135h081	1	0	0	0	0	0	0	0	at 7 th TSP 36.7
Subtotal No. 4	**77**	**1**	**14**	**0**	**23**	**1**	**8**	**0**	

Table A (continued)

	Wavelet				FIS				Human Analysis				Missed Call			
	Out. TSP		In. TSP		Out. TSP		In. TSP		Out. TSP		In. TSP		Out. TSP		In. TSP	
Tube No.	T	NQI	T	NQI	T	NQI	T	NQI	T	NQI	T	NQI	T	NQI	T	NQI
151o011	0	1	0	0	0	0	0	0	0	1	0	0	0	1	0	0
151h011	1	0	0	0	0	0	0	0	1	0	0	0	1	0	0	0
151o016	1	0	0	0	1	0	0	0	1	0	0	0	0	0	0	0
151h016	2	0	0	0	2	0	0	0	2	0	0	0	0	0	0	0
Subtotal No. 5	**4**	**1**	**0**	**0**	**3**	**0**	**0**	**0**	**4**	**1**	**0**	**0**	**1**	**1**	**0**	**0**
Subtotal																
No. 1	**15**	**5**	**7**	**3**	**15**	**4**	**7**	**3**	**16**	**5**	**8**	**3**	**1**	**1**	**1**	**0**
No. 2	**7**	**1**	**6**	**3**	**6**	**1**	**6**	**3**	**7**	**1**	**7**	**4**	**1**	**0**	**1**	**1**
No. 3	**10**	**0**	**6**	**4**	**9**	**0**	**6**	**4**	**10**	**0**	**6**	**4**	**1**	**0**	**0**	**0**
No. 4	**7**	**0**	**8**	**4**	**7**	**0**	**8**	**3**	**9**	**0**	**8**	**4**	**2**	**0**	**0**	**1**
No. 5	**4**	**1**	**0**	**0**	**3**	**0**	**0**	**0**	**4**	**1**	**0**	**0**	**1**	**1**	**0**	**0**
Total	**43**	**7**	**27**	**14**	**40**	**5**	**27**	**13**	**46**	**7**	**29**	**15**	**6**	**2**	**2**	**2**
Sum	**91**				**85**				**97**				**12**			

Table A (continued)

	Wavelet				FIS				
	Out. TSP		In. TSP		Out. TSP		In. TSP		
Tube No.	**F**	**T***	**F**	**T***	**F**	**T***	**F**	**T***	**NOTE**
151o011	7	0	2	0	1	0	2	0	False positives show on 92 & 94 and
151h011	6	0	3	0	0	0	1	0	locate at 10 th 0.8 & 15 th 0.84
151o016	4	1*	0	0	2	1	0	0	* called on 94
151h016	8	0	2	0	1	0	1	0	
Subtotal No. 5	**23**	**1**	**7**	**0**	**3**	**1**	**4**	**0**	
Subtotal									
No. 1	**152**	**13**	**32**	**1**	**25**	**9**	**17**	**1**	
No. 2	**120**	**0**	**16**	**1**	**28**	**0**	**10**	**1**	
No. 3	**71**	**0**	**24**	**0**	**18**	**0**	**15**	**0**	
No. 4	**77**	**1**	**14**	**0**	**23**	**1**	**8**	**0**	
No.5	**23**	**1**	**7**	**0**	**3**	**1**	**4**	**0**	
Total	**443**	**15**	**93**	**2**	**97**	**11**	**54**	**2**	

Table B Test results on steam generator unit B of Oconee

	Wavelet				FIS				Human Analysis				Missed Call			
	Out. TSP		In. TSP		Out. TSP		In. TSP		Out. TSP		In. TSP		Out. TSP		In. TSP	
Tube No.	T	NQI	T	NQI	T	NQI	T	NQI	T	NQI	T	NQI	T	NQI	T	NQI
002o002	1	0	0	0	0	0	0	0	1	2	0	1	1	2	0	1
002h002																
002o005	0	1	0	0	0	1	0	0	0	2	0	0	0	1	0	0
002h005	1	0	0	0	1	0	0	0	2	1	0	0	1	1	0	0
002o009	1	1	0	0	1	0	0	0	1	1	0	0	0	1	0	0
002h009	1	0	0	0	1	0	0	0	1	0	0	0	0	0	0	0
002o011	1	0	0	0	1	0	0	0	1	0	0	0	0	0	0	0
002h011	1	0	0	0	1	0	0	0	1	0	0	0	0	0	0	0
009i062	1	0	0	0	0	0	0	0	1	0	0	0	1	0	0	0
009h062	1	0	0	0	0	0	0	0	1	0	0	0	1	0	0	0
014o075	1	0	1	0	1	0	1	0	1	0	1	0	0	0	0	0
014h075	1	0	0	0	1	0	0	0	1	0	0	0	0	0	0	0
016i005	0	1	0	0	0	1	0	0	0	1	0	0	0	0	0	0
016h005	1	0	0	0	1	0	0	0	1	0	0	0	0	0	0	0
018o079	0	1	0	0	0	1	0	0	0	1	0	0	0	0	0	0
018h079	1	0	0	0	1	0	0	0	1	0	0	0	0	0	0	0
020i078	0	0	0	1	0	0	0	1	0	0	0	1	0	0	0	0
020h078	1	0	0	0	1	0	0	0	1	0	0	0	0	0	0	0
021i014	0	1	0	0	0	1	0	0	0	1	0	0	0	0	0	0
021h014	1	0	0	0	1	0	0	0	1	0	0	0	0	0	0	0
026o066	0	0	1	0	0	0	1	0	0	1*	1	0	0	1*	0	0
026h066	0	0	1	0	0	0	1	0	0	0	1	0	0	0	0	0
Subtotal No. 1	**14**	**5**	**3**	**1**	**11**	**4**	**3**	**1**	**15**	**10**	**3**	**2**	**4**	**6**	**0**	**1**

Table B (continued)

	Wavelet				FIS				
	Out. TSP		In. TSP		Out. TSP		In. TSP		
Tube No.	F	T*	F	T*	F	T*	F	T*	NOTE
002o002	10	0	0	0	3	0	0	0	Multiple flaws connected
002h002									Big interference located on flaw's position
002o005	1	0	3	0	0	0	0	0	Multiple flaws connected
002h005	0	0	8	0	0	0	5	0	
002o009	3	0	1	0	2	0	0	0	
002h009	0	1	17	0	0	0	14*	0	* TSP not suppressed well
002o011	6	0	0	0	0	0	0	0	
002h011	1	0	13	0	0	0	13*	0	* TSP not suppressed well
009i062	16	0	2	0	5	0	2	0	One false positive shows on 92 & 94
009h062	3	0	2	0	3	0	2	0	and located on 14 th TSP 30.5
014o075	5	0	3	0	3	1	0	0	
014h075	3	0	1	0	2	0	0	0	
016i005	3	0	1	0	0	0	1	0	
016h005	10	0	2	0	4	0	2	0	
018o079	15	0	4	0	0	0	4	0	
018h079	7	0	2	0	0	0	2	0	
020i078	6	0	1	0	2	0	1	0	
020h078	2	0	1	0	0	0	1	0	
021i014	3	0	0	0	1	0	0	0	
021h014	0	0	0	0	0	0	0	0	
026o066	1	0	1	0	0	0	1	0	* called on 92 but not called on 94
026h066	3	0	1	0	0	1	0	1	
Subtotal No. 1	**98**	**1**	**62**	**0**	**23**	**1**	**39**	**0**	

Table B (continued)

	Wavelet				FIS				Human Analysis				Missed Call			
	Out. TSP		In. TSP		Out. TSP		In. TSP		Out. TSP		In. TSP		Out. TSP		In. TSP	
Tube No.	T	NQI	T	NQI	T	NQI	T	NQI	T	NQI	T	NQI	T	NQI	T	NQI
032i006	0	0	0	0	0	0	0	0	0	0	1	0	0	0	1	0
032h006	0	0	1	0	0	0	1	0	0	0	1	0	0	0	0	0
033i004	0	0	0	1	0	0	0	1	0	0	0	1	0	0	0	0
033h004	0	0	0	0	0	0	0	0	0	0	1	0	0	0	1	0
033i030	0	0	0	1	0	0	0	1	0	0	0	1	0	0	0	0
033i030	0	0	1	0	0	0	1	0	0	0	1	0	0	0	0	0
034i103	1	0	0	0	1	0	0	0	1	0	0	0	0	0	0	0
034i103	1	0	0	0	1	0	0	0	1	0	0	0	0	0	0	0
037h003	1	0	1	0	1	0	1	0	1	0	1	0	0	0	0	0
037i005	1	0	0	0	1	0	0	0	1	0	0	0	0	0	0	0
037h005	1	0	0	0	1	0	0	0	1	0	0	0	0	0	0	0
040i001	1	0	0	0	1	0	0	0	1	0	0	0	0	0	0	0
040h001	1	0	0	0	1	0	0	0	1	0	0	0	0	0	0	0
040i080	0	1	0	0	0	1	0	0	0	1	0	0	0	0	0	0
040h080	1	0	0	0	1	0	0	0	1	0	0	0	0	0	0	0
041i004	0	0	1	0	0	0	1	0	0	0	1	0	0	0	0	0
041h004	0	0	1	0	0	0	1	0	0	0	1	0	0	0	0	0
046i004	1	0	1	0	1	0	1	0	1	0	1	0	0	0	0	0
046h004	0	0	1	0	0	0	1	0	0	0	1	0	0	0	0	0
046i099	0	0	0	1	0	0	0	1	0	0	0	1	0	0	0	0
046i099	0	0	1	0	0	0	1	0	0	0	1	0	0	0	0	0
Subtotal No. 2	**9**	**1**	**8**	**3**	**9**	**1**	**8**	**3**	**9**	**1**	**10**	**3**	**0**	**0**	**2**	**0**

Table B (continued)

	Wavelet				FIS				
	Out. TSP		In. TSP		Out. TSP		In. TSP		
Tube No.	**F**	**T***	**F**	**T***	**F**	**T***	**F**	**T***	**NOTE**
032i006	23	0	0	0	6	0	0	0	One false positive shows on 92 & 94
032h006	5	0	0	0	3	0	0	0	and located on 9 th TSP 16.18
033i004	15	0	1	0	5	0	1	0	
033h004	2	0	0	0	2	0	0	0	
033i030	1	0	0	0	0	0	0	0	
033h030	2	0	0	0	1	0	0	0	
034i103	4	0	0	0	1	0	0	0	
034h103	6	0	0	0	1	0	0	0	
037h003	0	0	1	0	0	0	1	0	
037i005	3	0	4	0	1	0	3	0	
037h005	1	0	1	0	0	0	1	0	
040i001	3	0	2	0	1	0	1	0	
040h001	1	0	1	0	0	0	0	0	
040i080	*								* Data oscillation results lots of false
040h080	*								positives.
041i004	6	0	1	0	3	0	0	0	
041h004	8	0	0	0	3	0	0	0	
046i004	15	0	3	0	4	0	1	0	
046h004	17	0	1	0	1	0	1	0	
046i099	14	0	2	0	7	0	0	0	
046h099	8	0	1	0	1	0	0	0	
Subtotal No. 2	**134**	**0**	**17**	**0**	**40**	**0**	**9**	**0**	

Table B (continued)

	Wavelet				FIS				Human Analysis				Missed Call			
	Out. TSP		In. TSP		Out. TSP		In. TSP		Out. TSP		In. TSP		Out. TSP		In. TSP	
Tube No.	T	NQI	T	NQI	T	NQI	T	NQI	T	NQI	T	NQI	T	NQI	T	NQI
047i004	0	0	1	0	0	0	1	0	0	0	1	1*	0	0	0	1*
047h004	0	0	1	0	0	0	1	0	0	0	1	0	0	0	0	0
047o122	1	0	0	0	1	0	0	0	1	0	0	0	0	0	0	0
047h122	1	0	0	0	1	0	0	0	1	0	0	0	0	0	0	0
049i119	2	0	0	0	2	0	0	0	2	0	0	0	0	0	0	0
049h119	1	0	0	0	1	0	0	0	1	0	0	0	0	0	0	0
053i055	1	0	0	0	1	0	0	0	1	0	0	0	0	0	0	0
053h055	1	0	0	0	1	0	0	0	3	0	0	0	2	0	0	0
059i008	0	0	0	1	0	0	0	1	0	0	0	1	0	0	0	0
059h008	0	0	1	0	0	0	1	0	0	0	1	0	0	0	0	0
062o115	1	0	0	0	1	0	0	0	1	0	0	0	0	0	0	0
062h115	1	0	0	0	1	0	0	0	1	0	0	0	0	0	0	0
069 001																
069o124	0	0	1	0	0	0	1	0	0	0	1	0	0	0	0	0
083i071	0	1	0	0	0	1	0	0	0	1	0	0	0	0	0	0
083h071	1	0	0	0	1	0	0	0	1	0	0	0	0	0	0	0
083o108	0	2	0	0	0	0	0	0	0	2	0	0	0	2*	0	0
083h108	0	1	0	0	0	1	0	0	0	1	0	0	0	0	0	0
083o127	1	0	0	0	0	0	0	0	1	0	0	0	1	0	0	0
083h127	1	0	0	0	1	0	0	0	1	0	0	0	0	0	0	0
Subtotal No. 3	**12**	**4**	**4**	**1**	**11**	**2**	**4**	**1**	**14**	**4**	**4**	**2**	**3**	**2**	**0**	**1**

Table B (continued)

	Wavelet				FIS				
	Out. TSP		In. TSP		Out. TSP		In. TSP		
Tube No.	**F**	**T***	**F**	**T***	**F**	**T***	**F**	**T***	**NOTE**
047i004	10	0	2	0	0	0	0	0	* called on 92 but not called on 94
047h004	10	0	0	0	2	0	0	0	Check 9 th TSP 25.0
047o122	1	0	2	0	0	0	1	0	
047h122	3	0	2	0	2	0	1	0	
049i119	3	0	4	0	0	0	4	0	
049h119	2	0	3	0	2	0	3	0	
053i055	2	0	4	0	1	0	2	0	
053h055	8	0	0	0	3	0	0	0	
059i008	2	0	2	0	2	0	2	0	
059h008	0	0	0	0	0	0	0	0	
062o115	8	0	1	0	5	0	1	0	
062h115	15	0	4	0	7	0	4	0	
069 001									Incomplete data set
069o124	3	0	0	0	0	0	0	0	
083i071	32	0	1	0	5	0	1	0	
083h071	11	0	0	0	2	0	0	0	
083o108	4	0	0	0	1	0	0	0	* One positive called on 92 but not called
083h108	4	0	0	0	2	0	0	0	on 94
083o127	10	0	0	0	2	0	0	0	
083h127	10	0	0	0	4	0	0	0	
Subtotal No. 3	**128**	**0**	**25**	**0**	**40**	**0**	**19**	**0**	

Table B (continued)

	Wavelet				FIS				Human Analysis				Missed Call			
	Out. TSP		In. TSP		Out. TSP		In. TSP		Out. TSP		In. TSP		Out. TSP		In. TSP	
Tube No.	T	NQI	T	NQI	T	NQI	T	NQI	T	NQI	T	NQI	T	NQI	T	NQI
083o132	0	0	1	0	0	0	1	0	0	0	1	0	0	0	0	0
083h132	0	0	1	0	0	0	1	0	0	0	1	0	0	0	0	0
089o042	1	0	0	0	1	0	0	0	1	0	0	0	0	0	0	0
089h042	1	0	0	0	1	0	0	0	1	0	0	0	0	0	0	0
092o113	0	0	1	0	0	0	1	0	0	0	1	0	0	0	0	0
092h113	0	0	1	0	0	0	1	0	0	0	1	0	0	0	0	0
093o119	0	0	1	0	0	0	1	0	0	0	1	0	0	0	0	0
093h119	0	0	0	0	0	0	0	0	0	0	1	0	0	0	1	0
107o045	1	0	0	0	1	0	0	0	1	0	0	0	0	0	0	0
107h045	1	0	0	0	1	0	0	0	1	0	0	0	0	0	0	0
112o013	0	0	1	0	0	0	1	0	0	0	1	0	0	0	0	0
112c013	0	0	1	0	0	0	1	0	0	0	1	0	0	0	0	0
124o038	0	1	0	0	0	0	0	0	0	1	0	0	0	1	0	0
124c038	2	0	0	0	2	0	0	0	2	0	0	0	0	0	0	0
125o011	0	0	0	1	0	0	0	1	0	0	0	1	0	0	0	0
125c011	0	0	2	0	0	0	2	0	0	0	2	0	0	0	0	0
125o012	0	0	0	1	0	0	0	0	0	0	0	1	0	0	0	1
125c012	0	0	1	0	0	0	0	0	0	0	1	0	0	0	0	0
126c011	0	0	1	0	0	0	1	0	0	0	1	0	0	0	0	0
127c010	0	0	0	0	0	0	0	0	0	0	1	0	0	0	1	0
Subtotal No. 4	**6**	**1**	**11**	**2**	**6**	**0**	**10**	**1**	**6**	**1**	**13**	**2**	**0**	**1**	**3**	**1**

Table B (continued)

	Wavelet				FIS				
	Out. TSP		In. TSP		Out. TSP		In. TSP		
Tube No.	**F**	**T***	**F**	**T***	**F**	**T***	**F**	**T***	**NOTE**
083o132	5	0	2	0	2	0	2	0	
083h132	1	0	0	0	1	0	0	0	
089o042	2	0	2	0	0	0	1	0	
089h042	21	0	1	0	7	0	0	0	
092o113	9	0	0	0	2	0	0	0	
092h113	14	0	0	0	1	0	0	0	
093o119	9	0	0	0	3	0	0	0	
093h119	5	0	1	0	2	0	1	0	
107o045	15	0	1	0	5	0	0	0	
107h045	8	0	1	0	1	0	1	0	
112o013	5	0	1	0	2	0	0	0	
112c013	0	0	0	0	0	0	0	0	
124o038	5	1*	0	0	1	1*	0	0	* called on 94 but not called on 92
124c038	3	0	0	0	2	0	0	0	
125o011	3	0	0	1*	1	0	0	1*	* called on 94 but not called on 92
125c011	1	0	0	0	1	0	0	0	
125o012	4	0	0	0	1	0	0	0	
125c012	3	0	0	0	0	0	0	0	
126c011	2	0	0	0	0	0	0	0	
127c010	0	0	0	0	0	0	0	0	
Subtotal No. 4	**115**	**1**	**9**	**1**	**32**	**1**	**5**	**1**	

Table B (continued)

	Wavelet				FIS				Human Analysis				Missed Call			
	Out. TSP		In. TSP		Out. TSP		In. TSP		Out. TSP		In. TSP		Out. TSP		In. TSP	
Tube No.	T	NQI	T	NQI	T	NQI	T	NQI	T	NQI	T	NQI	T	NQI	T	NQI
127o037	0	0	1	0	0	0	1	0	0	0	1	0	0	0	0	0
127c037	0	0	1	0	0	0	1	0	0	0	1	0	0	0	0	0
134o033	0	1	0	0	0	1	0	0	0	1	0	0	0	0	0	0
134c033	1	0	0	0	1	0	0	0	1	0	0	0	0	0	0	0
138o029	0	1	0	0	0	1	0	0	0	1	0	0	0	0	0	0
138c029	1	0	0	0	1	0	0	0	2	1	0	0	1	1	0	0
141o004	0	0	0	1	0	0	0	0	0	0	0	1	0	0	0	1
141c004	0	0	1	0	0	0	1	0	0	0	1	0	0	0	0	0
144o012	0	0	0	1	0	0	0	1	0	0	0	1	0	0	0	0
144c012	0	0	1	0	0	0	1	0	0	0	1	0	0	0	0	0
144o015	0	0	1	0	0	0	1	0	0	0	1	0	0	0	0	0
144c015	0	0	0	1	0	0	0	1	0	0	0	1	0	0	0	0
144i056	1	0	0	0	1	0	0	0	1	0	0	0	0	0	0	0
144h056	1	0	0	0	1	0	0	0	1	0	0	0	0	0	0	0
149i023	0	1	0	0	0	1	0	0	0	1	0	0	0	0	0	0
149h023	1	0	0	0	1	0	0	0	1	0	0	0	0	0	0	0
Subtotal No. 5	**5**	**3**	**5**	**3**	**5**	**3**	**5**	**2**	**6**	**4**	**5**	**3**	**1**	**1**	**0**	**1**
Subtotal																
No. 1	**14**	**5**	**3**	**1**	**10**	**5**	**3**	**1**	**15**	**10**	**3**	**2**	**5**	**5**	**0**	**1**
No. 2	**9**	**1**	**8**	**3**	**9**	**1**	**8**	**3**	**9**	**1**	**10**	**3**	**0**	**0**	**2**	**0**
No. 3	**12**	**4**	**4**	**1**	**11**	**2**	**4**	**1**	**14**	**4**	**4**	**2**	**3**	**2**	**0**	**1**
No. 4	**6**	**1**	**11**	**2**	**6**	**0**	**10**	**1**	**6**	**1**	**13**	**2**	**0**	**1**	**3**	**1**
No. 5	**5**	**3**	**5**	**3**	**5**	**3**	**5**	**2**	**6**	**4**	**5**	**3**	**1**	**1**	**0**	**1**
Total	**46**	**14**	**31**	**10**	**42**	**10**	**30**	**8**	**50**	**20**	**35**	**12**	**8**	**10**	**5**	**4**
SUM	**101**				**90**				**117**				**27**			

Table B (continued)

	Wavelet				FIS				
	Out. TSP		In. TSP		Out. TSP		In. TSP		
Tube No.	**F**	**T***	**F**	**T***	**F**	**T***	**F**	**T***	**NOTE**
127o037	3	0	0	0	0	0	0	0	
127c037	4	0	0	0	1	0	0	0	
134o033	5	0	1	0	0	0	0	0	
134c033	1	0	0	0	1	0	0	0	
138o029	6	0	0	0	1	0	0	0	
138c029	1	0	0	0	0	0	0	0	
141o004	13	0	0	0	7	0	0	0	
141c004	10	0	0	0	2	0	0	0	
144o012	11	0	0	0	1	0	0	0	
144c012	5	0	0	0	0	0	0	0	
144o015	11	0	0	0	0	0	0	0	
144c015	3	0	0	0	3	0	0	0	
144i056	13	0	1	0	6	0	1	0	
144h056	4	0	0	0	2	0	0	0	
149i023	11	0	3	0	1	0	2	0	
149h023	3	0	2	0	2	0	2	0	
Subtotal	**104**	**0**	**7**	**0**	**27**	**0**	**5**	**0**	
Subtotal									
No. 1	**98**	**1**	**62**	**0**	**23**	**1**	**39**	**0**	
No. 2	**134**	**0**	**17**	**0**	**40**	**0**	**9**	**0**	
No. 3	**128**	**0**	**25**	**0**	**40**	**0**	**19**	**0**	
No. 4	**115**	**1**	**9**	**1**	**32**	**1**	**5**	**1**	
No. 5	**104**	**0**	**7**	**0**	**27**	**0**	**5**	**0**	
Total	**579**	**2**	**120**	**1**	**162**	**2**	**77**	**1**	

APPENDIX B: LIST OF ABBREVIATIONS

In this appendix, the abbreviations used in this dissertation are listed below:

1. NDE = Nondestructive evaluation.
2. NDT = Nondestructive testing.
3. MFEC (eddy current technology) = Multifrequency (eddy current technology).
4. MPEC = Multiparameter (eddy current technology).
5. ID (flaw) = Inside diameter (flaw).
6. OD (flaw) = Outside diameter (flaw).
7. LS (algorithm) = Least squares (algorithm).
8. %TW = Percent through-wall.
9. FIR (filter) = Finite impulse response.
10. FFT = Fast Fourier transform.
11. TSP = Tube support plate.
12. FLS = Fuzzy logic system.
13. FIS = Fuzzy inference system.
14. NQI = Non-qualified indication.

REFERENCES

[1] S. S. Udpa and W. Lord, "A Fourier Descriptor Classification Scheme for Differential Probe Signals", *Material Evaluation*, Vol. 42, pp. 1136-1141, 1984.

[2] D. J. Hagemaier, Fundamentals of Eddy Current Testing, ASNT, Columbia, OH, 1990.

[3] R. S. Sharpe, *Research Techniques in Nondestructive Testing Vol. VIII*, Academic Press, London, 1985.

[4] R. S. Sharpe, *Research Techniques in Nondestructive Testing Vol. VII*, Academic Press, London, 1984.

[5] W. G. Clark, " Multiple-Element Eddy Current Probes For Enhanced Inspection", Material Evaluation, Vol. , pp. 794-802, 1993.

[6] R. A. Baker and R. S. Tombaugh, "Eddy Current Examination of Heat-Exchanger Tubing with Inside-surface Pitting", *Material Evaluation*, Vol. 48, pp. 55-58, 1990.

[7] C. V. Dodd and W. E. Deeds, "In-Service Inspection of Steam-Generator Tubing Using Multiple-Frequency Eddy-Current Techniques", in G. Birnbaum and G. Free (eds.), *Eddy-Current Characterization of Material and Structures*, ASTM, Philadelphia, 1981.

[8] T. J. Davis, "Advanced Multifrequency Eddy-Current System for Steam-Generator Inspection", in G. Birnbaum and G. Free (eds.), *Eddy-Current Characterization of Material and Structures*, ASTM, Philadelphia, 1981.

[9] *ET Analysis for Windows - User Guide*, Zetec Inc., Issaquah, WA, 1994.

[10] P. G. Doctor, T. P. Harrington, T. J. Davis, C. J. Morris, and D. W. Fraley, "Pattern-Recognition Methods for Classifying and Sizing Flaws Using Eddy-Current Data", in G. Birnbaum and G. Free (eds.), *Eddy-Current Characterization of Material and Structures*, ASTM, Philadelphia, 1981.

[11] A. N. Mucciardi, "Elements of Learning Control Systems with Applications to Industrial Processes", *Proceedings of the IEEE Conf. on Decision and Control*, New Orleans, LA, 1972.

[12] A. N. Mucciardi, E. C. Orr, J. R. Gouge, R. Shankar, and M. F. Whalen, "Signal Processing for ISI", *EPRI NP 1421*, May 1980.

[13] T. Stepinski and N. Maszi, "Conjugate Spectrum Filters for Eddy Current Signal Processing", *Material Evaluation*, Vol. 51, pp. 839-844, 1993.

[14] A. J. Levy, J. E. Oppenlander, D. M. Brudnoy, J. M. Englund, K. C. Loomis, and A. M. Barsky, "Dodger: an Expert System for Eddy Current Evaluation", *Material Evaluation*, Vol. 51, pp. 34-44, 1993.

[15] L. Udpa and S. S. Udpa, "Eddy Current Defect Characterization Using Neural Networks", *Material Evaluation*, Vol.48, pp. 342-347, 1990.

[16] L. Udpa, W. Lord, and S. S. Udpa, "Frequency Domain Methods for the Analysis of Multifrequency Eddy Current Data', Review of Progress in Quantitative Nondestructive Evaluation, edited by D.O. Thompson and D.E. Chimenti, Vol. 8A, pp. 821-830, 1988.

[17] A. V. Oppenheim, R. W. Schafer, *Discrete-Time Signal Processing*, Prentice Hall, Englewood Cliffs, New Jersey, 1989.

[18] W. H. Press, S. A. Teukolsky, W. T. Vetterling, and B. P. Flannery, *Numerical Recipes in C Second Edition.*, Cambridge, University Press, 1994.

[19] I. Daubechies, *Ten Lectures on Wavelets*, SIAM, Philadelphia, 1992.

[20] C. K. Chui, *An Introduction to Wavelets*, Academic Press, New York, 1992.

[21] Y. Meyer, *Wavelets: Algorithms and Applications*, SIAM, Philadelphia, 1993.

[22] G. Kaiser, A Friendly Guide to Wavelets, Birkhauser, Boston, 1994.

[23] Y. T. Chan, Wavelet Basics, Kluwer Academic Publishers, Boston, 1995.

[24] M. Vetterli, and C. Herley, "Wavelets and Filter Banks: Theory and Design", *IEEE Transactions on Signal Processing*, Vol. 40, No. 9, Sep. 1992.

[25] R. Bracewell, *The Fourier Transform and its Applications*, Second Ed., New York, McGraw-Hill, 1986.

[26] M. R. Portnoff, " Time-Frequency Representation of Digital Signals and System Based on Short-Time Fourier Analysis", *IEEE Tran. Acoust., Speech, Signal Processing*, Vol. 28, pp. 55-69, Feb. 1980.

[27] S. G. Mallat, "A Theory for Multiresolution Signal Decomposition: The Wavelet Representation", *IEEE Transactions on Pattern Analysis and Machine Intelligence*, Vol. 11, No. 7, pp. 674-693.

[28] G. Strang, "Wavelet and Dilation Equations: A Brief Introduction", *SIAM Review*, Vol. 31, No. 4, pp. 614-627, Dec 1989.

[29] S. Mallat, and S. Zhong, "Characterization of Signals from Multiscale Edges", *IEEE Transaction on Pattern Analysis and Machine Intelligence*, Vol. 14, No. 7, pp. 710-732, Jul. 1992.

[30] S. Mallat, "Zero-Crossings of a Wavelet Transform", *IEEE Transactions on Information Theory*, Vol. 37, No. 4, Jul. 1991.

[31] R. A. Carmona, "Wavelet Identification of Transients in Noisy Time Series", *SPIE, Mathematical Imaging*, Vol. 2034, pp. 392-400, 1993.

[32] M. Sugeno, *Industrial Applications of Fuzzy Control*, Amsterdam, North-Holland, 1985.

[33] M. M. Gupta, and T. Yamakawa, *Fuzzy Computing*, Amsterdam, North-Holland, pp. 263-284, 1991.

[34] J. R. Boston, "Effect of Membership Function Parameters on the Performance of a Fuzzy Signal Detector", *IEEE Transactions on Fuzzy Systems*, Vol. 5., No. 2, pp. 249-255, May, 1997.

[35] L. A. Zadeh, "Fuzzy Sets", *Inform. Contr.*, Vol. 8, pp. 338-353, 1965.

[36] G. Bojadziev, and M. Bojadziev, *Fuzzy Sets, Fuzzy Logic, Applications*, Singapore, World Scientific, 1995.

[37] A. Kandel, *Fuzzy Mathematical techniques with Application. Reading*, MA, Addison-Wesley, 1986.

[38] L. X. Wang and J. M. Mendel, "Generating fuzzy rules from numerical data, with applicaitons", IEEE Trans. Systems, Man, and Cybern., Vol. SMC-22, pp. 1414-1427, 1992.

[39] C. C. Lee, "Fuzzy Logic in Control System: Fuzzy Logic Controller—Part I", *IEEE Transactions on Systems, Man, and Cybernetics*, Vol. 20, No. 2, pp. 404-418, 1990.

[40] J. M. Mendel, "Fuzzy Logic Systems for Engineering: A Tutorial", *Proceedings of the IEEE*, Vol. 83, No. 3, pp. 345-377, Mar. 1995.

[41] B. Kosko, *Neural Networks and Fuzzy Systems*, Englewood Cliffs, NJ, Prentice Hall, 1996.

[42] P. Craven and G. Wahba, "Smoothing Noisy Data with Spline Functions", *Numer. Math.*, Vol. 31, pp. 377-403, 1979.

[43] E. Oja, "A Simplified Neuron Model as a Principal Component Analyzer", *J. Math. Biology*, Vol. 15, pp. 267-273,1982.

[44] E. Oja, "Neural Networks, Principal Components, and Subspaces", *Int. J. Neural Systems*, Vol. 1, pp. 61-68, 1989.

[45] T.D. Sanger, "Optimal Unsupervised Learning in a Single-Layer Linear Feedforward Neural Network", *Neural Networks*, Vol. 12, pp. 459-473, 1989.

[46] S. Haykin, *Neural Networks: A Comprehensive Foundation*, Macmilan, New York, 1994.

[47] S. Ergezinger and E. Thossen, "An Accelerated Learning Algorithm for Multilayer Perceptron: Optimization Layers by Layers", *IEEE Tran. Neural Networks*, Vol. 6, pp. 31-42, 1995.

[48] M. J. D. Powell, "Radial Basis Functions for Multivariable Interpolation: a Review" in *Algorithms for Approximation*, edited by J. C. Mason and M. G. Cox, pp. 143-167, Oxford, 1987.

[49] S. Elanayar V. T. and Y. C. Shin, "Radial Basis Function Neural Network for Approximation and Estimation of Nonlinear Stochastic Dynamic Systems", *IEEE Trans. Neural Network*, Vol. 5, pp. 594-603, 1994.

[50] J. A. Leonard, M. A. Kramer, and L. H. Ungar, "Using Radial Basis Functions to Approximate a Function and its Error Bounds", *IEEE Trans. Neural Networks*, Vol. 3, pp. 624-627, 1992.

[51] J. Durkin, *Expert Systems Design and Development*, Macmillan, New York, 1994.